ENGINEERING APPLICATIONS USING THE INNATE REDOX ENVIRONMENT OF *RHODOPSEUDOMONAS PALUSTRIS*

A Dissertation

Presented to the Faculty of the Graduate School

of Cornell University

In Partial Fulfillment of the Requirements for the Degree of

Doctor of Philosophy

By

Devin Forest Reed Doud

August 2014

ENGINEERING APPLICATIONS USING THE INNATE REDOX ENVIRONMENT OF *RHODOPSEUDOMONAS PALUSTRIS*

Devin Forest Reed Doud, Ph.D.

Cornell University 2014

Rhodopseudomonas palustris is currently the most metabolically versatile organism known. Because of this, it has become a model organism not only for it's many forms of metabolism, but also for the complex coordination required to regulate them. Under anaerobic conditions, *R. palustris* has received considerable attention regarding how it handles excess reducing equivalents. Herein, I investigated alternate routes for either pushing or pulling reducing equivalents into the metabolism of *R. palustris* for applications relating to bioenergy. Of particular interest to my research are the anaerobic metabolic processes of: i. anoxygenic photosynthesis; ii. metabolism of the molecules *n*-butyrate and *p*-coumarate; iii. photoautotrophic growth with iron(II) as a sole electron donor; iv. nitrogenase based production of H_2; and v. fixation of CO_2. In my first study, I focused on the lethal redox imbalance that *R. palustris* encounters when growing on *n*-butyrate with no viable electron sinks. Excess reducing equivalents were harnessed to drive the metabolically engineered production of the biofuel *n*-butanol. Because the reduction of *n*-butyrate to *n*-butanol became the only route of maintaining redox balance, this metabolically engineered activity became obligate for growth. In the second study, I co-cultured *R. palustris* and the model exoelectrogen *Geobacter sulfurreducens* together in a bioelectrochemical system to investigate metabolite sharing of the lignin monomer *p*-coumarate by *R. palustris*. The electrochemical system functioned as a tool for measuring the

effect of *G. sulfurreducens* aiding *R. palustris* in maintaining redox balance. The third study characterized the ability of *R. palustris* to take up electrons from a negatively poised electrode through mediated iron cycling as a sole source of electrons for growth. It was observed that volumetric rates of electron uptake were very low, so to improve these rates and demonstrate that this mechanism could be the foundation of a future microbial electrosynthesis technology, improvements in reactor design were made. The electrode was removed from the growth reactor, which allowed optimization of both the photosynthetic bioreactor and the abiotic electrochemical reactor. These two components were then connected through a closed recirculation loop to recycle and regenerate the iron substrate. This resulted in increased volumetric iron consumption 56 times higher in the illuminated reactor compared to previously measured in conventional bioelectrochemical reactors.

BIOGRAPHICAL SKETCH

Devin F. R. Doud graduated Summa Cum Laude with a B.S. in Biochemistry from California State University Long Beach in 2009 and continued directly into the Ph.D. program in microbiology at Cornell University. During the program, he rotated through the research labs of Drs. Ian Hewson, David Wilson, and Ruth Richardson before joining the lab of Dr. Lars Angenent in the Biological and Environmental Engineering department. He worked as a teaching assistant for general microbiology for 4 semesters and served as the 2010 vice president for the Field Of Microbiology Students. While at Cornell, Devin joined the North American – International Society for Microbial Electrochemical Technologies and co-organized the 2013 conference at Cornell. He was later selected to speak about his research at the same conference in 2014 at Penn State University.

This dissertation is dedicated to my fiancée, Charlotte, and my entire family.

Your continuous support is what has enabled me to be where I am today.

ACKNOWLEDGEMENTS

Countless people have contributed to my development in the field of scientific research. I would like to thank Dr. Lars Angenent, my advisor, who taught me the importance of the patience, dedication, and repetition necessary to achieve success in research. I now understand that nothing is easy in research, and nothing ever works the first time. My committee, composed of Dr. Stephen Zinder, Dr. David Wilson, Dr. Georg Jander, and Dr. Matt DeLisa, whom were critical in the support of my research with their expertise and advise. My study at Cornell University was supported financially by many avenues, all of which I am very grateful for. The graduate microbiology TA fellowship, the Atkinson Center for a Sustainable Future, and the Advanced Research Projects Agency – Energy, all facilitated the progress I made through their generous financial support. And lastly, the many people I have had the opportunity to interact with in my time in the Angenent lab: you have always provided a wealth of advise, support, encouragement, and just plain old-fashioned fun. To name a few: Dr. Michaela TerAvest, Dr. Elliot Friedman, Juan Guzman, Dylan Webster, Aadhar Jain, Nina Voulis, Joe Usack, Drs. Hanno and Lubna Richter, Dr. Matt Agler, Dr. Miriam Rosenbaum, Dr. Zhongjian Li, Dr. Arvind Venkatraman, Dr. Erik Bland, Dr. Michael Kalontarov, Dr. Erica Jung, Catherine Spirito, Leo Kucek, and Lauren Haroff.

TABLE OF CONTENTS

LIST OF FIGURES

LIST OF TABLES

CHAPTER 1

INTRODUCTION: CENRAL AIM AND SUMMARY OF RESEARCH

1.1 Central aim

Biofuels provide one potential form of alleviation from fossil fuels. As mandated by the Energy Independence and Security Act of 2007, production of liquid biofuels must increase to 36 billion gallons by 2022 with at least 21 billion gallons derived from non-cornstarch feedstock. Since the 15 billion gallon limit for cornstarch-based fuels has already been reached, efforts are turning to lignocellulosic, algal, and waste-based sources to sustainably produce a wide range of alcohols, alkanes, gasses, and diesels. Though strong efforts are being made in researching chemical and enzymatic pretreatments to transition this process to non-sugar based feedstocks, this has not yet become economical at the scale required. *Rhodospeudomonas palustris* is an attractive microbe for biofuel production due to: i. the diversity of substrates it can metabolize; ii. its ability to perform photosynthesis; and iii. its innate redox imbalance. Previous research efforts have harnessed these three traits for the production of hydrogen as a biofuel, however, there is opportunity for the production of a wider spectrum of bioenergy by developing new systems within *R. palustris*. In an effort to help realize these applications, I focused on alternate routes for harnessing energy from *R. palustris* that center around metabolic engineering and growth inside bioelectrochemical systems.

1.2 Introduction

This dissertation investigates the microbe *Rhodopseudomonas palustris* as a platform for multiple bioenergy technologies. Fundamental to this is the unique metabolism of *R. palustris*, which displays an inherent drive to dissipate excess reducing equivalents. Chapter 2 is a review of previous literature relating to the metabolism of *R. palustris*, previous metabolic engineering strategies that have been used for biofuel production, and bioelectrochemical systems, which harbor microbes for bioenergy production. Chapter 3, 4, and 5 describe the three studies of the dissertation, and present the research that was performed in support of these objectives (Chapter 3 and 5) and hypothesis (Chapter 4). Chapter 3 describes a metabolic engineering approach for the production of the biofuel *n*-butanol from waste-derived *n*-butyrate. This activity was inspired by the solventogenic bacterium *Clostridium acetobutylicum*. Chapter 4 presents a strategy for utilizing electrochemical systems as a tool for measuring fundamental metabolic interactions that exist between two organisms in a controlled environment. Chapter 5 focuses on the ability of *R. palustris* to grow using an electrode as the sole source of electrons. To improve rates of electron uptake from the electrode, a new bioelectrochemical reactor was constructed. Chapter 6 gives conclusions on the presented findings and suggestions for future research to expand the field. Appendices 1, 2, and 3 contain supplementary information for Chapters 3, 4, and 5, respectively. Appendix 4 contains work that was performed beyond the concentration of the dissertation and focused on utilizing UV light to disinfect the same novel photobioreactor used in Chapter 5. This reactor was designed in a collaborative effort as part of a grant awarded through Advanced Research Projects Agency- Energy.

1.3 Summary of experiments

Section 1- Objective: To metabolically engineer the *n*-butyrate to *n*-butanol reduction pathway in *R. palustris*.

- The known *n*-butyrate to *n*-butanol activity from *Clostridium acetobutylicum* 824 was engineered into *R. palustris*.
- This was achieved by codon optimization of the wild type *Clostridium* alcohol/aldehyde dehydrogenase AdhE2 and was also attempted with a homologous protein found in *R. palustris* strain BisB18.
- Growth rates, pH, all relevant metabolites, and carbon conversion efficiency of the engineered strain and empty vector control under both restrictive ($-HCO_3^-$) and permissive ($+HCO_3^-$) conditions were measured.

Section 2- Hypothesis: Acetate sharing alleviates redox burden in *R. palustris* degrading *p*-coumarate.

- Two different strains of *R. palustris*; wild type and the H_2 secretor NifA*, were grown with *p*-coumarate as the sole organic carbon source in a bioelectrochemical reactor harboring *Geobacter sulfurreducens* to investigate metabolite sharing.
- Growth rates, Coulombic efficiency, maximum current production, pH, and *p*-coumarate intermediates were measured.
- Using electrical current produced from *G. sulfurreducens* as a proxy for acetate sharing, it was determined that *R. palustris* does not release acetate as a redox balance strategy while consuming *p*-coumarate.

Section 3- Objective: To improve volumetric electron uptake rates of *R. palustris* growing with the electrode as a sole electron donor.

- *R. palustris* was grown photoautotrophically with a negatively poised electrode as a sole source of electrons through an iron-mediated electron transfer mechanism.
- To increase rates of electron transfer above the state-of-the-art, a new photobioelectrochemical reactor strategy was designed and operated.
- Current uptake, optical density, and pH were measured as a function of growth under darkened and illuminated conditions.

CHAPTER 2

INTRODUCTION TO ANAEROBIC METABOLISM OF *RHODOPSEUDOMONAS PALUSTRIS* AND ITS APPLICATION IN BIOENERGY

2.1 Rhodopseudomonas palustris

2.1.1 Photosynthetic purple non-sulfur bacteria

Rhodopseudomonas palustris is a mesophilic purple non-sulfur bacterium (PNSB) belonging to the alphaproteobacteria class. The PNSB are a non-taxonomic group of bacteria capable of anoxygenic photosynthesis *via* cyclic photophosphorylation while using a wide range of organics, reduced sulfur species (such as sulfide, sulfite and elemental sulfur), Fe(II) or H_2 to fix CO_2 (Garrity 2007). The photosynthetic center contains either bacteriochlorophyll a or b and is expressed usually only in anaerobic environments. Unlike chlorophyll a that is found in cyanobacteria and plants, the photosynthetic center of bacteriochlorophyll a absorbs energy in the infrared region (peaks at 805 and 870 nm) and derives its electrons from reduced organic or inorganic sources rather than H_2O. Because of this, PNSB are often found in transition zone sediments with low-level light exposure.

2.1.2 Rhodopseudomonas palustris *metabolism*

R. palustris is best known for its diverse metabolism as it is capable of living by all four methods of growth: photoautotrophic, photoheterotrophic, chemoautotrophic, and chemoorganotrophic (Larimer et al. 2004). With the sequencing of the 5.46 Mb genome and 8.4 kb plasmid of *R. palustris* CGA009 in 2003, *R. palustris* was verified to be the most metabolically versatile organism yet known and was adopted as a model organism for the study of metabolic regulation

due to the complex networks necessary to orchestrate these different growth modes. In addition, *R. palustris* has been widely studied for its ability to degrade aromatic hydrocarbons, both aerobic and anaerobically, produce hydrogen (even when growing photoautotrophically), and is capable of fixing nitrogen and carbon (Joshi et al. 2009).

R. palustris is capable of growing photoautotrophically through two forms of RuBisCO, type I and II. For this process, the Calvin-Benson-Bassham (Calvin) cycle in *R. palustris* utilizes NADH as a reducing cofactor to fix CO_2 as opposed to NADPH used by other autotrophic organisms (McFadden 1973). The potential reason for this deviation from traditional autotrophic strategy could be that during cyclic photophosphorylation, production of NADPH is not directly coupled with photosynthesis (as in a photosystem II like method) and reducing equivalents must be generated later by the reverse flow of electrons through the electron transport chain to reduce NAD^+ at the expense of proton motive force. Thus, the predominance of the NADH reducing equivalent, as the direct product of the reverse electron transport chain, compared with NADPH may be the reason for the altered cofactor specificity in the Calvin cycle for the PNSB. In addition, due to the mechanism of energy production by cyclic photophosphorylation, the production of cellular reducing equivalents is uncoupled from photosynthesis.

2.1.3 Rhodopseudomonas palustris *as a potential host for biofuel production*

R. palustris has been investigated as a potentially advantageous organism for the production of renewable biofuels due to its ability to produce H_2 by multiple methods of growth. *R. palustris* is capable of photoheterotrophic growth under anaerobic conditions with a range of organic substrates. It has long been known that catabolism of a substrate with a more reduced oxidation state than biomass requires a parallel process functioning as an electron sink (*i.e.,* H_2 evolution,

N_2/CO_2 fixation) in PNSB to adjust the redox state of the substrate to that of biomass (Muller 1933). This was verified by Hillmer and Gest growing *Rhodobacter capsulatus* with *n*-butyrate (Hillmer and Gest 1977). When HCO_3^- was added to the medium, growth of *R. capsulatus* occurred, but when HCO_3^- was omitted, no growth occurred. However, if NH_4^+ was omitted from the medium and conditions for N_2 fixation were allowed, *R. capsulatus* was able to again grow even in the absence of HCO_3^-. This result suggests that when excess reducing equivalents accumulate during photoheterotrophic cell growth, the processes of carbon and nitrogen fixation are used as electron sinks to regenerate reduced cofactors and maintain cell redox equilibrium in PNSB. This finding was further verified by the observation that *R. capsulatus* could be grown with *n*-butyrate under non-carbon/nitrogen fixing and non-H_2 evolution conditions if DMSO was included in the media, further suggesting these processes function as electron sinks (Richardson et al. 1988).

To gauge the magnitude of this activity in maintaining redox balance in PNSB, McKinlay and Harwood provided labeled acetate as the sole carbon source for photoautotrophic growth of *R. palustris (McKinlay and Harwood 2010)*. By following the label, the authors determined that while 22% of the acetate was released from the system as CO_2, 68% of this released carbon was subsequently reassimilated into biomass by the Calvin cycle. This level of CO_2 fixation corresponded to the consumption of roughly half of the reducing equivalents generated by acetate oxidation and suggests that *R. palustris* is only capable of using half of the reduced cofactors produced from acetate oxidation for synthesis of biomass. When this experiment was repeated with *R. palustris* mutant NifA*, which demonstrates constitutive expression of its nitrogenase, a reduction in the levels of CO_2 fixation occurred and a concurrent increase in H_2 production was observed. Unsurprisingly, these combined activities accounted for the

consumption of half of the reducing equivalents produced by acetate oxidation. These results suggest that when grown on acetate, the total catabolic activities of *R. palustris* generate roughly twice as many reducing equivalents than they can use for anabolism and *R. palustris* must obligately dispose of the additional equivalents through any manner possible.

Table 2.1. Oxidation states of different carbon substrates and H_2 production during photoheterotrophic growth of *R. palustris* NifA* Adapted from J.B. McKinlay, C. S. Harwood, Mbio 2, (Mar-Apr, 2011).

Compound	Formula	Oxidation State	H_2 yield (mol H_2/100 mol C)
Fumarate	$C_4H_4O_4$	+1	18 ± 3
Succinate	$C_4H_6O_4$	+0.5	23 ± 1
Acetate	$C_2H_4O_2$	0	21 ± 3
Biomass	$CH_{1.8}N_{0.18}O_{0.38}$	-0.5	N/A
***n*-Butyrate**	$C_4H_8O_2$	-1	41 ± 10

In a follow-up study, *R. palustris* was inoculated into mineral medium with either fumarate, succinate, acetate, or *n*-butyrate as the carbon source (McKinlay and Harwood 2011). These substrates were chosen to monitor metabolic fluxes as a function of substrate oxidation state, ranging from more oxidized (fumarate, succinate, acetate) to more reduced (*n*-butyrate) than biomass. Growth and evolution of H_2 was measured in all conditions when NH_4^+ was omitted (**Table 2.1**). When NH_4^+ was added, it was again observed that HCO_3^- played a similar role in maintaining redox equilibrium in *R. palustris* because with its omission the *n*-butyrate culture was unable to grow. The observation that H_2 was produced across the entire range of carbon substrates, even with fumarate, is intriguing as it suggests that even with substrates more oxidized than biomass, there is still a need to remove reducing equivalents from the system

(McKinlay and Harwood 2010). Understanding why H_2 is evolved from *R. palustris* growing on substrates at a more oxidized state compared to biomass requires tracing these components as they enter into metabolism.

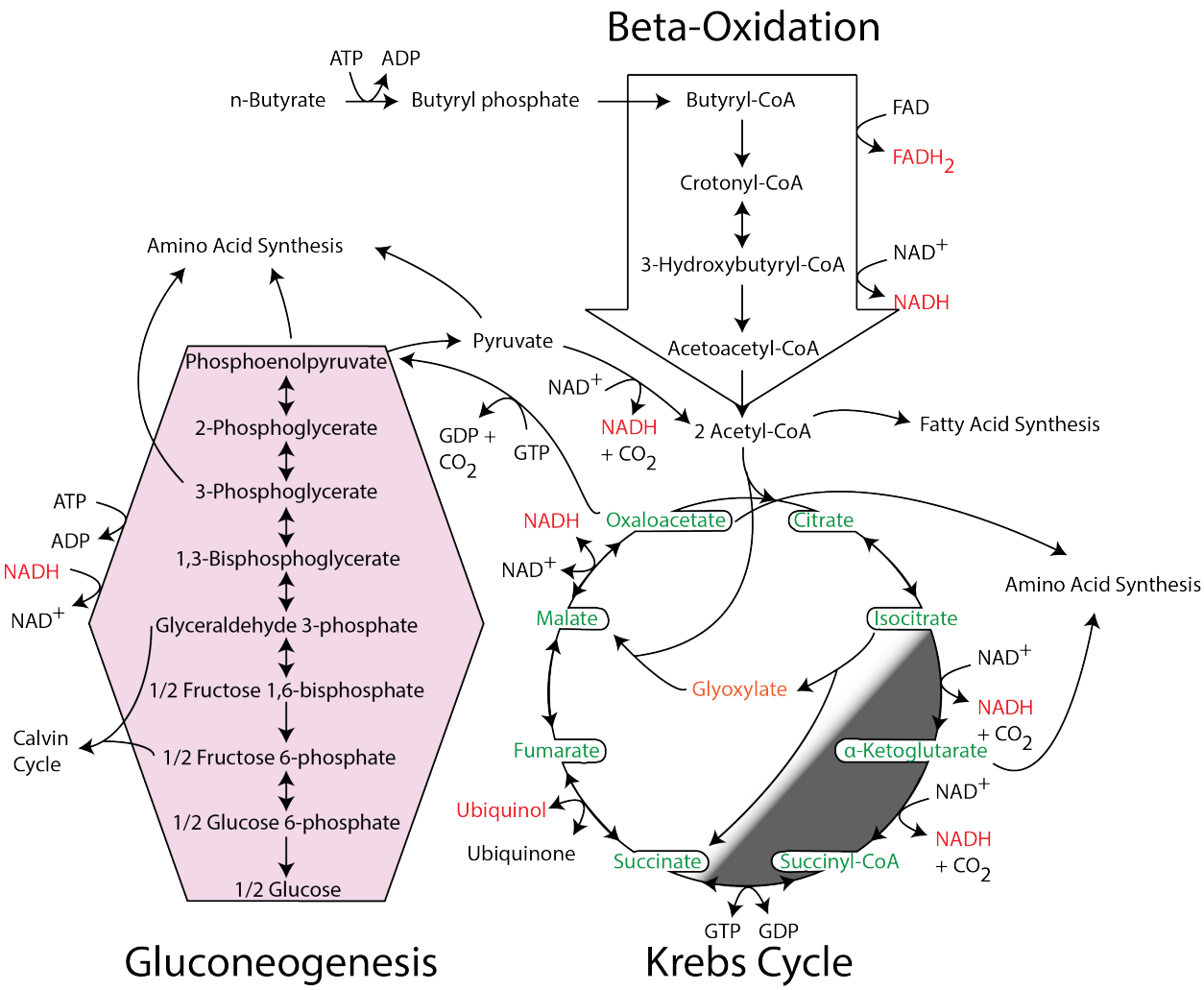

Figure 2.1. Central metabolism of *R. palustris* growing photoheterotrophically.

As an example, the formation of 1 mol of glucose by gluconeogenesis will be traced for all carbon sources tested in the 2011 McKinlay and Harwood study. Fumarate and succinate, as intermediates in the Krebs cycle, enter central metabolism easily and are capable of directly funneling into the gluconeogenic pathway. To create 1 mol of glucose from succinate requires

the expense of 4 mols ATP and has the net production of two ubiquinol. Similar to succinate, fumarate also requires the consumption of 4 ATP but does not yield ubiquinol. *n*-Butyrate and acetate are not direct intermediates of the Krebs cycle and because of this, organisms able to grow solely on these carbon sources require a strategy similar to the glyoxylate shunt to allow incorporation instead of oxidation of their substrate. Briefly, bypassing the oxidative portions of the Krebs cycle (**Fig. 2.1**), the glyoxylate shunt allows synthesis of larger carbon structures by allowing acetyl-CoA to be integrated with glyoxylate into malate, which is then oxidized to oxaloacetate in the Krebs cycle. Oxaloacetate can then be subsequently decarboxylated to phosphoenolpyruvate, which is a critical intermediate in the gluconeogenesis pathway. As a result of the glyoxylate shunt, the formation of 1 mol of glucose from acetate produces two mols of reduced ubiquinol and consumes 8 mols ATP. Alternatively, *n*-butyrate is not directly compatible for the Krebs cycle and must be cleaved to two molecules of acetyl-CoA before entering as acetate does. This cleavage of *n*-butyrate proceeds through an anaerobic β-oxidation like mechanism in *R. palustris* (McKinlay and Harwood 2011) and produces 1 mol of NADH and 1 mol of $FADH_2$. With this additional step, the synthesis of 1 mol of glucose from *n*-butyrate produces 2 mols of NADH, $FADH_2$, and ubiquinol each, and consumes 6 mols of ATP.

Table 2.2. ATP and cofactors generated by gluconeogenesis during photoheterotrophic growth of *R. palustris* on different substrates.

Compound	NADH	$FADH_2$ or Ubiquinol	ATP
Fumarate	0	0	-4
Succinate	0	+2	-4
Acetate	0	+2	-8
***n*-Butyrate**	+2	+4	-6

Although fumarate does not produce any reducing equivalents directly in the process of gluconeogenesis, the synthesis of precursor metabolites, including α-ketoglutarate, acetyl-CoA, pyruvate, and phosphoenolpyruvate, result in the net production of cellular reducing equivalents that could ultimately be responsible for the observed H_2 production when growing on this substrate. To gain a better understanding of the central metabolism of *R. palustris*, a predictive metabolic model was constructed to analyze pathway flux under these various growth methods.

Stoichiometric network analysis of core metabolism for *R. palustris,* constructed to model flux through 143 central reactions and 119 metabolites, investigated conditions growing photoheterotrophically on different carbon sources (Hadicke, Grammel, and Klamt 2011). This model confirmed that regardless of the synthetic pathway taken, the uptake of a certain substrate always corresponded to the yield of a fixed amount of biomass synthesized and CO_2 released, with increasing levels of CO_2 released for more oxidized substrates. These results concurred with a non-zero calculated flux through the Calvin cycle for each substrate and supported previous empirical findings that carbon fixation occurred when growing on with a wide oxidation range of organic carbon sources. However, because the uncoupling of ATP production and substrate consumption allow a number of potentially futile pathways (*i.e.,* oxidation of acetyl-CoA by TCA and subsequent fixation this CO_2 with the produced NADH), the oxidative flux through TCA was set to zero for these calculations. This assumption, which could underestimate the potential of the cells to fix CO_2 or evolve H_2 if this pathway is even slightly active, resulted in flux values that strongly agree with the reported findings discussed previously. It is widely agreed that the tight coupling between carbon and redox balance found in this model is the governing principle for the photoheterotrophic growth of *R. palustris*.

The metabolism of *R. palustris* growing photoheterotrophically is attractive in the field of biofuels as a large proportion of produced reducing equivalents must be eliminated to maintain cellular growth. While the production of H_2 has been the primary focus for the industrial application of *R. palustris*, the reducing power of its innate imbalanced redox metabolism has potential to drive the production of any number of biofuels. One attractive biofuel that has gained interest recently due to its chemical advantages over ethanol is *n*-butanol

2.2 Butanol

2.2.1 History of n-*butanol production*

Microbial production of *n*-butanol was first described in 1862 by the father of microbiology, Louis Pasteur (Pasteur 1862). This discovery evolved from a previous characterization of a mixed culture that produced the pungent compound *n*-butyrate. Within this culture, Pasteur described the presence of an organism, which he called *Vibrion butyrique* due to its shape and metabolism (Pasteur 1861a), and went on to describe that this organism's inability to grow in air was attributed to its intolerance of oxygen, and thus first coined the term "anaerobic" (Pasteur 1861b). *Clostridium butyricum* along with closely related *n*-butanol producing relatives, are believed to be closely related to the previously described *Vibrion butyrique*, and have, thus, had a long and politically charged history paralleling their 150-years of scientific inquiry.

Soon after Pasteur's discovery of fermentative *n*-butanol production, a number of microbiologists including Albert Fitz and Martinus Beijerinck identified a number of organisms of the genus *Clostridium* that also produced solvents, including acetone, isopentanol, and isopropanol, as part of their fermentation metabolism. While these "solventogenic" *Clostridia* remained relatively in the shadows in their respective research labs between 1860 and 1900, the

demand for their metabolic capabilities pushed them into their industrial debut in early 20th century.

A shortage of natural rubber, which was triggered by the increasing popularity of cars and a blight of Brazilian rubber trees in the early 1900's, prompted a "rubber race" between the United States, Britain, and Russia, each striving to discover a method to produce rubber synthetically. British scientists at Strange and Graham Ltd. in 1910 determined a method for the production of rubber from the polymerization of 1,3-butadiene and 2-methyl-1,3-butadiene (isoprene). These chemicals were not available in the bulk quantities required for commercial synthetic rubber production, so methods for producing the *n*-butanol and isopentanol precursors to isoprene were sought by Strange and Graham. They recruited a number of scientists, including Chaim Weizmann, to investigate the possibility of producing large volumes of these chemicals by clostridial fermentation of sugars. Weizmann became fervent that the success of synthetic rubber rested on future solvent production by microbial fermentation and eventually isolated an organism, *Clostridium acetobutylicum*, which produced unprecedented amounts of both *n*-butanol and acetone (Gabriel 1928).

Soon after, with the outbreak of WWI in 1914, global demand for gunpowder skyrocketed and again *Clostridia* were enlisted for their solvent producing abilities. Cordite, which was the bullet propellant used at the time, required large volumes of acetone as a solvent for production and *Clostridia* were utilized for their solvent production, this time purely for acetone. During this process, *n*-butanol was produced in large volumes as a side product, however, as there was no apparent use for *n*-butanol, it was stored until later needed. Following the war, uses for the stockpiled *n*-butanol, including as an auto paint lacquer, were found but with the discovery of cheaper petrochemical based methods of production, clostridial production

of both acetone and *n*-butanol fell out of favor (Jones and Woods 1986). Time and time again, *Clostridia* have demonstrated their value for solvent production at an industrial scale. Their ability to produce a range of flammable solvents is due to their unique metabolism that has been the focus of much research since its discovery in 1861.

2.2.2 Metabolism of Clostridium acetobutylicum

C. acetobutylicum is capable of growing by two metabolic modes: acedogenesis, and solventogenesis. The arrangement of these metabolic modes of growth is exclusive, sequential, and aids in surviving the increasingly stressful conditions created by excretion of its own metabolic end products. The progression of these metabolic strategies is best illustrated by following growth in a batch-type environment.

When inoculated into neutral medium, *C. acetobutylicum* expends its exponential growth phase fermenting a range of sugars into acetic and butyric acids by the acedogenic pathway highlighted in blue (**Fig. 2.2**) (Sauer and Durre 1995). These acids accumulate to concentrations above 100 mM (Grimmler et al. 2011) and induce a drop in the pH to below 5 as the organism reaches late exponential phase. The acidification of the medium induces an "acid crash" response in the cells as their intracellular pH drops to 6, prevented from dropping further only by the activity of its H^+-translocating ATPase (Nolling et al. 2001). The reduced pH causes stress on the cells not only through the increased transmembrane proton gradient, but accumulation of intracellular dissociated acids (Gottwald and Gottschalk 1985).

The dissociation equilibrium for a weak acid is governed by the Henderson-Hasselbalch equation and is dependent solely on pH. For example, a given amount of *n*-butyrate at a pH of 4.8 has a ~16 times higher proportion of the undissociated acid form compared to a pH of 6.

Following acidification of the batch fermentation, the extracellular *n*-butyrate equilibrium is shifted predominantly to the uncharged *n*-butyric acid, enabling diffusion through the clostridial cellular membrane. The higher intracellular pH facilitates the dissociation equilibrium shift and rapidly deprotonates a majority of the *n*-butyric acid to the charged and non-diffusible *n*-butyrate. This event acidifies the intracellular pH and sequesters *n*-butyrate inside the cell at high concentrations (Russell 1992).

In addition, throughout the course of acedogenic metabolism, the cellular redox balance is shifted to a more reduced state. This is due to the rapid fermentation of glucose to acids with H_2 production as the only metabolic outlet for the excess NADH reducing equivalents produced. Highlighted in **Table 2.3**, acedogenic production of acetate and *n*-butyrate produces two molecules of NADH per acid with the fermentation of glucose to acetate producing 4 NADH and glucose to *n*-butyrate producing 2 NADH overall. While the cue to transition from acedogenesis to solventogenesis remains an area of debate in the field, it is agreed that transmembrane proton stress, cytosolic accumulation of unprotonated acids, and the highly reduced redox state of the cell triggers the next phase of metabolism: solventogenesis.

Table 2.3. NADH and ATP yields from acedogenic (blue) growth and regeneration of NAD^+ by solventogenic (red) conversion of acids to alcohols.

	Acetate	*n*-Butyrate	Ethanol	Butanol	Acetone
NADH	2	2	-2	-2	4
ATP	2	3	0	0	2

To increase intracellular pH, reduce the concentration of accumulating acids, and oxidize its pool of reduced cofactors, *C. acetobutylicum* undergoes a fundamental shift in its metabolism. This shift is characterized by transitioning from an overall acid producing to acid reducing central metabolism (from blue to red path illustrated in **Fig. 2.2**).

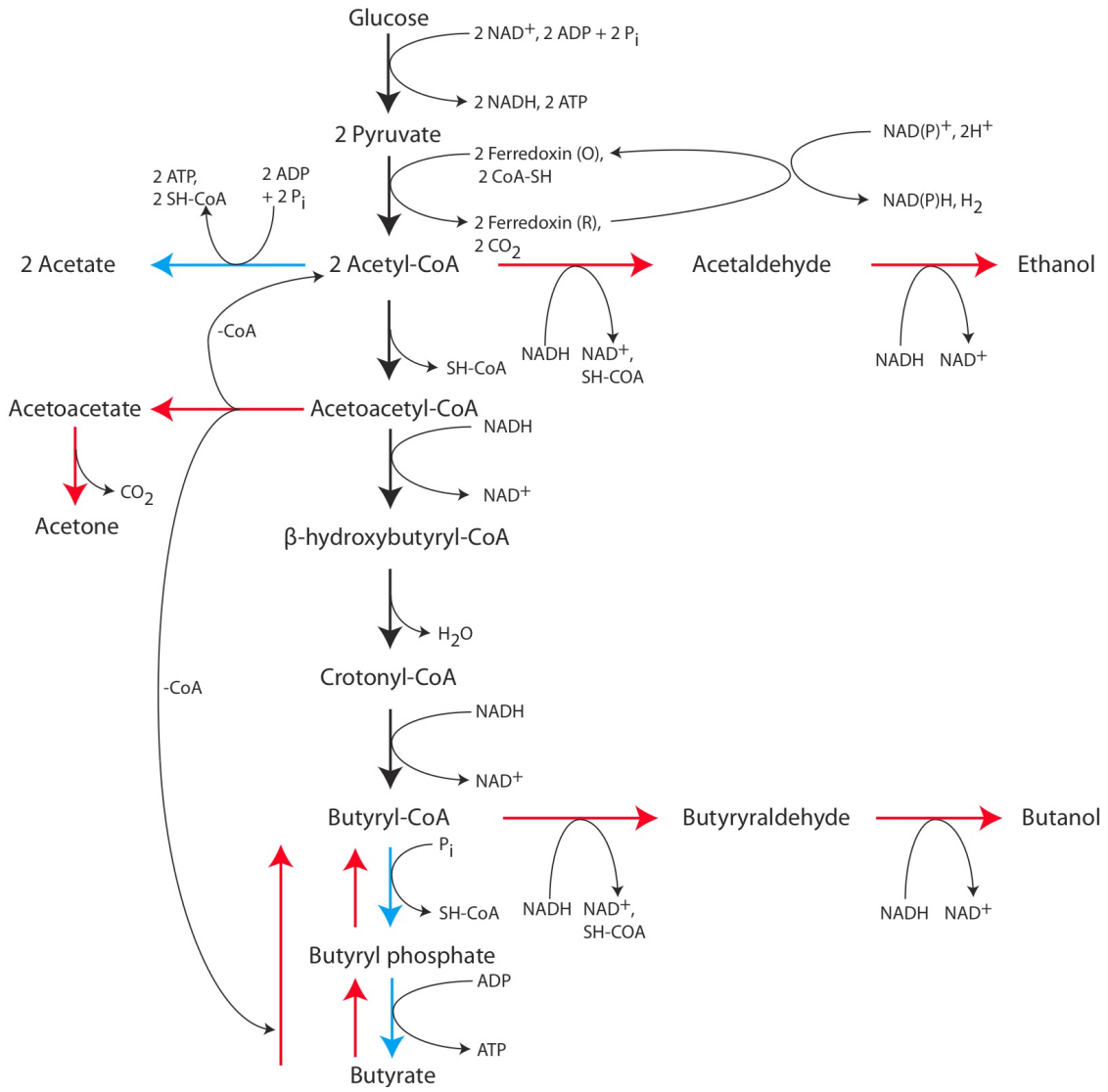

Figure 2.2. Central metabolism of *C. acetobutylicum*. Acedogenic pathway is highlighted in blue. Solventogenic pathway is highlighted in red.

As part of this metabolic strategy, *C. acetobutylicum* has been noted to produce solvents in a characteristic 3:6:1 ratio of acetone:butanol:ethanol (Jones and Woods 1986), which consumes the reducing equivalents produced from acetone formation with the reduction of *n*-butyrate and acetate (**Table 2.3**). The reduction of acetate and *n*-butyrate to their corresponding alcohols has been well characterized in *C. acetobutyicum* and both proceed through a similar mechanism. Below, the reduction of *n*-butyrate will be discussed.

2.2.3 Mechanism of n-*butyrate to* n-*butanol conversion*

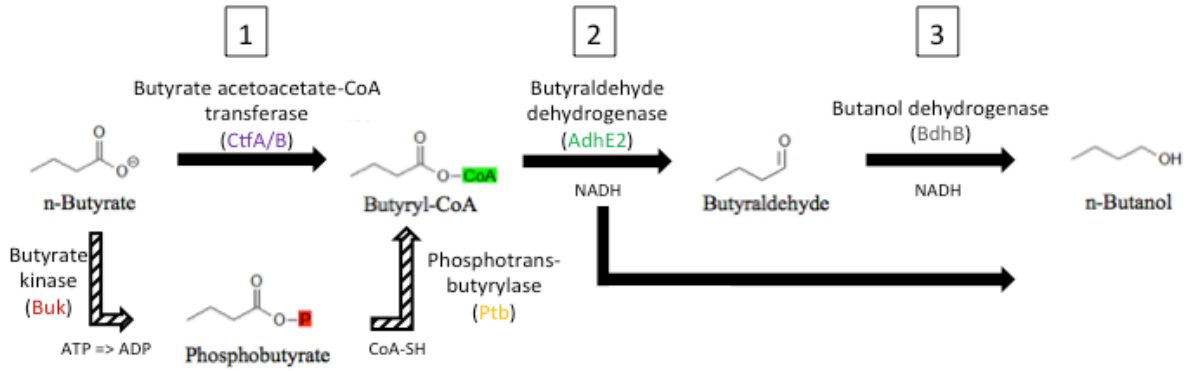

Figure 2.3. Mechanism of *n*-butyrate reduction to *n*-butanol in *C. acetobutylicum*.

n-Butyrate is converted into *n*-butanol in three sequential steps in *C. acetobutylicum*: 1) activation of *n*-butyrate to butyryl-CoA *via* one of two alternative mechanisms; 2) reduction of butyryl-CoA to butyraldehyde *via* either of the two AdhE isoenzymes; and ultimately 3) the reduction of butyraldehyde to *n*-butanol with a host of potential enzymes including either of the two AdhE isoenzymes or one of two butanol dehydrogenase isoenzymes, BdhA, and BdhB (**Fig. 2.3**).

2.2.3.1 n-*Butyrate acetoacetate-CoA transferase*

n-Butyrate is first activated by the *n*-butyrate acetoacetate-CoA transferase enzyme, which transfers an activated -CoA group from acetoacetyl-CoA to *n*-butyrate. Acetoacetate is subsequently irreversibly decarboxylated to acetone to drive the reversible transfer mechanism forward. This step favors the irreversible formation of activated butyryl-CoA and likely supports a much higher flux than through the alternate *n*-butyrate kinase/phosphotransbutyrylase mechanism responsible for originally forming *n*-butyrate from butyryl-CoA (Sillers, A-Hinai, and Papoutsakis 2009, Desai et al. 1999). In addition, the elimination of acetoacetate from the

cell as acetone facilitates the uptake of additional extracellular acids for reduction (Hartmanis, Klason, and Gatenbeck 1984).

2.2.3.2 Bifunctional aldehyde/alcohol dehydrogenases:

AdhE1 and AdhE2 are both bifunctional aldehyde/alcohol dehydrogenases capable of reducing butyryl-CoA to butanal and subsequently to *n*-butanol in a two-step process. These enzymes are both encoded on the pSOL1 plasmid and appear to be evolutionary protein fusions of an aldehyde- and an alcohol dehydrogenase, since they both possess two primary domains, 49-395 and 455-850, that show high homology to the aldehyde dehydrogenase and Fe-containing alcohol dehydrogenase family, respectively (Fontaine et al. 2002).

AdhE1 was discovered and characterized early on in the study of *n*-butanol production from *C. acetobutylicum* and was long believed to be the sole enzyme responsible for the aldehyde reduction of butyryl-CoA. However, following sequencing of the *C. acetobutylicum* genome and pSOL1 plasmid in 2001, the gene encoding AdhE2 was found 47 kb away from *adhE1* on the pSOL1 plasmid. Although these two enzymes share 66.1% amino acid identity (Fontaine et al. 2002), *in vitro* studies of both enzymes indicate that while their sequence dissimilarity has little effect on their alcohol dehydrogenase activity, it strongly affects their aldehyde dehydrogenase activity and cofactor specificity.

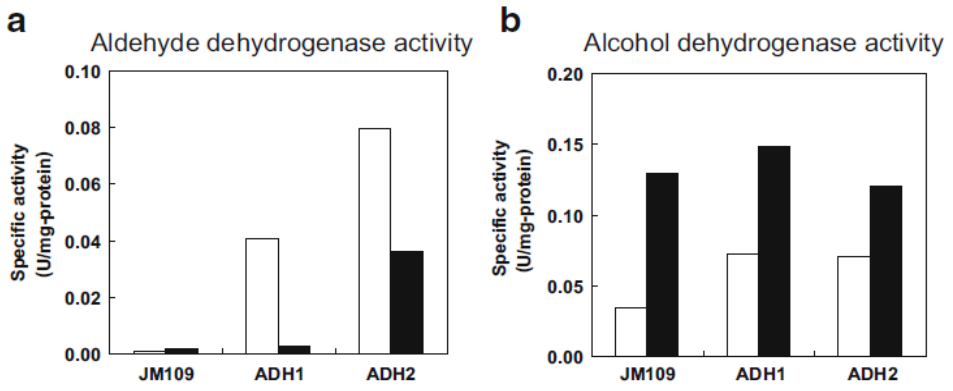

Figure 2.4. Aldehyde and alcohol dehydrogenase activity of AdhE1 and AdhE2. This figure was taken from Inui et al. 2008. a) Aldehyde and b) alcohol forming activities of AdhE1 (ADH1), AdhE2 (ADH2), and background *E. coli* host (JM109). The white bar represents acetyl-CoA (a), or acetaldehyde (b) as a substrate while the black bar represents butyryl-CoA (a) or butyraldehyde (b) as a substrate.

AdhE1 and AdhE2 were expressed in *E. coli* and activities of crude cellular extracts were measured to better understand the roles of these two enzymes in reductive solventogenesis. It was found that although AdhE2 had a comparable alcohol dehydrogenase activity to AdhE1 (neither of which was significantly higher than background levels in *E. coli*), its ability to reduce butyryl-CoA to butanal was 12 fold higher than AdhE1 (Inui et al. 2008). In addition, previous characterization of AdhE1 and AdhE2 individually expressed in a *C. acetobutylicum* cured of its pSOL1 plasmid found that AdhE1 reduced its substrates only with NADPH as a cofactor while AdhE2 demonstrated high NADH dependency (Fontaine et al. 2002).

2.2.3.3 Alcohol dehydrogenases

In addition to the alcohol dehydrogenase reductive ability of AdhE1/AdhE2, two cellular butanol dehydrogenases are also capable of participating in the final reduction step in *n*-butanol production. The *C. acetobutylicum* ATCC 824 chromosome contains two primary butanol dehydrogenases (BdhA and BdhB), which carry out this reaction. In 1992, Walter et al. isolated and sequenced a 4 kb DNA fragment containing the complete sequence for both genes. Sequence

results indicated that *bdhA* and *bdhB* encode for proteins that are respectively 389 and 390 amino acids long, share 73% amino acid identity, and display high homology to a bacterial class of iron containing alcohol dehydrogenase (which varied greatly from the extensively studied eukaryotic zinc dehydrogenases) (Yokoyama et al. 1990). In addition, they discovered that although the genes were arranged in tandem, they did not form an operon and were in fact individually regulated, contrary to previously believed (Walter, Bennett, and Papoutsakis 1992).

Characterization of these two butanol dehydrogenase isoenzymes revealed that BdhA has a two-fold greater activity in reducing butyraldehyde than acetaldehyde, yet BhdB is 46-fold more active with butyraldehyde than BdhA (Petersen et al. 1991). Similar to the two aldehyde/alcohol dehydrogenases AdhE1 and AdhE2, BdhA and BdhB also displayed different dependency for the cofactors NADH and NADPH, with BdhA using NADPH, and BdhB using NADH exclusively (Walter, Bennett, and Papoutsakis 1992). Thus, it is believed that of the butanol dehydrogenases, BdhB is primarily responsible for the reductive conversion of *n*-butanal to *n*-butanol at high levels under steady state conditions (Walter, Bennett, and Papoutsakis 1992).

Results from enzyme activity studies suggest, based on activities and cofactor preferences that the most efficient pathway for *C. acetobutylicum* to convert *n*-butyrate to *n*-butanol would be by expression of CtfA/B-AdhE2-BdhB as illustrated in **Fig. 2.3**. Surprisingly, this is not the route taken.

2.2.4 Transcriptional regulation of solventogenesis

In 2001, the complete genome sequence for *Clostridium acetobutylicum* ATCC 824 was released. While many of the genes and gene products pertinent to the metabolic activities of this strain had already been characterized, the complete genome provided an improved overall view

of how these networks fit together, are regulated, and facilitated deeper understanding of global responses during acedogenic to solventogenic transitions *via* whole genome transcriptomic studies.

Two studies (Alsaker and Papoutsakis 2005, Janssen et al. 2010) focused on the acedogenic to solventogenic transition and characterized the change in global transcript levels during this metabolic shift. Results from these studies pertaining to solventogenic and acedogenic pathway genes are highlighted in **Fig. 2.5**. Upon the transition from acedogenesis to solventogenesis, the enzymes involved with glucose fermentation (*thl*:thiolase, *hbd*:β-hydroxybuytyryl-CoA dehydrogenase, *crt*:crotonase and *bcd*:butyryl-CoA dehydrogenase along with its associated *etfA*/*B*:electron-transfer flavoprotein, and *pdc*:pyruvate decarboxylase) are strongly down regulated as expected. In addition, phosphotransbutyrylase (*ptb*) and *n*-butyrate kinase (*buk*), believed to be involved in converting butyryl-CoA to *n*-butyrate, were also found to be down regulated in both studies, although not as significantly in Alsaker et al. 2005. The strong up regulation of the acetoacetate decarboxylase (*adc*) and butyryl-CoA:Acetyl-CoA CoA tranferase (*ctfA*/B) during solventogenesis further suggests that CoA transfer is the primary activating pathway from *n*-butyrate to butyryl-CoA.

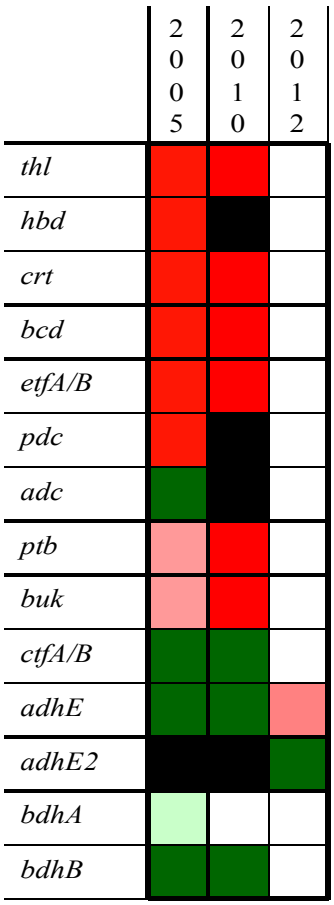

Figure 2.5. Heat map of transcriptional changes in *C. acetobutylicum* when undergoing acedogenic to solventogenic transition. Colors indicate increase (green), decrease (red), no change (white) or intermediate values (spectrum) between acedogenic and solventogenic conditions.

As expected, expression of both butanol dehydrogenase genes are up regulated, however, results indicate that only *bdhB* is expressed at high levels during solventogenesis with slight expression of *bdhA* at steady state. A higher resolution time series of the alcohol dehydrogenases revealed that *bdhA* is induced before *bdhB* during solvent production, and was associated only with low levels of *n*-butanol production in high-density cultures, while *bdhB* is expressed with the onset of high production rates of *n*-butanol (Sauer and Durre 1995).

The most surprising finding is that *adhE2* was not transcribed in either of these studies, suggesting that it is not involved in *n*-butanol production although it was found to have much

higher activity than AdhE1. However, a 2012 transcriptomic study by Hönicke et al. on a strain of *C. acetobutylicum* with an increased ratio of *n*-butanol:acetone is presented in the final column of **Fig. 2.5** where the addition of the artificial electron carrier methyl viologen to a culture of *C. acetobutylicum* was found increase its *n*-butanol:acetone ratio from 1.4 to 16.5. Transcriptomic studies looking for the metabolic rearrangement that facilitated this dramatic change in products found that the only effect on central metabolism genes of *C. acetobutylicum* was the induction of *adhE2* and repression of *adhE1* (Honicke et al. 2012). Although studies on the solventogenic ability of *C. acetobutylicum* have given great insight into the metabolism of *n*-butanol production, they have also highlighted the pitfalls associated with clostridial fermentations.

Production of *n*-butanol with Clostridia has a number of disadvantages including slow growth, strict intolerance to oxygen, dependence on sugars for fermentation, a close link between solvent formation and sporulation (Harris, Welker, and Papoutsakis 2002), difficulty controlling fermentation (Chauvatcharin et al. 1998), and degeneration of solventogenic ability (Cornillot et al. 1997). While one branch of research has focused on altering the wild type solvent producing *Clostridia* strains through genetic manipulation, others have taken an alternate route and attempted expression of the solventogenic pathway in advantageous heterologous hosts.

2.3 Engineering heterologous hosts with the n*-butanol production pathway*

Reconstructing the *C. acetobutylicum* ATCC 824 *n*-butanol fermentation pathway has been previously achieved in *E. coli* (Inui et al. 2008). The workhorse organism of choice, *E. coli* is one of the best-characterized organisms and comes with a large repertoire of genetic tools. *E. coli* is capable of rapid growth by fermentation, whereby large pools of NADH and acetyl-CoA

are produced, similar to the cellular conditions inside *C. acetobutylicum* at the onset of solventogenesis. Thus, the drive to regenerate oxidized cellular cofactors and high concentrations of precursors would likely aid in facilitating high flux production of *n*-butanol in *E. coli*. In addition, the *C. acetobutylicum n*-butyrate formation pathway had previously been expressed and demonstrated to be functional in *E. coli* (Boynton, Bennett, and Rudolph 1996). Because of this, *E. coli* presents itself as an advantageous candidate for producing *n*-butanol.

In a study by Inui et al. (2008), all *C. acetobutylicum* genes for converting acetyl-CoA to butyryl-CoA by the subsequent activities of thiolase, β-hydroxybutyryl-CoA dehydrogenase, crotonase, and 3-hydroxybutyryl-CoA dehydrogenase, as outlined previously (**Fig. 2.2**), were expressed under control of a constitutive promoter within *E. coli*. To reduce butyryl-CoA to *n*-butanol, both isoforms of the aldehyde/alcohol dehydrogenases (AdhE1 and AdhE2) were attempted individually. Following aerobic growth, the two synthetic *E. coli* strains were collected and resuspended in anaerobic medium to an OD_{660} value of 20 where they were allowed to incubate and ultimately produced 0.3 and 1.19 g/L of *n*-butanol from 40 g/L glucose for the two isoenzymes, respectively (Inui et al. 2008). Introduction of *bdhA* or *bdhB* was not attempted and all alcohol dehydrogenase activity was either provided by AdhE1, AdhE2, or any active endogenous *E. coli* alcohol dehydrogenases.

While the results from this study demonstrate that the *C. acetobutylicum n*-butanol forming genes could be functionally expressed in *E. coli* and that AdhE2 produced *n*-butanol *in vivo* at 4 fold higher levels compared to AdhE1, low productivities and the dependence on glucose as a substrate limit the applicability of this approach. Recent studies have built on these findings and drastically improved the yield of *n*-butanol production from clostridial based metabolic pathways inside *E. coli,* reaching yields of 4.66 g/L (Bond-Watts, Bellerose, and

Chang 2011) and 15 g/L (Shen et al. 2011) by knocking out pathways that compete for NADH and acetyl-CoA and selecting alternate isoenzymes that support higher flux through the *n*-butanol pathway. Although these approaches address a number of the limitations imposed by *Clostridia*, namely fermentation of *n*-butanol by a fast growing, easily controlled, oxygen tolerant organism with a fully developed genetic molecular system, they still remain dependent on the fermentation of glucose for production for *n*-butanol.

2.4 Electrochemically active bacteria

The electrochemical activity of *R. palustris* was first reported in 2007. The study focused on improving its electricigenic ability for power production from a pure-culture microbial fuel cell (Morishima et al. 2007). Since then, a handful of studies on other strains of *R. palustris* have supported the hypothesis that this ability may be present throughout the *R. palustris* species (Inglesby, Beatty, and Fisher 2012, Xing et al. 2008). These studies have focused solely on the application of electric current production in a microbial fuel cell and fundamental studies on the mechanism of conversion of organic substrates into electricity has received less attention. However, numerous other organisms have been extensively studied for their ability to convert organic substrates into electrical current. A majority of these well-characterized organisms belong to a group known as the dissimilatory metal reducing bacteria.

2.4.1 Dissimilatory metal reducing bacteria

Microbial metabolism continues to demonstrate an ever-expanding range of reactions to yield harnessable energy, regardless of the accompanying logistical complexity. While aerobic respiration and fermentation of organics are widely used in many environments, alternate

pathways in specialist organisms have adapted to derive energy from organic substrates under even more restrictive conditions. One major restriction in microbial metabolism is the use of substrates with poor solubility or substrates that are difficult to internalize.

Most bacteria require internalization (into the cytoplasm or periplasm) of a substrate before their cellular machinery can metabolize it. However, internalization presents a limitation that restricts metabolism to soluble electron acceptors and donors, and thus confines the breadth of potential metabolic forms. The discovery that insoluble metal oxides, such as Fe_2O_3 and MnO_2, are capable of being solubilized and liberated as Fe(II) and Mn(II) linked directly to microbial respiration was reported in 1988 (Myers and Nealson 1988, Lovley and Phillips 1988) and enlightened us to a novel form of metabolism. This ability has since been found present in a phylogenetically diverse group of bacteria with extracellular electron transfer capabilities, collectively referred to as the dissimilatory metal reducing bacteria (DMRB). These bacteria are capable of translocating metabolic electrons to a terminal electron acceptor outside of the cell. Beyond this novel method of respiration, these organisms possess ecological implications as they integrate the carbon cycle with the iron cycle and are responsible for liberating free Fe(II), which is a growth limiting nutrient in many environments (Behrenfeld and Kolber 1999, Jickells et al. 2005).

In addition to the respiration of solid iron and manganese, some DMRB have been identified to have an activity towards a number of other oxides including uranium, selenium, technetium, chromium, arsenic, and vanadium (Lovley 1991, Turick, Apel, and Carmiol 1996, Lloyd et al. 2000, Carpentier et al. 2003, Stolz et al. 2006), many of which are of environmental concern. This is primarily because, unlike iron and manganese, these oxides are soluble and travel freely through the aquifer, while their reduced counterparts are insoluble. Thus, respiration

of these compounds and precipitation of their reduced form helps prevent proliferation of site contamination and DMRB have been largely praised for their potential in bioremediation applications (Shelobolina et al. 2008, Turick, Apel, and Carmiol 1996, Stolz et al. 2006). While these oxides are soluble, and thus could physically be reduced in an intracellular mechanism, the highly insoluble products generated by their reduction warrant that the strategies employed by DMRB retain the terminal electron acceptor outside the cell to prevent cytosolic or periplasmic precipitation of the reduced product.

It has been found that the same cellular machinery is often implicated with the reduction of this wide range of substrates (Belchik et al. 2011, Beliaev et al. 2001, Sani, Peyton, and Dohnalkova 2008). The promiscuity of substrate specificity lends itself well to not only the organism, as they can utilize a wide range of electron acceptors without the need for major cellular reorganization, but also to the field of electrochemistry as the non-selective nature of their respiration is capable of coupling their metabolism to an solid-state electrode.

2.4.2 Microbial electrochemistry

With the integration of microbial metabolism and an electrochemical system, the field of microbial electrochemistry (ME) was conceived. Contained within the field of bioelectrochemistry, which encompasses all biologically oriented electrochemical systems, such as enzyme functionalized electrodes, ME focuses specifically on the metabolic interactions of living bacteria with electrochemical systems. This is accomplished by directing electrons between organisms and an electrode (in either direction) of an electrochemical cell.

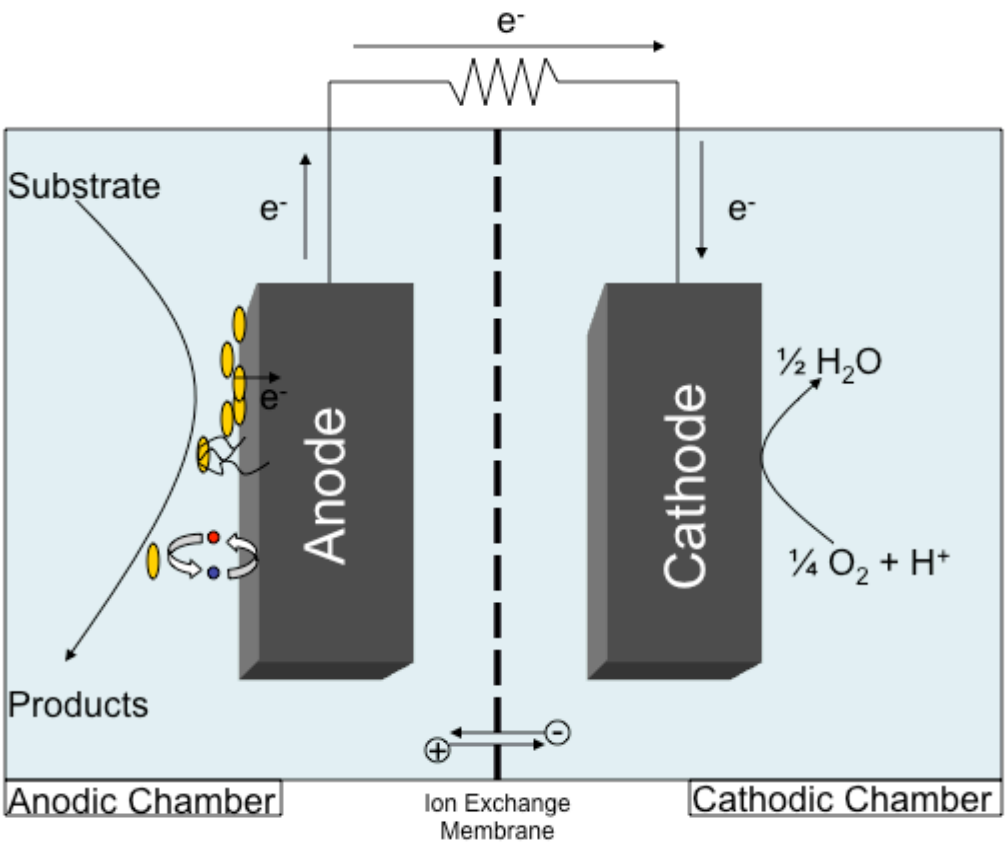

Figure 2.6. Schematic of a basic microbial fuel cell.

Electron flow is driven by the difference in redox potential between two electrodes. **Figure 2.6** is a schematic of a basic microbial fuel cell with an anaerobic anode and an aerobic cathode separated by an ion-permeable membrane. Many studies focused on the production of microbially derived electricity from organics have been conducted and continue to be the predominant form of applied research in this field (He, Minteer, and Angenent 2005, Fornero, Rosenbaum, and Angenent 2010, Yi et al. 2009, Pham et al. 2008, Rabaey et al. 2003), while monitoring microbial interactions in pure and mixed cultures with an electrochemical device has been the primary focus of fundamental research (Rosenbaum et al. 2012, Venkataraman et al. 2011, Venkataraman et al. 2010, Baron et al. 2009, Marsili et al. 2008). These efforts have resulted in the identification of a number of electrochemically active bacteria, including

Geobacter sulfurreducens, Shewanella oneidensis, and *Rhodopseudomonas palustris*. In this sense, electrochemical devices are invaluable tools for understanding wild type and manipulated microbial metabolisms as perturbations can be monitored directly as a function of electrochemical behavior. One of the most intriguing questions that has been answered with the aid of ME studies pertains to the mechanism of microbial extracellular respiration.

2.4.3 Mechanism of Microbial Electrochemistry

Due to the inherent challenges bacteria overcome to achieve extracellular respiration (*i.e.*, transporting electrons across the periplasmic gap, through the outer membrane, and to a substrate), elucidating mechanisms for extracellular electron transport to an electrode has been a central focus in the field of ME.

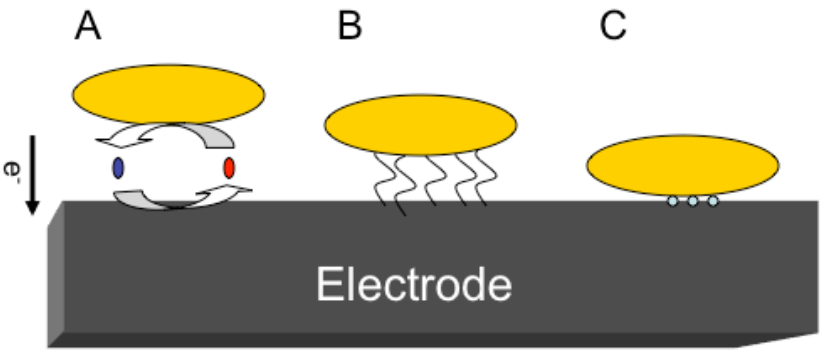

Figure 2.7. Extracellular electron transfer mechanisms: A) Mediated electron transfer allows "electron shuttling" between cell and solid-state acceptors at a distance. Cells release reduced shuttles (blue) that donate electrons to the substrate and return to the cell in the oxidized form (red). B) Direct electron transfer *via* conductive biopolymers ("nanowires") allow transfer of electrons over large distances. C) Direct electron transfer from cell surface cytochromes.

Three primary mechanisms have been proposed (**Fig. 2.7**). These three mechanisms were determined based on studies of two model organisms: *Geobacter sulfurreducens* PCA and *Shewanella oneidensis* MR-1 (Baron et al. 2009, Gorby et al. 2006, Reguera et al. 2005, Torres

et al. 2010). Mechanism A describes a c-type cytochrome mediated direct electron transfer. This mechanism requires that the cell be in direct contact with the electrode, which is reduced directly by contact with decaheme outer membrane cytochromes (Nevin and Lovley 2000). Both *G. sulfurreducens* and *S. oneidensis* have many decaheme c-type cytochromes, a number of which are predicted to be expressed at the outer membrane and have been demonstrated to be responsible for extracellular respiration (Rosenbaum et al. 2012). Mechanism B, similar to A, involves physical contact with the electrode, however, unlike A this contact is mediated through the extension of conductive biopolymers or "nanowires". These polymers are often associated with outer membrane cytochromes and are believed to be capable of transporting electrons to substrates over (relatively) long distances (Leang et al. 2010). Unlike mechanisms A and B, mechanism C does not require direct contact with the electrode and facilitates extracellular respiration by the shuttling of a reversibly oxidized mediator between the organism and electrode (Marsili et al. 2008). Without the restrictions imposed by direct electron transfer, organisms using redox mediators in ME systems are capable of growing planktonically, while those organisms that only use direct methods for extracellular respiration are confined to growth on the electrode in a biofilm. While both *G. sulfurreducens* PCA and *S. oneidensis* MR-1 are capable of mechanisms A and B, *S. oneidensis* MR-1 also performs mediated electron transfer *via* electron shuttles (riboflavin and flavin mononucleotide), and thus provides a more encompassing model organism for the study of extracellular electron transfer (Marsili et al. 2008). In addition, as the *S. oneidensis* mechanism of extracellular electron transfer has been the most extensively characterized, it will be the primary focus of this review.

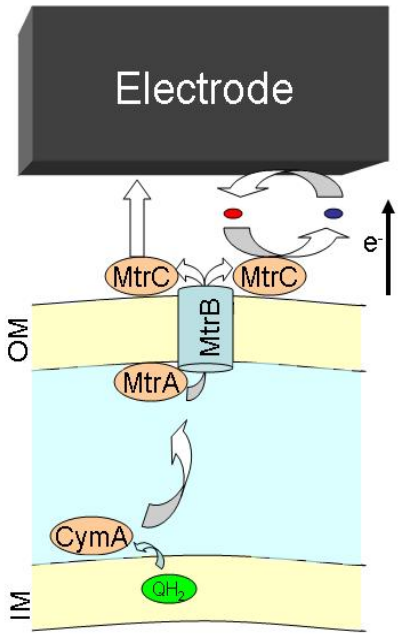

Figure 2.8. Metal reducing pathway mechanism for extracellular electron reduction by *S. oneidensis*

The *S. oneidensis* MR-1 metal reduction (Mtr) pathway is comprised of a proteinaceious conduit that facilitates the transfer of electrons from the quinol pool in the inner membrane to the outer leaf of the outer membrane (**Fig. 2.8**). The conduit is composed of three essential proteins: MtrA, MtrB, and MtrC. The structure of the *S. oneidensis* extracellular electron transport has been found amenable to investigation as these three components have proven necessary and sufficient to facilitate electron transfer across the outer membrane in both *S. oneidensis* as well as in abiotic liposomes and *E. coli* (Hartshorne et al. 2009, Jensen et al. 2010). While portions of the mechanism for electron transport remain unclear, it is understood that electrons for this process originate from the inner membrane menaquinol pool, where they are then transferred to an inner membrane associated tetraheme cytochrome, CymA (Myers and Myers 2000). Soluble periplasmic electron carriers or protein-protein bridges are predicted to shuttle these electrons to the outer membrane associated decaheme cytochrome (MtrA) (Ross et al. 2007). At the outer

membrane, MtrA forms a complex with MtrB, which is a beta-barrel transmembrane protein. MtrB is predicted to contain 28 transmembrane β-strands, making it one of the largest known outer membrane porins (Schulz 2002, Koebnik, Locher, and Van Gelder 2000) with a diameter predicted to be larger than 35 Å (Schulz 2002). MtrC, which is an outer membrane decaheme cytochrome, resides on the outer membrane exterior surface (Lower et al. 2009) at the extracellular face of MtrB and has been found responsible for catalyzing the reduction of metal oxides and riboflavin directly (Beliaev et al. 2001, Hartshorne et al. 2007).

Reconstitution experiments with *Shewanella* mutants lacking different components have found that in the absence of either MtrA or MtrB, neither of the other components localizes to the outer membrane and ability to reduce metals was abolished (Hartshorne et al. 2009). However, in the absence of MtrC, the MtrAB still forms a tight complex in the outer membrane (Hartshorne et al. 2009). The MtrAB containing mutant still possesses slight electrochemical activity due to the presence of less active outer membrane cytochromes, including OmcA (Meitl et al. 2009). These results indicate two modular forms to the *S. oneidensis* electron conduit, the MtrAB structure to facilitate electron flow through the outer membrane and MtrC for ultimate reduction of the terminal substrate. The last step in the Mtr electron transport in which electrons are transferred from MtrA to MtrC still remains largely uncertain. Based on high affinity protein-protein interactions between MtrA and MtrC it is believed, although still speculative, that MtrA and MtrC partially enter the pore of MtrB and come close enough to each other to facilitate electron transfer between their network of heme groups (Hartshorne et al. 2009).

2.4.4 *Potential Activity of Mtr Outside of* Shewanella

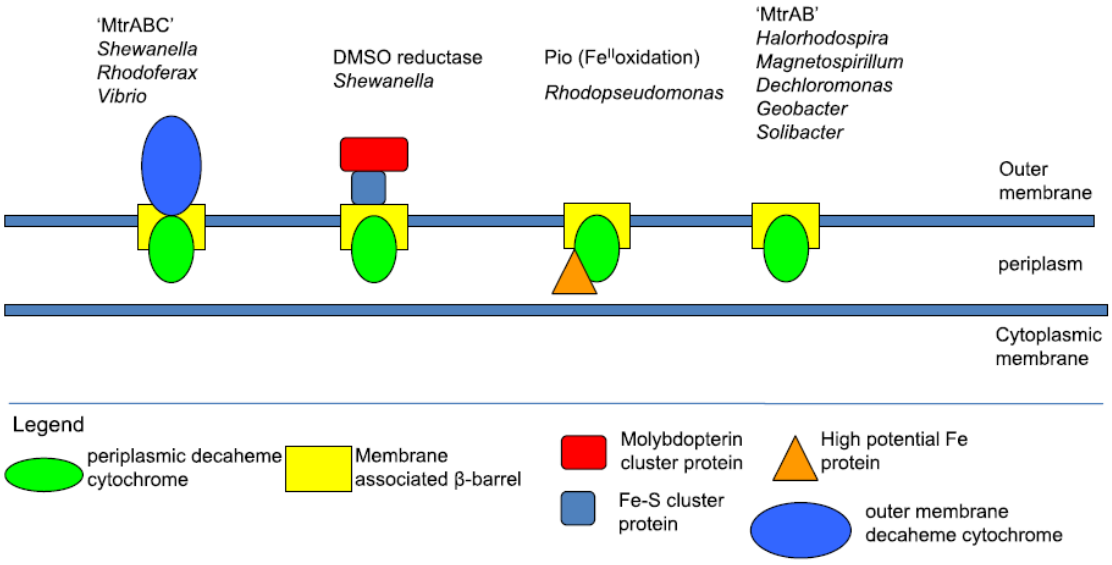

Figure 2.9. Homologous structures to the *S. oneidensis* Mtr complex, including the Pio machinery of *R. palustris*. This figure was taken from Hartshorne et al. 2009.

Homologs of the Mtr pathway have been found in a wide range of known electrochemically active bacteria including *Geobacter sp.* and *R. palustris*, as well as in organisms that are not yet known to be electrochemically active (**Fig. 2.9**). The homolog in *R. palustris* comprises the phototrophic iron oxidation (*pio*) operon and has been found to be functionally responsible for oxidizing Fe(II) when growing photoautotrophically (Jiao and Newman 2007). Similar to Mtr, the *pio* operon encodes PioA, which is a periplasmic c-type cytochrome, PioB, which is a putative outer membrane beta-barrel protein, and PioC, which is a putative high potential iron sulfur protein, of which the first two demonstrate high homology to MtrA and MtrB, respectively. As expected, all the components are marked for secretion into the periplasm by either the general secretory pathway (PioA and PioB) or the twin arginine transport pathway (PioC). Deletion of any of the *pio* pathway components resulted in decreased or abolished ability to grow on Fe(II).

Recently, it was found that the Mtr pathway is capable of functioning in reverse, allowing internalization of electrons derived from solid external sources (Ross et al. 2011). This finding demonstrates a potential route that could be utilized to study the largely uncharacterized process of microbial electrosynthesis.

2.4.5 Microbial electrosynthesis

Microbial electrosynthesis, which is the production of reduced compounds from CO_2 by microbial metabolism supported by an electric current, is nascent in the field of microbial electrochemistry. Driving microbial metabolism with electricity in an electrochemical system may seem counterintuitive at first since historically ME has focused on deriving electricity from organics. However, the ability to convert electricity to defined reduced forms of carbon is an attractive solution to the problem of how to store renewably produced electricity. In addition, because the catalyst is a microorganism, all advantages associated with ME, such as generation of a (relatively cheap) biocatalyst with high substrate specificity, apply.

While numerous publications describe the theory and potential application of this direct renewable energy to chemical conversion (Rosenbaum et al. 2011, Rabaey, Girguis, and Nielsen 2011, Rabaey and Rozendal 2010, Lovley , Ross et al. 2011), to date only three strategies have described the metabolic production of organic compounds (*i.e.*, acetate, 2-oxobutyrate, and methane from electricity (Nevin et al. 2011, Nevin et al. 2010, Cheng et al. 2009)). Electrosynthetic organisms have, thus far, all been fermenters using unknown mechanisms, and all energy for metabolism was provided *via* a strong reducing potential applied (-0.4 V *vs.* standard hydrogen electrode (SHE)). This approach has two potential drawbacks. First, it has not yet been confirmed that there is a cellular mechanism that generates metabolic energy from

externally supplied electrical current to sustain microbial growth. The achieved product concentrations are low (sub-millimolar) and cells had to be grown in the system with H_2 to an appreciable biomass density before the transition to electrosynthesis could be made. These results suggest that severe thermodynamic or metabolic limitations exist in the electrosynthetic operation of these organisms.

Second, supplying electrons at increasingly negative potentials requires increased input of electrical energy. Driving the transfer of electrons from H_2O (0.816 V *vs*. SHE) to -0.4 V *vs*. SHE to produce 1 mmol of acetate from *S. ovata* requires a minimal energy input of 486 joules (disregarding over potentials that may be present). The standard reduction potential for Acetate/CO_2 however is only -0.29 V *vs*. SHE (Thauer, Jungermann, and Decker 1977) and requires an input of 442 joules, resulting in a 9% energetic efficiency loss by *S. ovata* electrosynthesis. These inefficiencies demonstrated by current electrosynthetic approaches could be overcome by an organism capable of accepting electrons from a more positive potential at the cathode.

One route to reducing the potential that must be applied at the cathode is by utilizing the known mechanism of mediated iron transfer. Various iron species exist and many of these have a wide range of redox values, from +0.1 to -0.3 V *vs*. SHE (Bird, Bonnefoy, and Newman 2011). Because of this, it is possible to supply electrons derived from the electrode to bacteria mediated by reversible cycling of iron. This was demonstrated in pure culture with an obligate Fe(II) chemolithotroph, *Mariprofundus ferrooxydans* PV-1, under aerobic conditions at a potential of -0.07 V *vs*. SHE (Summers, Gralnick, and Bond 2013), and recently with *R. palustris* under anaerobic conditions in the light at a potential of +0.1 V *vs*. SHE (Bose et al. 2014). This route of

providing electrons to microbes at much higher potentials than previously described could be advantageous for future microbial electrosynthesis efforts.

2.5 Conclusion

The central metabolism of *Rhodopseudomonas palustris* growing photoheterotrophically produces an inherent redox imbalance. The introduction of a pathway to divert these reducing equivalents into an alternate carbon sink could harness reducing equivalents to produce reduced carbon compounds of interest, such as *n*-butanol. In addition, further characterizing of how *R. palustris* manages these excess reducing equivalents when oxidizing molecules relevant to renewable energy, such as lignin derivatives, could provide insights into future energy technologies. Further, *R. palustris* could function to consume electrons from an electrode at potentials close to 0 V *vs*. SHE for applications related to microbial electrosynthesis.

CHAPTER 3

METABOLIC ENGINEERING OF *RHODOPSEUDOMONAS PALUSTRIS* FOR THE OBLIGATE REDUCTION OF *N*-BUTYRATE TO *N*-BUTANOL

Adapted from: Devin F. R. Doud, Eric C. Holmes, Hanno Richter, Georg Jander, and Largus T. Angenent. In preparation for *Metabolic Engineering*.

3.1 Abstract

The innate redox imbalance of *Rhodopseudomonas palustris* that can occur while growing photoheterotrophically has inspired interest in the ability to harness this metabolism for production of bioenergy in the form of H_2. However, these excess reducing equivalents and ATP from photosynthesis could be used to drive more advantageous reactions as an obligate cellular activity. Harnessing the photoheterotrophic metabolism of *R. palustris* to provide reducing equivalents and energy for the metabolically engineered production of *n*-butanol from *n*-butyrate is a potential strategy that could be taken as an alternate pathway for maintaining redox balance in *R. palustris*. Here, modeled after the well-characterized *n*-butyrate to *n*-butanol reduction pathway from *Clostridium acetobutylicum* ATCC 824, a homologous pathway for *n*-butanol production was constructed and expressed in *R. palustris*. Because this pathway functions as the sole route to reoxidizing excess reducing equivalents under anaerobic conditions with no alternate electron sinks, the engineered production of *n*-butanol functions as an obligate metabolism for growth. To date, we have achieved 0.6 mM *n*-butanol production with 40% carbon conversion efficiency.

3.2 Introduction

Rhodopseudomonas palustris, which is a member of the purple non-sulfur bacteria (PNSB) group, is often noted for its metabolic versatility. Of the many metabolic activities *R. palustris* demonstrates, H_2 production by photofermentation – the utilization of organic carbon under anaerobic conditions with light - has become a central focus for bioenergy production from *R. palustris* (McKinlay and Harwood 2010). The unique ability to produce H_2 at high levels may be due to two attributes: i. an excess of reducing equivalents that accumulate during photoheterotrophic growth (Hillmer and Gest 1977); and ii. expression of a vanadium-dependent nitrogenase (Oda et al. 2005), which has been found to form H_2 at levels 3x higher than the molybdenum-dependent nitrogenases that are known to exist in the rest of the PNSB (Eady 1996). This inherent requirement to eliminate excess reducing equivalents, and the metabolic routes by which *R. palustris* accomplishes this, have only recently been elucidated.

When growing on acetate, McKinlay and Harwood (2010) found that only approximately half of all reducing equivalents that were generated from acetate were being used for biosynthesis and that the other half of reducing equivalents derived from acetate required obligate reoxidation by some alternate metabolic strategy such as CO_2 fixation, H_2 evolution, or a combination of both. These two pathways were found to be complimentary in this role, and when one route was made unavailable, the other facilitated the reoxidation of all reducing equivalents with minimal changes occurring elsewhere in the central metabolism. However, when fed a more reduced substrate, such as *n*-butyrate (hereafter butyrate), it was observed that under non-H_2 evolving conditions, *R. palustris* could only grow if exogenous CO_2 was supplemented into the medium (McKinlay and Harwood 2011, Hillmer and Gest 1977). This finding demonstrates that under these conditions *R. palustris* generates more reducing equivalents than available electron

sinks can accommodate and ultimately suffers a lethal redox imbalance. Numerous studies have investigated methods for improving H_2 yields from photofermentations using *R. palustris* (Barbosa et al. 2001, Gosse et al. 2007, Chen et al. 2008), many of which used principles discussed above to improve native metabolic fluxes to H_2, but diverting this flow of electrons into alternate fuel forms has not yet been attempted. One attractive route to redirect these reducing equivalents is into the production of the biofuel *n*-butanol (herafter butanol) through a reduction reaction.

Butanol is traditionally produced *via* fermentation of monosaccharides by certain strains of clostridia. *Clostridium acetobutylicum* ATCC 824, which has widely been studied for this activity, is generally seen as the model organism for solvent production and has been used as a source of genes for engineered butanol production previously (Nolling et al. 2001, Inui et al. 2008, Atsumi et al. 2008). In *C. acetobutylicum*, reduction of butyrate proceeds through a two-phase pathway with: i) activation of butyrate to butyryl-CoA; and ii) reduction to butanol through the butyraldehyde intermediate (Desai et al. 1999, Sillers, A-Hinai, and Papoutsakis 2009). This strategy includes two alternative routes in the pathway for generating butyryl-CoA from butyrate. Activation of butyrate proceeds either through a two-step butyrate kinase/phosphotransbutyrylase reaction or a one-step rection with butyrate/acetoacetyl-CoA transferase, which transfers a -CoA group from acetoacetyl-CoA to butyrate. In the reduction phase of the butanol pathway, the AdhE2 enzyme (hereafter 824 AdhE2) reduces butyryl-CoA to butyraldehyde and subsequently butanol (Durre et al. 1995). Analysis of 824 AdhE2 has revealed that the protein is a bifunctional NADH dependent fusion protein with the N terminal domain retaining highly conserved sequences of the aldehyde dehydrogenase family, while the C terminal domain of 824 AdhE2 retains the iron-containing alcohol dehydrogenase family (Nair,

Bennett, and Papoutsakis 1994). A second alcohol dehydrogenase enzyme (*i.e.*, BdhB) has also been found to aid in the reduction of butyraldehyde to butanol, though its activity is not necessary (Fontaine et al. 2002).

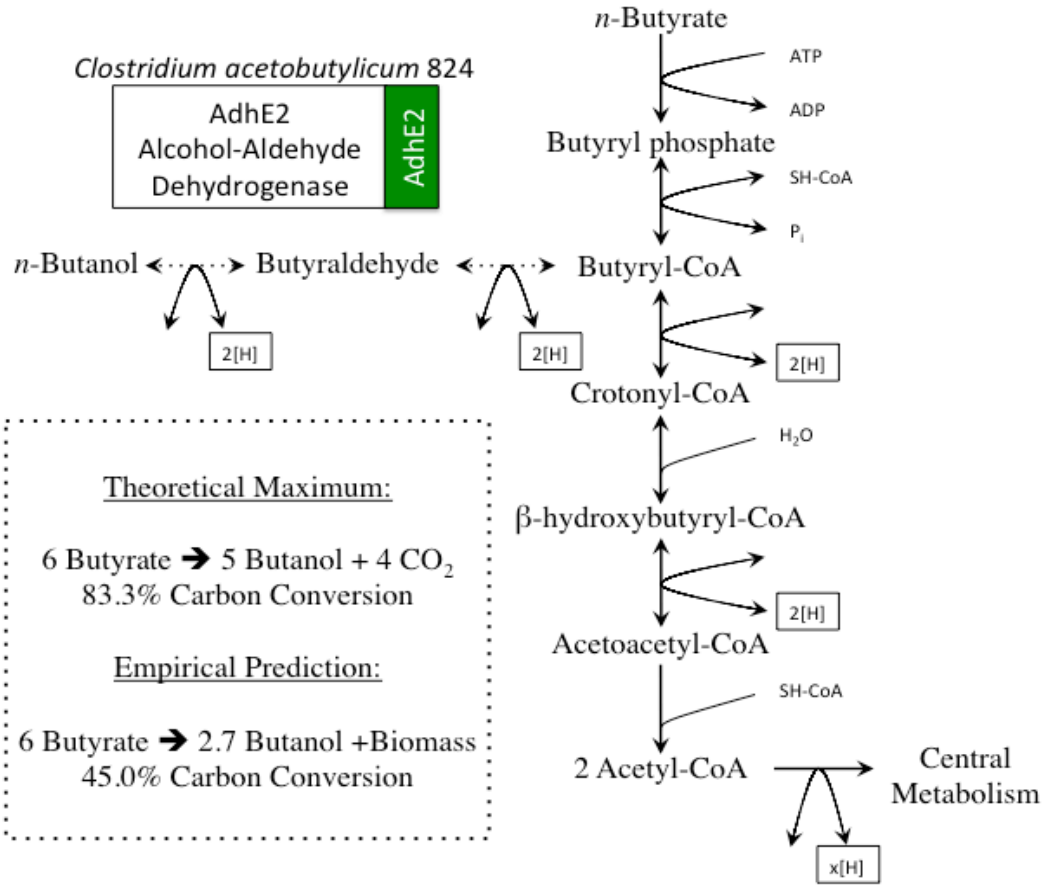

Figure 3.1. Butyrate metabolism and proposed route for butanol production in *R. palustris* by the activity of the 824 AdhE2 enzyme. Theoretical butanol production based upon all electrons derived from complete oxidation of one molecule of butyrate reducing 5 molecules of butyrate to butanol. Empirical prediction based upon measured excess reducing equivalents of *R. palustris* growing with butyrate by McKinlay et al. (2011).

Comparing the clostridial conversion pathway to the known mechanism for catabolism of butyrate by *R. palustris*, it is observed that before butyrate can be converted to 2 molecules of acetyl-coA by anaerobic β-oxidation, butyryl-CoA is first formed through native butyrate

kinase/phosphotransbutyrylase enzymes (**Fig. 3.1**). However, under the conditions of photoheterotrophic redox imbalance, the first oxidation reaction for the metabolism of butyrate, butyryl-CoA to crotonyl-CoA, would likely be inhibited by the thermodynamic limitations of the reduced cofactor pool. Because of this, the butyryl-CoA intermediate would be expected to accumulate and would provide an ideal target for shunting excess reducing equivalents onto for the production of butanol. Engineered butanol synthesis in *R. palustris* could, therefore, be achieved with the introduction of only the *C. acetobutylicum* 824 AdhE2 bifunctional aldehyde/alcohol dehydrogenase. However, due to the major incompatibilities in codon utilization preference between the *C. acetobutylicum* source and the *R. palustris* host, it was found that a direct introduction of the 824 *adhE2* gene did not result in expression of the 824 AdhE2 protein. Here, we demonstrate the successful construction of the butyrate to butanol pathway through codon optimization of the AdhE2 enzyme. This activity restored growth with butyrate in the absence of exogenous CO_2, enabled by shunting butyryl-CoA from its flux into central metabolism towards reoxidizing reduced cell cofactors with the production butanol. In addition, we attempted an alternate route by expressing an enzyme homologous to AdhE2 found in *R. palustris* BisB18, however, no butanol activity was observed.

3.3 Materials and methods

3.3.1 Media and culture conditions

R. palustris CGA009 was routinely cultured in anaerobic butyrate *Rhodospirillaceae* medium (RM) (Lee et al. 2002) consisting of 1.64 g $NaHCO_3$, 0.5 g KH_2PO_4, 0.5 g K_2HPO_4, 0.2 g $MgSO_4$ x 7 H_2O, 0.4 g NaCl, 0.05g $CaCl_2$ x 2 H_2O, 0.01g Fe-Citrate, 1.0 g $(NH_4)_2SO_4$, 1.12 mL 10 M NaOH, and 1 mL trace metals, per L. After autoclaving, 1.0 g sterile butyric acid and 1 ml trace

vitamins were added to the medium. The trace metal solution consisted of 0.25 mL concentrated HCl, 70.0 mg $ZnCl_2$, 100.0 mg $MnCl_2$ x 4 H_2O, 60.0 mg H_3BO_3, 200.0 mg $CoCl_2$ x 6 H_2O, 20.0 mg $CuCl_2$ x 2 H_2O, 20.0 mg $NiCl_2$ x 6 H_2O, and 40.0 mg Na_2MoO_4 x 2 H_2O per liter. The trace vitamin solution consisted of 1.0 g *p*-aminobenzoic acid, 1.0 g thiamine, and 0.1 g biotin per liter. 50 mL of sterile medium with a final pH of 7.0 was added to autoclaved serum bottles and sparged for 20 min with sterile filtered 80:20 N_2/CO_2 gas. For growth of engineered strains under restrictive butyrate to butanol conversion conditions, $NaHCO_3$ was omitted from the medium, the addition of 10 M NaOH was increased to 2.3 mL total, and serum bottles were sparged for 20 min with N_2. In addition, 200 μg/mL of kanamycin sulfate was added for retention of the selective marker in all growth conditions with engineered strains. All serum bottle cultures were grown in an environmental growth chamber (GC8-2VH, EGC, Chagrin Falls, OH) at 30.0°C with 80 μmol of photosynthetically active photons/s/m^2 (photons between 400-700 nm) illumination from both fluorescent and incandescent lamps.

3.3.2 DNA manipulation and cloning

The 824 *adhE2* and BisB18 *adhE* homolog gene were amplified from their respective hosts, *C. acetobutylicum* 824, and *R. palustris* BisB18, using Phusion HF polymerase (New England Biolabs, Ipswich, MA) and directionally ligated into the pBBR1MCS-2 expression vector using the XhoI/XbaI cloning sites. Reverse primers included a 6X His tag prior to termination site for detection by immunoreaction. All primers used are listed in **Table 3.1**. GFPmut2, which was used as a vector based a reporter gene, was inserted into the pBBR1MCS-2 and pMG105P vectors with a range of promoters including the *lac*, *ara,* and the endogenous *ppckA* from *R. palustris*. Restriction and ligation enzymes were purchased from Promega (Fitchburg, WI) and all constructs were verified with Sanger sequencing (Cornell University Genomics Facility).

Escherichia coli DH5α was used for routine cloning of constructs. Both *E. coli* and *R. palustris* were transformed by electroporation with a BioRad GenePulser II Electroporator (Bio-Rad, Hercules, CA) with 1.8kV, 200 Ω, 25 μF for *E. coli*, and 1.8 kV, 400 Ω, 25 uF for *R. palustris*. Electroporated cells were recovered in SOC for 1 and 3 h before plating on lysogeny broth (LB) plates with 50 μg/mL and 200 μg/mL kanamycin sulfate for isolation of individual *E. coli* and *R. palustris* transformants, respectively.

Table 3.1. Sequences of primers used for this study. Restriction sites are underlined.

Primer	Length	Sequence (5' -> 3')	Purpose
pBBR1MCS-2 Vector			
XhoI GFPmut2 F1	60	GGCGGCCTCGAGAGGAGGATCTATTCATGAGTAAAGGAGAAGAACTTTTCACTGGAGTTG	Cloning GFP
XbaI GFPmut2 R1	51	GCCGCCTCTAGACTATTTGTATAGTTCATCCATGCCATGTGTAATCCCAGC	
BamHI RBS 824 AdhE2 F1	68	GCCGCGGATCCAGGAGGATCTATTCATGAAAGTTACAAATCAAAAAGAACTAAAACAAAAGCTAAATG	Cloning 824 *adhE2*
SacI 6X His 824 AdhE2 R1	62	CACCCGGAGCTCTAAGTGGTGATGGTGATGATGAAATGATTTTATATAGATATCCTTAAGTT	
SacI 824 AdhE2 R1	43	CACCCGGAGCTCTAAAATGATTTTATATAGATATCCTTAAGTT	
XhoI RBS BisB18 AdhE F1	57	GACGACCTCGAGAGGAGGATCTATTCGTGACCTTATCTACCCCGTCCGACCTCGACA	Cloning BisB18 *adhE*
XbaI 6X His BisB18 AdhE R1	60	CACCCGTCTAGACTAGTGGTGATGGTGATGATGTTCCGCGGCGTTCGCCGTCGCCACCGA	
XbaI BisB18 AdhE R1	52	CAGTCACCCGTCTAGACTATTCCGCGGCGTTCGCCGTCGCCACCGACAATGT	
pMG105P Vector			
XbaI GFPmut2 F1	60	GGCGGCTCTAGAAGGAGGATCTATTCATGAGTAAAGGAGAAGAACTTTTCACTGGAGTTG	Cloning GFP
SalI GFPmut2 R1	53	GGCGGCCGGTCGACCTATTTGTATAGTTCATCCATGCCATGTGTAATCCCAGC	

3.3.3 Codon optimization of C. acetobutylicum *824 adhE2*

To express the *C. acetobutylicum* 824 AdhE2 enzyme in *R. palustris*, codon optimization was required. Optimization was performed in-house and largely utilized the one amino acid one codon approach, except in cases of multiple codon repeats and unfavorable energetics of mRNA secondary structure (Supplementary information). Synthesis of the gene was performed by GenScript (Piscataway, NJ). The *R. palustris* codon optimized *adhE2* gene (hereafter *adhE2* Opti) was synthesized with flanking XhoI/XbaI restriction sites that were used for directional cloning into pBBR1MCS-2.

3.3.4 Metabolite detection

Butyrate and butanol were detected *via* HPLC (600 HPLC, Waters, Milford, MA) with a refractive index detector and an Aminex HPX-87H column (Bio-Rad, Hercules, CA). The column temperature was set to 60°C, and a 5 mM sulfuric acid eluent at a flow rate of 0.6 mL/min was used as the mobile phase. Butanol and butyraldehyde were detected with a gas chromatograph (HP 5890, Hewlett Packard, Palo Alto, CA) with a 7673 autoinjector and flame ionization detector. The gas chromatograph contained a custom-made packed bed glass column of 1.8m x 2 mm id (Supelco, Sigma-Aldrich, St. Lous, MO). The support matrix of the column was Chromosorb W/AW80 over 100 mesh; phases were preconditioned: phase A was 10% Carbowax-20M; phase B was 0.1% phosphoric acid. The inlet and detector temperatures were 220°C and 240°C. The column temperature profile was 100°C for 2 min, a ramp of 40°C/min to 180°C with a 5 min hold. Concentrations of butanol were verified by both HPLC and GC platforms.

3.3.5 SDS-PAGE and Western blot detection.

For both SDS-PAGE and subsequent western blot detection, 50 mL of late-log *E. coli* and *R. palustris* cells were harvested by centrifugation (10 min, 12,000 x g, 4°C) and resuspended in 1 mL 1X Laemmli buffer (Protocols 2006) with a protease inhibitor (Protease inhibitor cocktail, Promega, Fitchburg, WI). The suspension was sonicated on ice using three 30 s on/1 min off pulses of 20W (Branson Sonifier 150, Emerson, Danbury, CT). After sonication, debris was removed by centrifugation and the total soluble protein concentration was determined by BCA assay (Pierce BCA protein assay kit, Thermo Scientific, Rockford, IL). 45 µl of 3 mg/mL soluble protein samples and 10 µl of Precision Plus Protein™ standard (BioRad, Hercules, CA) were loaded into each lane of a Mini-PROTEAN® TGX gel (BioRad, Hercules, CA) and run at 100V for 1.5 h before blotting onto PVDF membranes at 100 V for 1 h. Immunoreactive bands were developed using manufacturer suggested protocols for One-Hour WesternTM Standard Kit for rabbit (Genscript, Piscataway, NJ) and a 6X His primary antibody (Rabbit polyclonal, GeneTex, Irvine, CA).

3.4 Results

3.4.1 GFP screen of expression vectors in R. palustris *CGA009.*

GFPmut2 (Cormack, Valdivia, and Falkow 1996) was used as a reporter protein to screen for the activity of different expression vectors tested in *R. palustris* under aerobic conditions. Two different plasmids; the endogenously derived pMG105 (Inui et al. 2000), and the broad-host pBBR1MCS-2 (Kovach et al. 1995), were used as expression vectors. Different combinations of vector and promoter sequences were screened for best levels of expression within *R. palustris*.

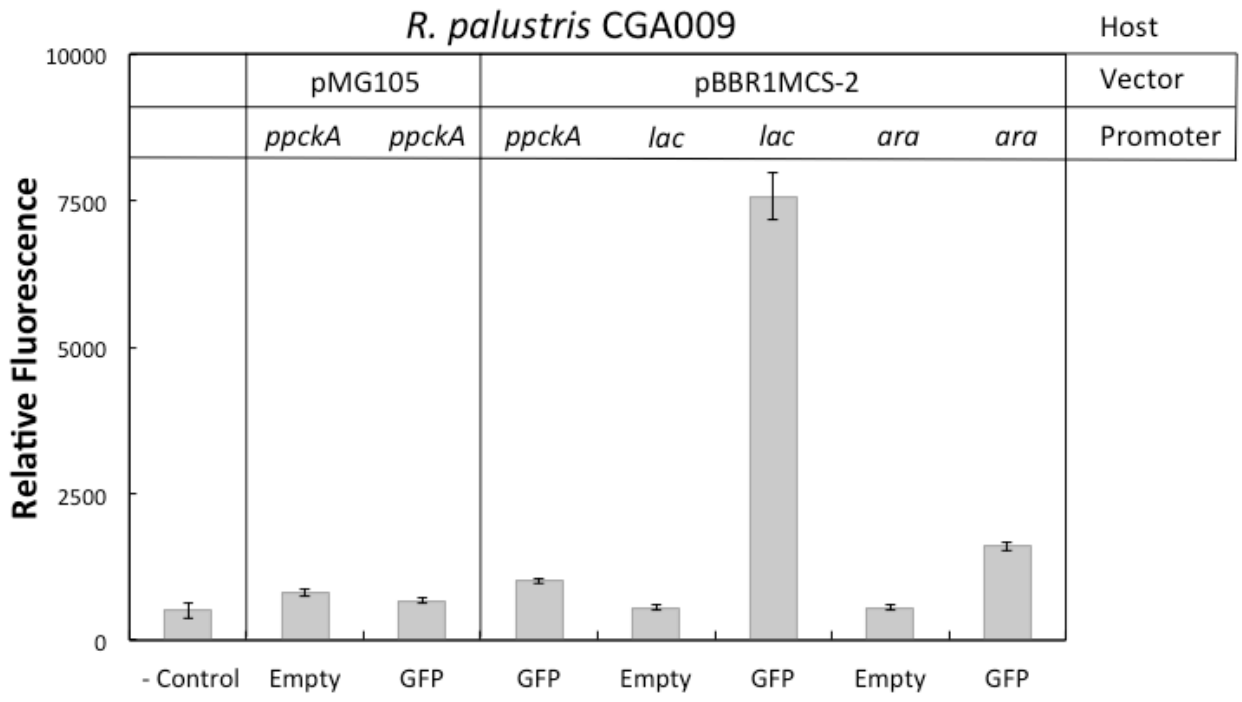

Figure 3.2. Fluorescence screen of potential expression vectors in *R. palustris* CGA009. Fluorescence from each strain is expressed as relative fluorescence per 1 unit of OD_{600}. Technical triplicates with standard deviation are shown. Excitation/emission was measured at 480:510 nm. The control contained no cells. Different empty vector and constructs with GFP are designated by vector/promoter heading.

The endogenous phosphoenolpyruvate carboxykinase (*ppckA*) promoter of *R. palustris* is one of the few promoter sequences that has been previously characterized in *R. palustris* to be active under all gluconeogenic conditions (Inui et al. 1999). However, only a minimal increase in fluorescence was observed for both the pMG10P and pBBR1MCS *ppckA* GFP constructs compared to the empty vector controls (**Fig. 3.2**). While the pBBR1MCS *ara* GFP construct yielded slightly higher levels compared to the *ppckA*, the pBBR1MCS *lac* promoter offered the best expression overall and was selected as the vector for expression in *R. palustris*. Expression from the *lac* promoter in *R. palustris* was not affected by the addition of the inducer IPTG and catabolite repression only showed a minor decrease in fluorescence (**Fig. A1.1**). This suggests

that although *R. palustris* recognizes the lac promoter, the *lac* regulatory response system utilized by *E. coli* (**Fig. A1.2**) is not functional in *R. palustris*.

3.4.2 Engineering the butyryl-CoA to butanol activity in R. palustris.

3.4.2.1 BisB18 AdhE

As determined by the lack of growth under restrictive conditions and lack of a band in a western blot (**Fig. 3.4** lanes 3 and 7), direct introduction of the 824 *adhE2* gene did not result in expression of 824 AdhE2 in *R. palustris*. This is likely due to the large genomic GC discrepancy, 30% *vs*. 65%, and codon utilization preference between *C. acetobutylicum* and *R. palustris,* respectively (Gustafsson, Govindarajan, and Minshull 2004). Because of this, we pursued modifying *R. palustris* by introducing an aldehyde/alcohol dehydrogenase gene homologous to 824 *adhE2* identified in *R. palustris* BisB18.

Endogenous alcohol/aldehyde dehydrogenases in other organisms with homology to 824 AdhE2 have been found to function in the production of butanol from butyrate when expressed in conjunction with the correct pathway. This was previously demonstrated with the *fucO* gene in *E. coli*, where overexpression allowed production of butanol from an engineered reverse β-oxidation pathway where no butanol production was observed previously (Dellomonaco et al. 2011). In an attempt to enable butanol production in *R. palustris*, a BLAST search for an endogenous enzyme yielded the identification of RPC_4481 (hereafter BisB18 AdhE), an aldehyde/alcohol dehydrogenase with high homology to both domains of the *C. acetobutylicum* 824 AdhE2 enzyme in *R. palustris* strain BisB18.

Before utilizing BisB18 AdhE as a candidate butanol pathway protein, *R. palustris* BisB18 was screened for its ability to grow by producing butanol from butyrate under restrictive electron sink conditions (No HCO_3^-). Although no growth or butanol production occurred (data

not shown), it is possible that wild type expression of this protein under these conditions is either inactive or insufficient for an observable effect, similar to previously described with *FucO* in *E. coli* (Dellomonaco et al. 2011). Because no experimental studies have previously characterized the activity of the BisB18 AdhE protein, its highly conserved primary sequence was further investigated for its structural homology to the verified butanol producing 824 AdhE2 protein.

Using Swiss PDBviewer/Deep View (Guex and Peitsch 1997), a three dimensional structure of the individual protein domains for both 824 AdhE and BisB18 AdhE was generated. The predicted tertiary structure of both aldehyde/alcohol dehydrogenases appeared highly conserved with regard to overall shape, location and conservation of active site residues, channel volume and surface charge (**Fig. 3.3**). Because of this, the *R. palustris* BisB18 AdhE was used for the engineered conversion of butyryl-CoA to butanol.

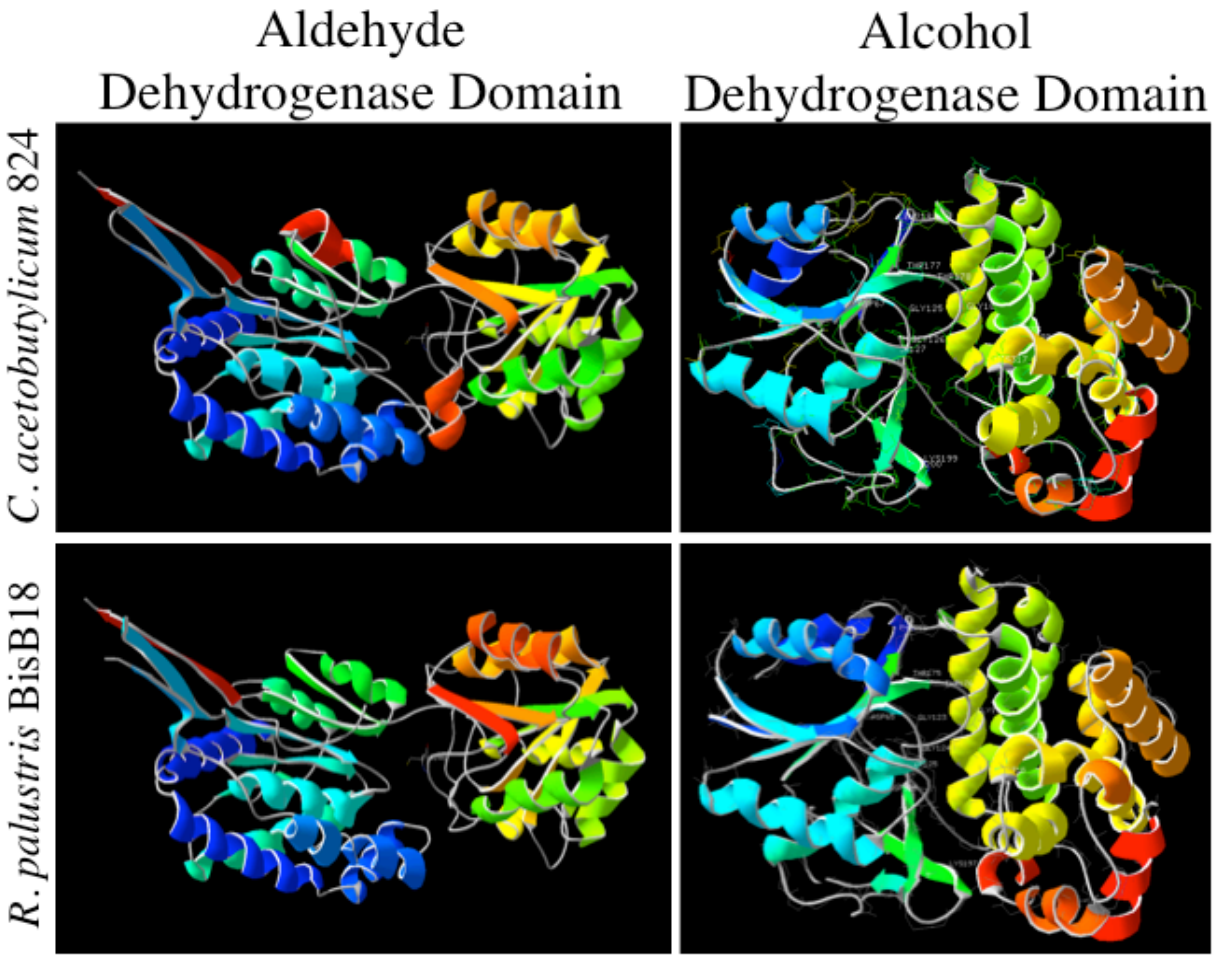

Figure 3.3. Predicted structures of the *C. acetobutylicum* 824 AdhE2 and *R. palustris* BisB18 AdhE individual aldehyde and alcohol domains. Structures were created with Swiss PDBViewer using pdb3m7C (e^{-132} structural similarity) as a scaffold for modeling the alcohol dehydrogenase domain and pdb3zdr (e^{-114} structural similarity) as a scaffold for the alcohol domains.

BisB18 *adhE* was expressed in *R. palustris* using the pBBR1MCS-2 *lac* construct. Transformants were inoculated into both RM butyrate ± HCO_3^- to screen for ability to produce butanol and viability. Although transformants grew up in the +HCO_3^- conditions, no growth was observed under -HCO_3^- conditions, suggesting that either BisB18 AdhE was not successfully expressed or did not have butyryl-CoA to butanol activity. To investigate this further, a crude

cell extract of the +HCO_3^- culture, along with *E. coli* harboring the same construct, was analyzed *via* western blot. However, the presence overlapping photosynthetic pigments (produced under anaerobic conditions) with the expected band for the AdhE protein on the western blot required that expression of the BisB18 AdhE protein be screened under aerobic conditions (**Fig. 3.4** lane 8).

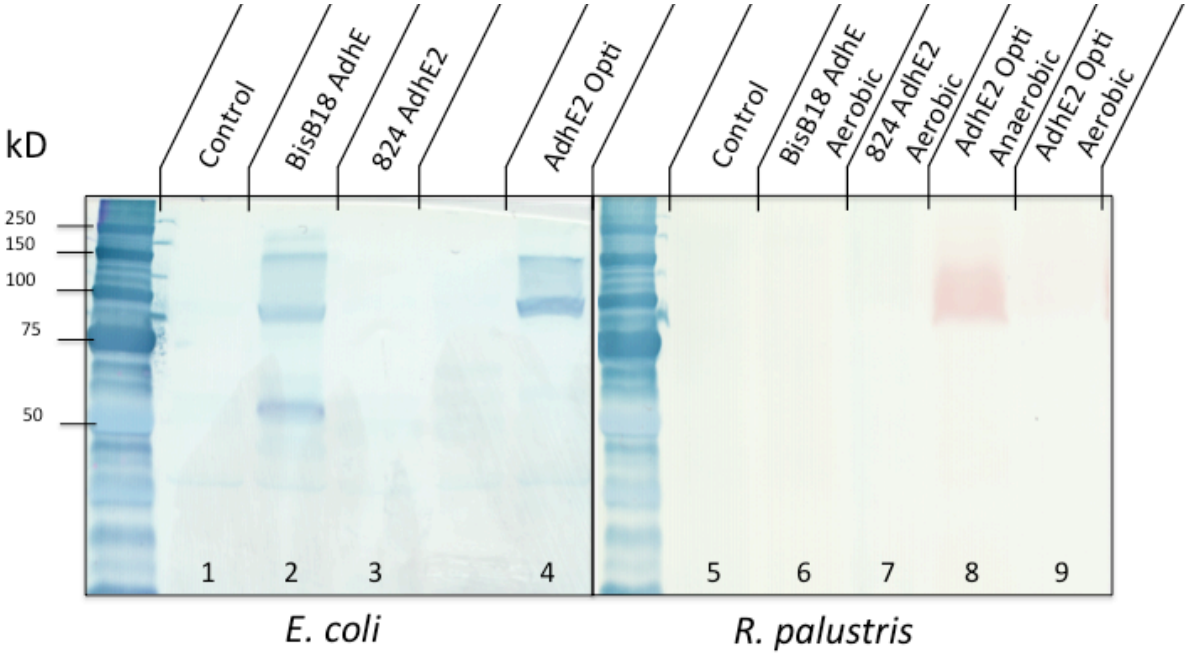

Figure 3.4. Western blot of engineered 6X His AdhE strains in both *E. coli* and *R. palustris*. Expected 824 AdhE2 (and AdhE2 Opti) and BisB18 AdhE sizes are 94.3 and 94.7 kD, respectively. Downfield band of ~ 50 kD likely corresponds to the fragmented C-terminal alcohol dehydrogenase domain where the 6X His tag is located. Protein concentrations of 135 µg were loaded into all sample lanes.

Although the strong band at the expected size of 94.5 kD for BisB18 AdhE in *E. coli* (**Fig 3.4** lane 2) demonstrates the construct is functional, the lack of a signal from the *R. palustris* BisB18 *adhE* construct (**Fig 3.4** lane 6) and no growth under restrictive occurred suggests that either the construct is not functional in *R. palustris*, or that the protein expression level in *R. palustris* is below detection. Comparing fluorescence levels from the previously screened GFP

reporter strains for the pBBR1MCS-2 *lac* construct, expression in *R. palustris* is predicted to be ~ 13x lower than in *E. coli* (**Fig. A1.2**). However, the lack of growth under restrictive $-HCO_3^-$ conditions demonstrates that regardless of the reason, butyrate to butanol was not observed from the BisB18 *adhE* construct and a second approach using a codon-optimized copy of 824 *adhE2* (*adhE2* Opti) was attempted.

3.4.2.2 AdhE2 Opti

The optimization of 824 *adhE2* resulted in an overall increase of the average codon utilization frequency in *R. palustris* from 23% (for the original 824 *adhE2* form) to 64% (for the optimized form) (**Fig. 3.5**). Codon utilization frequency describes how often in the coding regions of the genome a particular codon is used for a given amino acid. The codon utilization table for *R. palustris* CGA009 was determined by analysis of all genomic coding sequences and was retrieved from the Kazusa database (Nakamura, Gojobori, and Ikemura 2000). Codon optimization resulted in a shift from a 32.5% GC content of 824 *adhE2* to 62%. In addition, the presence of rare codons (<10% utilization frequency), which previously composed 47.4% of all codons for the 824 *adhE2* gene, was entirely eliminated. One disadvantage to this approach of codon optimization is that rare codons are known to induce ribosomal pausing, which has been demonstrated important for proper folding of expressed proteins. With the elimination of all rare codons from the *adhE2* Opti gene, the elimination of codon-dependent ribosomal pausing could lead to improper folding and aggregation of the target protein (Rosano and Ceccarelli 2009). For comparison with the *adhE* Opti gene, the codon utilization frequency of the endogenous *R. palustris* BisB18 *adhE* gene averaged 55%, the gene possessed an overall 63% GC content, and the frequency of rare codons within the gene was 5%, demonstrating that even in endogenous alcohol/aldehyde genes, *R. palustris* may utilize rare codons for proper translation of proteins.

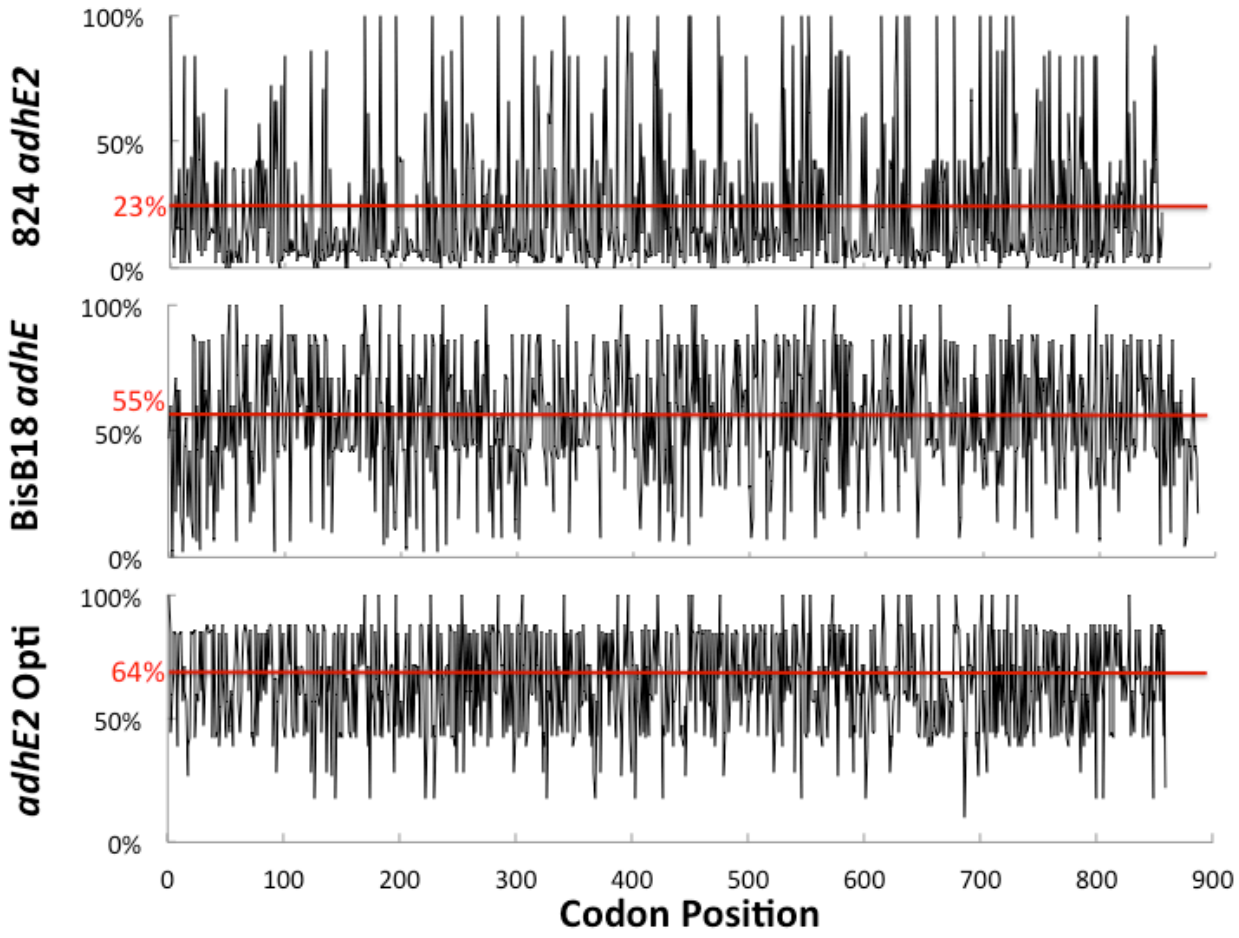

Figure 3.5. Codon utilization frequency for each codon position appearing in the three candidate enzymes for butyryl-CoA to butanol conversion. Top panel) *C. acetobutylicum* 824 *adhE2*, middle panel) *R. palustris* BisB18 *adhE*, and lower panel) codon optimized *adhE2*.

To test if *adhE2* Opti would be expressed in *R. palustris* and enable growth by conversion of butyrate to butanol, the gene was introduced as previously described using the pBBR1MCS-2 *lac* construct and inoculated into RM butyrate ± HCO_3^- for growth screening and western blot analysis. As with the BisB18 *adhE* construct, a detectable band was observed in the *E. coli* sample, however no band was detected from *R. palustris* (**Fig. 3.4** lanes 4, 9). Although western blot analysis remained inconclusive if the construct was successfully expressed in *R. palustris*,

growth and butanol production from *R. palustris* with the *adhE2* Opti construct demonstrated evidence of the functional activity. *R. palustris* pBBR1MCS *adhE2* Opti was further investigated for its ability to grow under both permissive and restrictive ± HCO_3^- compared to the pBBR1MCS-2 GFP strain as a control.

3.4.3 Butanol production rates and efficiency from adhE2 *Opti*.

Although the western blot remained inconclusive on which constructs were successfully expressed in *R. palustris*, the demonstration of growth and butanol production under –HCO_3^- conditions by *adhE* Opti suggests both functional expression and butyryl-CoA to butanol activity. This strain was further investigated for its ability to grow under both permissive and restrictive ± HCO_3^- conditions and was compared to the pBBR1MCS-2 GFP strain as a control.

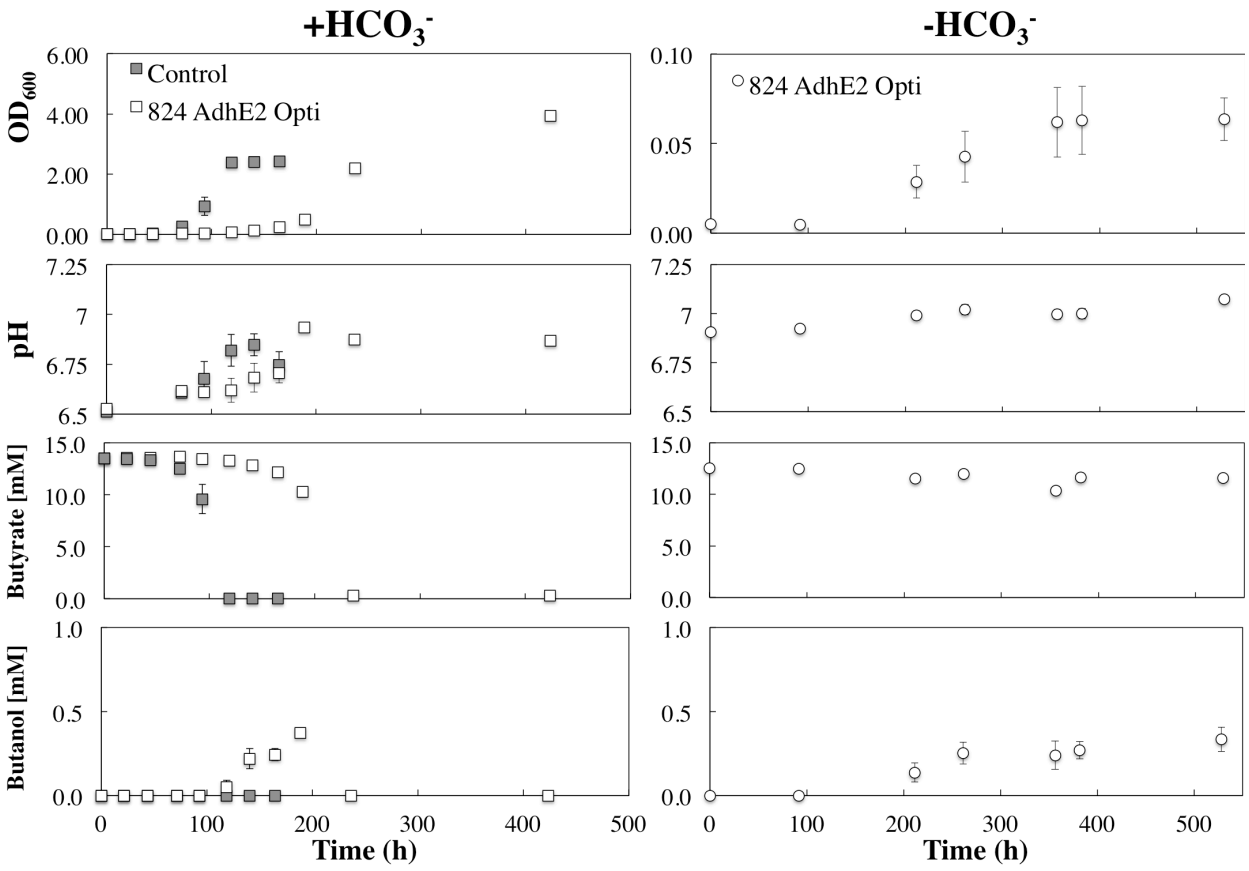

Figure 3.6. Growth of engineered *R. palustris* strains *adhE2* Opti and control (pBBR1MCS GFP) in permissive ($+HCO_3^-$, squares), and restrictive ($-HCO_3^-$, circles) conditions. Control and *adhE2* Opti represented by grey and white symbols, respectively. Average and standard deviation of triplicates are shown.

Growth in $-HCO_3^-$ did not occur for the control strain, and while the engineered strain was capable of growth under these restrictive conditions, it occurred on a long time scale and only reached a plateau of ~ 0.06 OD_{600}. Following the onset of stationary phase, consumption of butyrate and production of butanol still occurred, however, achieving a maximum butanol concentration of 0.6 mM after extended incubation. Although only low levels of butyrate were consumed, butanol production occurred with a 39.7 ± 7.6% carbon conversion efficiency. When inoculated into $+HCO_3^-$ conditions, surprisingly the engineered strain was still observed to produce butanol and grow slower compared to the GFP strain although exogenous CO_2 was

available for maintaining redox balance. One possible reason for this observation is that upon switching from -HCO_3^- to +HCO_3^- conditions, *R. palustris* experiences a long lag phase adjusting to using CO_2 where butanol production is still required for growth. Butanol production was observed by the engineered strain in the +HCO_3^- conditions at a maximum measured concentration of 0.37 mM, with an 11.5% carbon conversion efficiency.

3.5 Discussion

Here we demonstrate the obligate conversion of butyrate to butanol as a metabolically engineered strategy for maintaining redox balance in *R. palustris* under photoheterotrophic growth conditions. As far as the authors are aware, this is the first metabolically engineered fuel production activity that proceeds as an obligate strategy for growth. Though growth and butanol production levels we observe were low, the production of butanol proceeded with a carbon conversion efficiency of 39.7 ± 7.6% (**Fig. 3.6**). Based on previous quantitative measurements of *R. palustris* growing with butyrate, in addition to the excess reducing equivalents reoxidized by fixing CO_2 released from catabolic processes, 16.4% of electrons originally contained in butyrate must be reoxidized (McKinlay and Harwood 2011). This corresponds to an estimated 0.45 mol butanol produced per mol butyrate consumed, or 45.0% carbon conversion efficiency. This value agrees well with our findings and suggests that all reducing equivalents predicted to be in excess are being converted into butanol.

Since the theoretical maximum yield of butanol from butyrate is 83.3% (**Fig. 1**), with *R. palustris* functioning as an ideal biocatalyst and not consuming any substrate, strategies at improving carbon conversion for this reaction could be undertaken. For example, metabolism under stationary conditions has been shown to increase available reducing equivalents by shifting

central metabolism from the glyoxylate shunt to the oxidative steps of the tricarboxylic acid cycle for further oxidation of the substrate (McKinlay et al. 2014). Alternatively, if this engineered activity was introduced to a ΔRuBisCO strain of *R. palustris* and none of the CO_2 emitted from butyrate was refixed, 34% of all electrons originally contained in butyrate would be available for production of butanol, resulting in a 63.0% carbon conversion efficiency from butyrate to butanol. Further, a combination of these two situations could yield butanol production with carbon conversion efficiencies approaching the theoretical maximum.

To investigate the cause of the low growth levels observed *R. palustris* was screened for butanol toxicity. However, no inhibition of growth was observed in *R. palustris* at butanol concentrations below 30 mM (**Fig. A1.3**), and thus it is unlikely that the production of butanol at the concentrations observed here (0.6 mM) is leading to inhibition of the culture. The intermediate butyraldehyde is another metabolite that could have toxic effects within *R. palustris*. Although it was only detected at low levels in the supernatant (a maximum of 50 μM), the accumulation of aldehydes at higher concentrations within the cell could result in inhibition of growth. However, due to the fusion nature of the AdhE2 Opti protein, butyraldehyde would be expected to rapidly proceed to butanol with a high rate of flux and low effective concentration due to the physical colocalization of the aldehyde and alcohol domains of AdhE2 Opti (DeLisa and Conrado 2009).

More likely, inhibited growth is due to overall redox flux limitations through the engineered AdhE2 Opti pathway. Because AdhE2 Opti is provided as the sole route to maintaining redox balance, all excess electrons must be funneled through this pathway. If the capacity of the AdhE2 Opti protein pool is outweighed by the demand for regenerating oxidized reducing equivalents, this will introduce a bottleneck in the maximum rate of metabolism.

Assaying cell extracts for specific activity of this engineered pathway could be performed to verify if this is the cause. In addition, reduced growth through constrained redox flux could also be investigated by using improved expression vector/promoter combinations for AdhE2 Opti and screening for improved growth and butanol production levels. Alternatively, since the growth rate of the engineered strain is now linked directly with the ability to produce butanol, a directed evolution strategy could be used to select for faster growing, and likely higher butanol producing, strains.

3.6 Conclusion

Although growth and production rates were low for this system, our carbon conversion efficiency of 39.7 ± 7.6% matched well with the predicted 45.0% under these conditions. Because the low growth levels are likely constrained by redox flux through the engineered pathway, rational design and directed evolution could be used to further improve the performance of this activity and increase overall growth rates and butanol yields. While this proof-of-concept for harnessing an obligate reducing metabolism to drive engineered reactions used butanol as a target molecule, this redox based driving force could be used to achieve other reactions for the production of desirable chemicals that require reduction reactions.

3.7 Acknowledgements

We would like to thank Dr. Meena Haribal, Dr. Lubna Richter, Dr. Matt DeLisa, Dr. Jason Boock for their expertise and advise. We would like to thank Dr. Caroline Harwood for providing the *R. palustris* BisB18 strain. This project and its researchers were funded in part by the Atkinson Center for a Sustainable Future, the Academic Venture Fund at the Atkinson Center

for a Sustainable Future, and the Advanced Research Projects Agency – Energy Open 2012 program project number DE-AR0000312

CHAPTER 4

SYNTROPHIC ACETATE SHARING BETWEEN *RHODOPSEUDOMONAS PALUSTRIS* CELLS WHILE DEGRADING THE LIGNIN MOLECULE *P*-COUMARATE IS NOT A STRATEGY USED TO AID REDOX BALANCE

Adapted from: Devin F. R. Doud, and Largus T. Angenent. In preparation for *Applied and Environmental Microbiology*.

4.1 Abstract

Lignin is one of the largest forms of biogenic carbon and plays a major role in the global carbon cycle. Because of this, the desire for a clear understanding of its fate under both aerobic and anaerobic environments has driven investigation into lignin metabolism throughout the last century. However, the degradation of lignin under anaerobic conditions remains unclear as no organism capable of degrading complex lignin under such conditions has been identified, and few are known to metabolize lignin monomers and derive sufficient energy for growth. *Rhodopseudomonas palustris* has emerged as a model organism for the metabolism of *p*-coumarate, which is a primary component of lignin, under anaerobic conditions. However, during metabolism of *p*-coumarate, a number of known obligate strategies for maintaining redox balance are used to eliminate excess reducing equivalents. It has been hypothesized that to ease the burden of this redox imbalance, *R. palustris* differentiates into a single-genotype pseudo-consortium with one subpopulation performing the aromatic moiety degradation, and one subpopulation oxidizing downstream products. In this study, we co-cultured *R. palustris* with *Geobacter sulfurreducens* in a bioelectrochemical system to investigate if acetate sharing was a viable strategy used by *R. palustris* under conditions inducing redox imbalance. Our findings

demonstrate that acetate sharing does not occur between different subpopulations of *R. palustris* while degrading *p*-coumarate as its sole organic carbon source under anaerobic conditions.

4.2 Introduction

Lignin is the most abundant source of organic aromatic compounds, and the second most abundant organic carbon source in the biosphere (Suhas, Carrott, and Ribeiro Carrott 2007). Due to its overwhelming supply, lignin presents itself as a prime substrate for biomass conversion to produce renewable resources and energy. Unfortunately, the abundance of lignin is rivaled only by the difficulty organisms have in metabolizing it, especially under anaerobic conditions. This is because lignin is a class of structurally complex, high molecular weight molecules that contain many aromatic groups and remain largely insoluble. Previous studies on anaerobic lignin metabolism have focused primarily on the degradation of lignin monomers and the demonstration of anaerobic aromatic ring fission (Evans 1963, Colberg and Young 1982, Healy and Young 1979). Since this discovery, degradation of lignin oligomers and lignin monomers have been demonstrated under strictly anaerobic conditions, though it is still debated if complex lignin can be degraded under these conditions (Kirk and Farrell 1987).

Rhodopseudomonas palustris, which is a model organism for lignin monomer degradation, has also emerged as an attractive organism for bioenergy production. A purple non-sulfur bacterium, *R. palustris* has been well characterized for its anaerobic metabolism of lignin monomers in the presence of light (Harwood and Gibson 1986, Hirakawa et al. 2012, Pan et al. 2008, Phattarasukol et al. 2012). However, while growing photoheterotrophically with *p*-coumarate, which is one of the primary components of lignin, *R. palustris* must employ a number of metabolic strategies for managing excess reducing equivalents that accumulate from this

substrate. While CO_2 fixation and H_2 evolution have both been previously implicated in aiding redox balance for *R. palustris* (McKinlay and Harwood 2010, 2011), determining whether every cell is performing these redox-balancing activities or if it is a strategy shared between an entire community remains obscured.

It has been proposed that while degrading *p*-coumarate in pure culture, *R. palustris* forms a pseudo-syntrophic single-genotype consortium in which one subpopulation degrades the aromatic moiety of *p*-coumarate, and other subpopulations utilize downstream products, such as acetate (Karpinets et al. 2009). By secreting reduced substrates to other subpopulations, this strategy uncouples the redox imbalance that would arise within a single cell oxidizing *p*-coumarate to CO_2 and reduces demand for terminal electron acceptors within the aromatic degrading population. This strategy, thus, enables redox balance to be shared between all members of the single-genotype consortium. Due to the metabolic versatility afforded within the genome of *R. palustris*, metabolite sharing would employ many of the thermodynamic advantages present within a complex consortium without requiring metabolic changes between different, and potentially incompatible growth modes within individual *R. palustris* cells. The observation that *R. palustris* releases acetate when growing with *n*-butyrate provides support that this strategy may be employed when growing on a variety of reduced substrates (McKinlay and Harwood 2011). However, complications in experimentally verifying this relationship exist since transcriptomic or proteomic analyses from pure culture studies measure both populations together as an average. To experimentally investigate if *R. palustris* utilizes acetate sharing as a redox strategy while metabolizing *p*-coumarate, we introduced the acetate-consuming electrochemically active organism *Geobacter sulfurreducens* within a bioelectrochemical system. *G. sulfurreducens* was used as an indicator organism for the hypothesized subpopulation

of *R. palustris* responsible for downstream acetate removal to maintain redox homeostasis for the aromatic degrading subpopulation of *R. palustris*.

G. sulfurreducens is an advantageous organism for the high efficiency conversion of both acetate and H_2 into electric current when grown at an oxidizing electrode (Bond and Lovley 2003). Conserving energy for growth in the process, *G. sulfurreducens* completely oxidizes acetate and H_2, yielding only CO_2 and H^+, with electrons exiting the system through an electrical circuit. By complementing a culture of *R. palustris* growing on *p*-coumarate with *G. sulfurreducens* in a bioelectrochemical system (BES), an anaerobic co-culture of these two organisms could investigate metabolite sharing of acetate that may occur from the aromatic degrading population of *R. palustris*. Because any acetate or H_2 consumed by *G. sulfurreducens* is converted into an electric signal within the BES, measured current production from *G. sulfurreducens* serves as a proxy for metabolite sharing from *R. palustris* and the extent that *R. palustris* secretes acetate as a strategy for maintaining redox balance within a single-genotype consortium while degrading *p*-coumarate can be deduced. To aid in understanding these interactions, wild type *R. palustris* CGA009 and NifA*, which is an obligate H_2 secreting derivative of *R. palustris* CGA009, were grown in BESs with *G. sulfurreducens* with *p*-coumarate as the sole carbon source in FW medium with and without HCO_3^-. Though *R. palustris* NifA* elicited an electrochemical response when grown on *p*-coumarate with *G. sulfurreducens via* H_2 secretion, growth of *R. palustris* CGA009 did not result in an electrochemical signal, indicating that acetate is not released from the *p*-coumarate degrading population as a strategy to aid redox balance.

4.3 Materials and methods

4.3.1 Growth

Rhodopseuomonas palustris strains CGA009 and NifA*, and *Geobacter sulfurreducens* were routinely cultivated in anaerobic fresh water (FW) medium. FW medium consists of 2.5 g $NaHCO_3$, 0.1 g KCl, 0.25 g NH_4Cl, 0.52 NaH_2PO_4, 10 mL FW Vitamins, and 1 mL FW Minerals per liter, neutralized to pH 7.0 (Li et al. 2012). Precultures of *G. sulfurreducens* were grown in FW medium with 10 mM acetate and 20 mM fumarate acting as carbon substrate and terminal electron acceptor, respectively. Precultures of *R. palustris* NifA* and CGA009 were grown in the light with 2 mM *p*-coumarate as the sole organic carbon source. $NaHCO_3$ was replaced with a 25 mM phosphate buffer at a final pH of 7.0 for precultures of NifA* intended for experiments in the absence of HCO_3^-. Serum bottle experiments for the characterization of CGA009 and NifA* strains were grown in an environmental growth chamber (GC8-2VH, EGC, Chagrin Falls, OH) at 30.0°C with 80 μmol of photons/s/m^2 (photons between 400-700 nm) from both fluorescent and incandescent lamps.

4.3.2 Bioelectrochemical reactors

Two chamber H-type reactors were used for all electrochemical experiments. The reactors were constructed of autoclavable glass with water jackets for temperature control and ports for electrochemical components (TerAvest et al. 2014). The working electrode consisted of 9 cm x 9 cm carbon cloth (PANEX ® 30 – PW06, Zoltek Corp, St Louis, MO) attached to a carbon rod with carbon cement (CCC Carbon Adhesive, EMS, Hatfield, PA). The working electrode was potentiostatically controlled (VSP, BioLogic USA, Knoxville, TN) at +0.300 V vs. Ag/AgCl using an Ag/AgCl/sat'd KCl reference electrode (made in-house). The counter electrode consisted of a 2 x 7 x 1 cm carbon block (Poco Graphite, Decatur, TX) attached to a carbon rod

with carbon cement (CCC Carbon Adhesive) and was separated from the counter chamber by a cation exchange membrane (Membranes International, Ringwood, NJ). Prior to operation, the reactors were autoclaved and only sterile components were added. The working chamber contained 450 mL of FW medium and the counter chamber contained 450 mL of FW medium with no carbon source. The reactors were maintained at 30°C with water jackets and a recirculating water heater (Model 1104, VWR Scientific, Radnor, PA) and uniformly illuminated with 60-W incandescent lamps at an intensity of ~ 40 W/m^2. Lids with butyl rubber stoppers were used to maintain gastight conditions while sampling and replacing media. Anaerobic conditions were maintained by sparging reactors with either N_2 or 80:20 N_2/CO_2 through sterile filters.

4.3.3 Electrochemical experiments

For co-culture experiments, *G. sulfurreducens* was initially grown at the anode in FW medium with 10 mM acetate under continuous flow. After a biofilm and stable current production were achieved, the working chamber was flushed at a rate of 0.75 L/h with 1.5 L of either sterile anaerobic FW medium 2 mM *p*-coumarate with HCO_3^- or FW medium 2 mM *p*-coumarate with a 25 mM phosphate buffer and no HCO_3^-. The reactors were then operated in batch with no sparging for the conditions with HCO_3^- and N_2 sparging for the conditions without HCO_3^-. Reactors were allowed to reach an electrical baseline before inoculating with *R. palustris*. Samples were taken throughout operation to monitor OD_{600}, pH and relevant metabolites. All non-aromatic metabolites were detected *via* HPLC (600 HPLC, Waters, Milford, MA) with a refractive index detector and an Aminex HPX-87H column (Bio-Rad, Hercules, CA). The column was maintained at a temperature of 60°C, and a 5 mM sulfuric acid eluent at a flow rate of 0.6 mL/min was used as the mobile phase. Aromatic metabolites were detected *via* a Thermo

Scientific Ion Chromatograph System (ICS-1100, Dionex, Sunnyvale, CA) with a Dionex IonPac™ AS22 column (4 x 250 mm) and a Dionex Variable Wavelength Detector set to 285 nm. AS22 eluent was used at a flow rate of 1.2 ml/min.

4.3.4 Microscopy

Mid-log phase cultures of *R. palustris* CGA009 and NifA* growing in FW 2 mM *p*-coumarate with HCO_3^- were visualized using a KH-7700 digital microscope system (Hirox, Hackensack, NJ). Liquid samples were removed from growing cultures, 10 μL was added directly to a microscope slide with coverslip, and was directly visualized from above with a Hirox MX(G)-10C OL-140II lens. Cell aggregate geometries were measured using the integrated Hirox software and approximately 50 measurements were averaged.

4.4 Results and discussion

4.4.1 Characterizing R. palustris strains CGA009 and NifA grown on* p-*coumarate*

The pathway for *p*-coumarate consumption by *R. palustris* has been previously studied with identification of all intermediates and routes (Pan et al. 2008). However, to deduce if any major phenotypic differences between strains CGA009 and NifA* should be expected in the electrochemical reactors, their growth was first characterized in anaerobic FW medium with 2 mM *p*-coumarate in serum bottles with and without the addition of HCO_3^-.

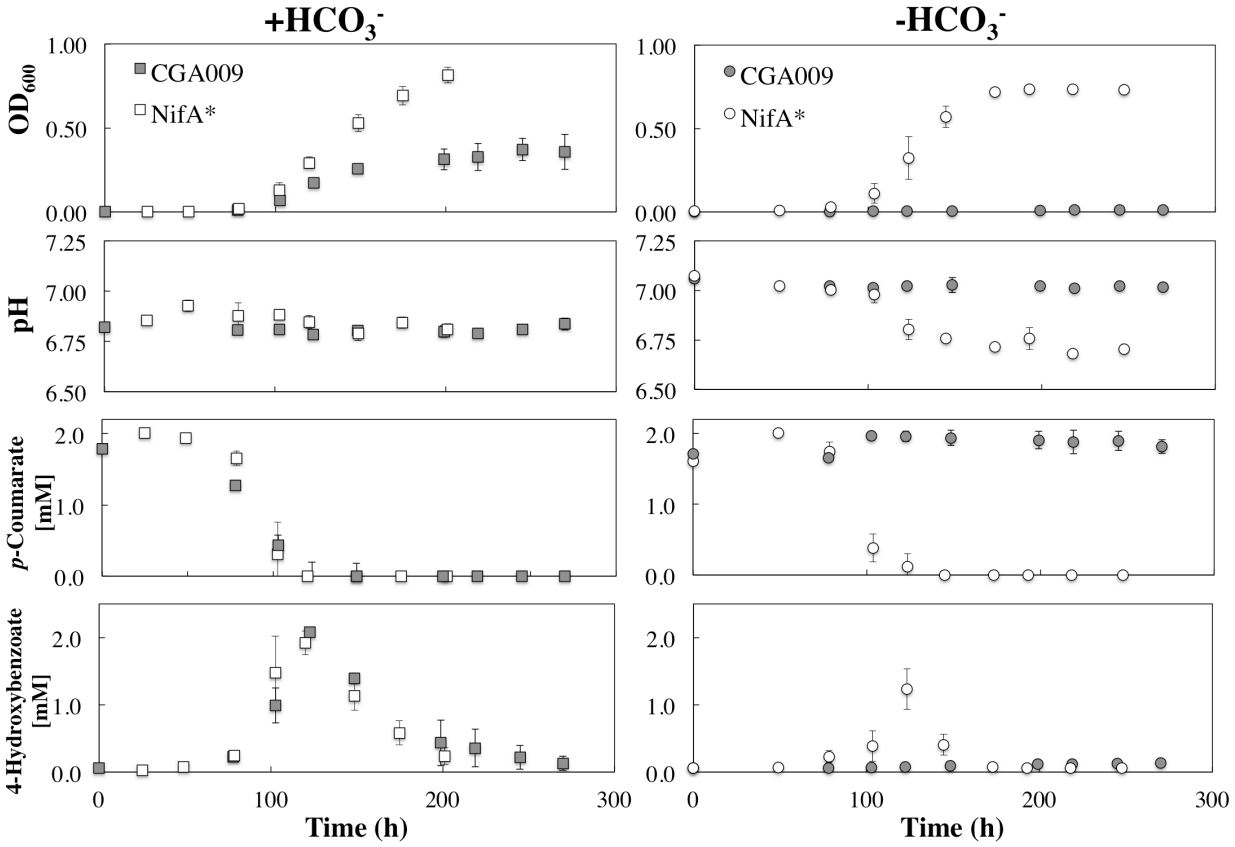

Figure 4.1. Growth of *R. palustris* strains CGA009 and NifA* in FW medium 2 mM *p*-coumarate ±HCO_3^-. Squares and circles represent +HCO_3^- and -HCO_3^- conditions, respectively. Grey icons denote *R. palustris* CGA009 and white icons denote *R. palustris* NifA*. All precultures for growth experiments were in FW 2 mM *p*-coumarate +HCO_3^- medium except for the NifA* culture for growth in -HCO_3^- to avoid the log lag phase when adapting from +HCO_3^- to -HCO_3^- conditions.

The metabolism of *p*-coumarate by *R. palustris* was observed to occur in distinctive phases starting with cleavage of the alkyl side chain, yielding a nearly stoichiometric conversion to 4-hydroxybenzoate. The hydroxyl group was then removed to benzoate (was not detected), which is rapidly degraded by beta-oxidation after activation and cleaving the aromatic ring (Pan et al. 2008). The transient production of 4-hydroxybenzoate began with the onset of *p*-coumarate metabolism and disappeared with the plateau of maximum culture OD, suggesting it is rapidly

consumed once taken up by the cell. When growing on *p*-coumarate in FW medium with HCO_3^- (**Fig. 4.1** left), *R. palustris* CGA009 and NifA* both have very similar rates of metabolism with *p*-coumarate and 4-hydroxybenozate showing very comparable consumption profiles. No other downstream metabolites were detected *via* HPLC. Despite nearly identical rates of substrate consumption, the optical density between the two cultures rapidly diverged with *R. palustris* NifA* reaching a density nearly three times that of CGA009 (0.301 *vs*. 0.847 maximum OD_{600}).

This observation is counterintuitive, as CGA009 should produce more biomass per unit of substrate consumed compared to NifA* due to the extra reducing equivalents available to CGA009 to fix CO_2 that are not lost to H_2 evolution (McKinlay and Harwood 2010). However, the observation that substrate consumption still occurred at the same rate within both environments suggests that a similar level of active cells must be present within both cultures.

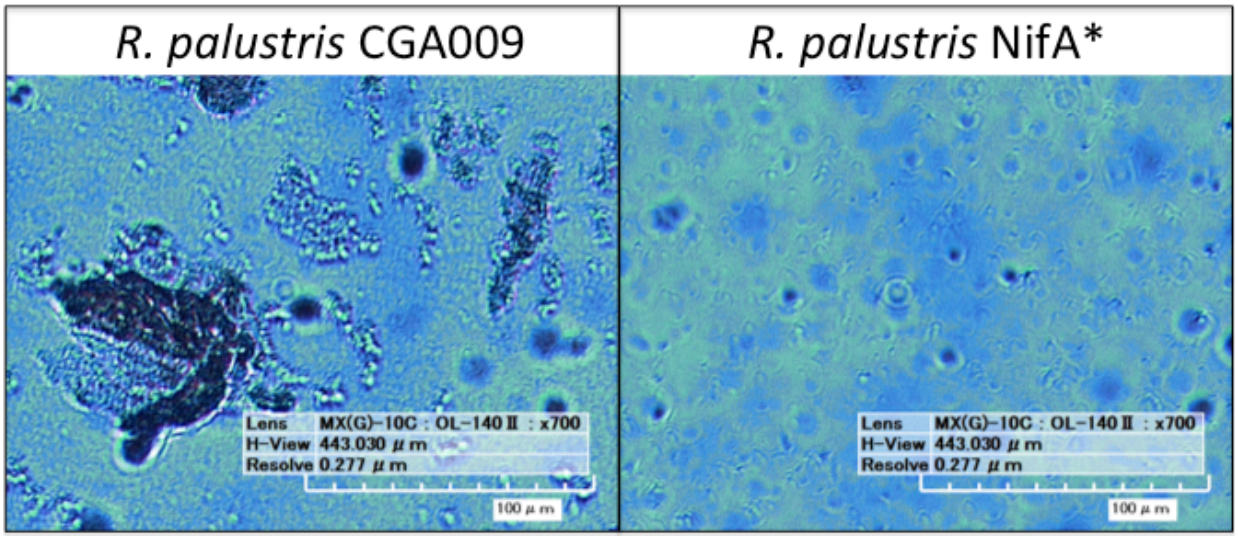

Figure 4.2. Digital microscopy of *R. palustris* CGA009 and NifA* grown on FW 2 mM *p*-coumarate with HCO_3^-. Aggregates of cells appear as dark clumps (CGA009), single cells can be seen as ~ 4 μM long rods (NifA*)

To investigate this, digital microscopy of the two cultures revealed that under these conditions CGA009 tended to grow primarily in granule-like aggregations ranging from 20 to

200 μm in width, and NifA* grew primarily as single cells with only infrequent small granules observed (**Fig. 4.2**). The reduced optical density of CGA009 compared to NifA* is likely due to this aggregation under these conditions, indicating that similar levels of active cells were likely present though optical densities varied between the two cultures. Because the only difference between strain CGA009 and NifA* is the constitutive expression of a nitrogenase in NifA*, this phenotypic distinction can possibly be attributed to differences between the strains utilizing alternate pathways for maintaining redox balance (*i.e.*, CO_2 fixation *vs*. H_2 evolution). This observation further suggests that metabolite sharing may be a viable strategy undertaken by a CO_2-fixing pseudo-consortium of *R. palustris* CGA009 due to the tendency to aggregate, since this aggregating phenotype is abolished when H_2 secretion by individual cells is utilized as the primary route to redox balance.

Under -HCO_3^- conditions (**Fig. 4.1** right), *R. palustris* CGA009 was unable to grow while NifA* performed similarly when compared to +HCO_3^- conditions. This confirms that CGA009 is restricted from growth in the absence of HCO_3^- due to redox imbalance (McKinlay and Harwood 2010), while NifA* is able to grow by using H_2 evolution to eliminate excess reducing equivalents.

4.4.2 R. palustris *CGA009 and NifA* BES co-culture with* G. sulfurreducens

R. palustris CGA009 and NifA* were both inoculated into *G. sulfurreducens*-pregrown BESs with 2 mM *p*-coumarate FW medium with HCO_3^- in batch. Because both strains of *R. palustris* are capable of growth in these conditions, the presence of *G. sulfurreducens* on the electrode as a potential electron sink is not obligate for growth for either strain under these conditions and any current produced would be through metabolite sharing of either acetate (CGA009 or NifA*) or H_2 (limited to NifA*). In addition, because the electrode is the only terminal electron acceptor

for growth of *G. sulfurreducens* under these conditions, any increase in the planktonic optical density was attributed to *R. palustris*.

Comparing metabolite profiles from the BESs (**Fig. 4.3**) to those previously determined in serum bottle experiments (**Fig. 4.1**), conversion of *p*-coumarate to *p*-hydroxybenzoate and subsequent consumption, occurred at nearly the same rate for both strains between both systems. While the optical density trend that CGA009 grew at lower levels than NifA* was maintained, the optical density for both strains was significantly lower in the BESs than when grown in serum bottles. This was likely due to preferential growth on the electrode and reactor surfaces compared to planktonic since biofilm growth on all surfaces was observed. While both strains appeared to perform similarly with regard to metabolism, NifA* was the only strain of the two to elicit an electrochemical response from *G. sulfurreducens* in the BES.

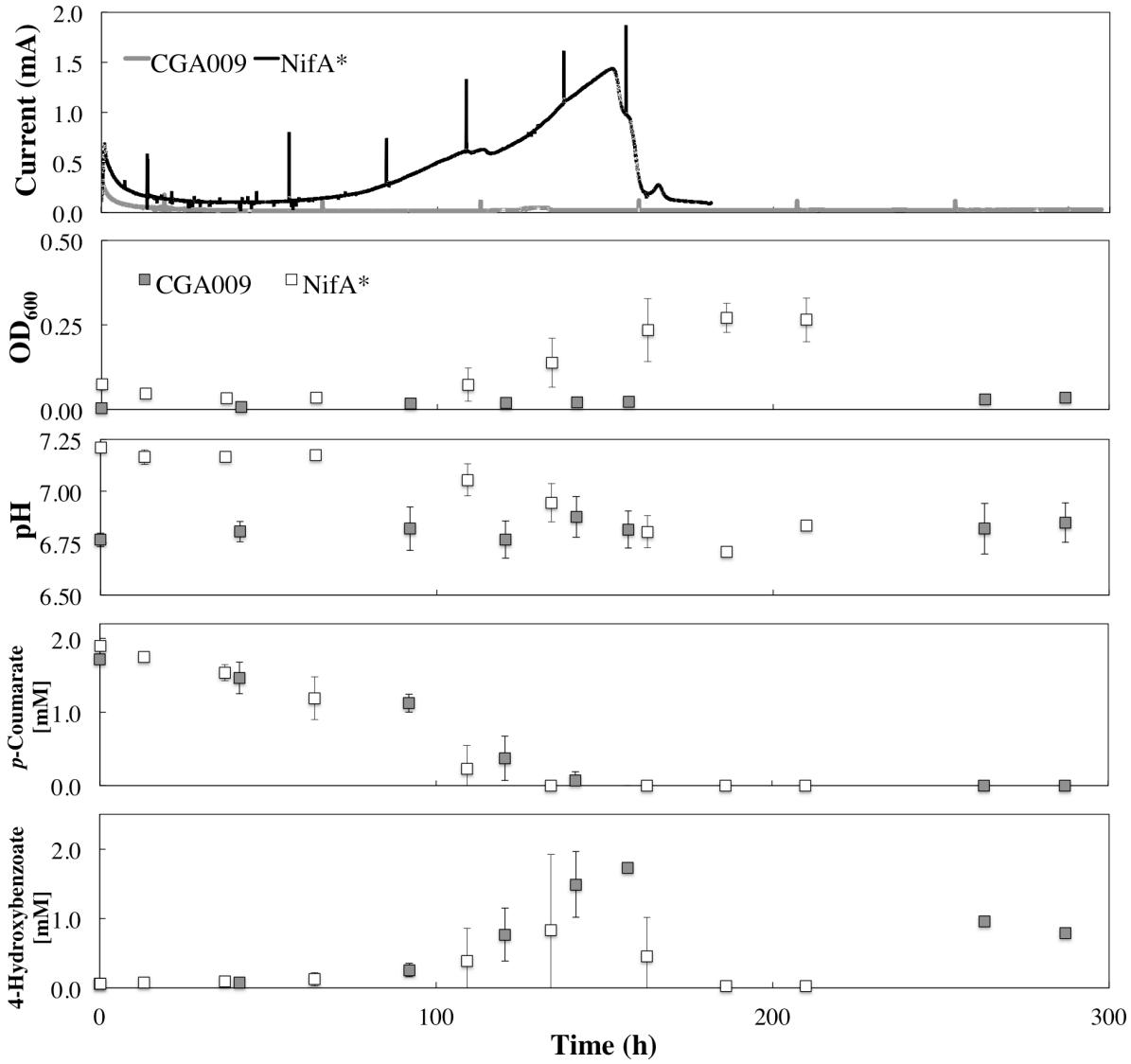

Figure 4.3. Co-culture growth of *R. palustris* CGA009 and NifA* with *Geobacter sulfurreducens* in FW medium 2 mM *p*-coumarate with HCO_3^-. Current for *R. palustris* CGA009 and NifA* denoted by black and grey lines, respectively. Growth and metabolites for *R. palustris* CGA009 and NifA* denoted by dark and white squares, respectively. Standard deviations of biological triplicates (CGA009) and duplicates (NifA*) shown.

The electrochemical signal produced in the *R. palustris* NifA* and *G. sulfurreducens* co-culture closely mirrored the metabolite profile, with current production beginning at the onset of *p*-coumarate consumption. Following the complete conversion of *p*-coumarate to 4-hydroxybenzoate, a short inflection in the current was observed while *R. palustris* transitioned to

consuming 4-hydroxybenzoate. Finally, current production peaked at 1.43 ± 0.15 mA, which coincided with the decrease in measured 4-hydroxybenzoate concentrations. Collectively, this suggests that the observed current from the NifA* *G. sulfurreducens* co-culture closely followed the metabolic trends of NifA* growing in the electrochemical system, and was likely mediated by H_2 evolution from the NifA* strain since negligible current was produced from CGA009 under identical conditions. The lack of current produced from CGA009 also demonstrates that no acetate was shared between *R. palustris* CGA009 and *G. sulfurreducens* under these conditions, though the possibility that secreted acetate remained within the aggregations of *R. palustris* that had previously been noted to form under these conditions (**Fig. 4.2**) cannot be ruled out.

Although *R. palustris* CGA009 did not provide any acetate to *G. sulfurreducens* through acetate sharing under conditions with HCO_3^-, we investigated if this activity would emerge if *G. sulfurreducens* were provided as the sole electron sink for *R. palustris* to grow under lethal redox balance conditions. To test this, *R. palustris* CGA009 and NifA* were separately introduced into *G. sulfurreducens*-pregrown BESs with 2 mM *p*-coumarate FW medium -HCO_3^- with a 25 mM phosphate buffer. As previously observed (**Fig. 4.1**), while NifA* is capable of growth under these conditions by H_2 evolution, *R. palustris* CGA009 is incapable of growth or metabolism of *p*-coumarate because of a buildup of excess reducing equivalents. To provide an opportunity for association between *G. sulfurreducens* and *R. palustris* at the electrode, as opposed to being inoculated in at the start of the experiment as previous, *R. palustris* CGA009 was precultured together with *G. sulfurreducens* on the electrode before switching to the restrictive -HCO_3^- conditions.

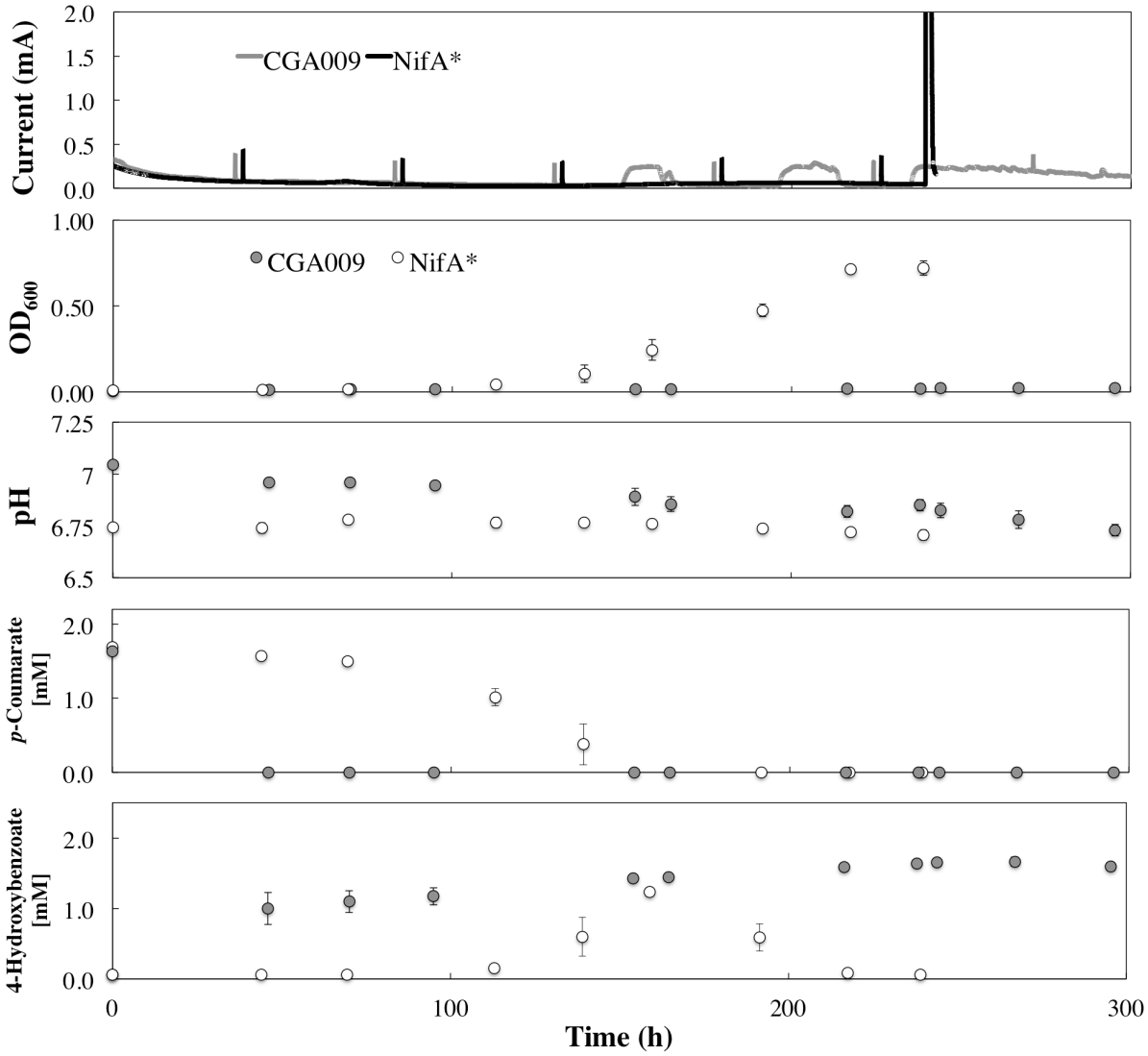

Figure 4.4. Co-culture growth of *R. palustris* CGA009 and NifA* with *Geobacter sulfurreducens* in FW medium 2 mM *p*-coumarate without HCO_3^-. *R. palustris* CGA009 and NifA* are represented by the grey line or grey circles and black line or white circles, respectively. Standard deviations of biological triplicates (NifA*) and duplicates (CGA009) shown. NifA* was precultured in FW medium 2 mM *p*-coumarate without HCO_3^- while CGA009 was pregrown with *G. sulfurreducens* at the electrode.

Although *R. palustris* CGA009 did not exhibit any planktonic growth within the BES once conditions were switched to -HCO_3^-, *p*-coumarate was rapidly taken up and metabolized to 4-hydroxybenozate after the medium replacement was completed. Because the acetyl-CoA unit

derived from the conversion of *p*-coumarate to 4-hydroxybenzoate can be metabolized without producing net excess reducing equivalents (McKinlay and Harwood 2010), it is expected that this conversion would be achieved without aid from *G. sulfurreducens* at the electrode. This conversion occurred much faster than in the serum bottle cultures (**Fig. 4.1**) due to the higher *R. palustris* biomass in the reactor from preculturing with *G. sulfurreducens*, however, following the initial metabolism of *p*-coumarate to 4-hydroxybenzoate, no further metabolism was observed (**Fig. 4.4**). This suggests that after consuming the alkyl moiety from *p*-coumarate, the excess of electrons from the aromatic group saturated the redox balance of *R. palustris* and growth was restricted. The absence of current production from *G. sulfurreducens* and inability of *R. palustris* to grow demonstrates that even under restrictive growth conditions where redox imbalance becomes lethal, *R. palustris* CGA009 did not eliminate excess reducing equivalents in the form of acetate for oxidation by another organism within a consortium. Notable however, when illumination was removed from the CGA009 -HCO_3^- culture, a transient increase in current was observed (**Fig. 4.4** time: 150, 190, and 230 h). This may indicate that release of acetate under redox imbalance conditions is linked with illumination levels, however insufficient evidence was gathered here to conclusively demonstrate this.

Growth and metabolism of NifA* was very similar to both the previous serum bottle and +HCO_3^- electrochemical experiments. However, while NifA* previously elicited a current response in FW medium 2 mM *p*-coumarate with HCO_3^-, no current was produced from growth of NifA* with *G. sulfurreducens* under the no HCO_3^- conditions. To verify that *G. sulfurreducens* was not inhibited following prolonged exposure to FW 25 mM phosphate with no HCO_3^-, sodium acetate was injected into the BES at hour 240 after all *p*-coumarate had been consumed and a large current signal was immediately produced (**Fig. 4.4**). Because evolution of

H_2 is the only route for redox balance by NifA* in the absence of HCO_3^-, this finding suggests that while *G. sulfurreducens* was capable of consuming the acetate provided exogenously, it could not use the H_2 produced by NifA* under no HCO_3^- conditions.

4.5 Conclusion

The hypothesis that *R. palustris* engages in metabolite sharing within a single genotype consortium to avoid complications of redox imbalance that can arise within a single cell was tested by investigating metabolite sharing of acetate between *R. palustris* CGA009 and *G. sulfurreducens*. *R. palustris* NifA* was used as a positive control under both $+HCO_3^-$ and $-HCO_3^-$ conditions for growth and metabolite sharing (of H_2) with *G. sulfurreducens*. An aggregating phenotype was initially observed for *R. palustris* CGA009, suggesting a desire to form close cellular interactions under these conditions, whereas NifA* demonstrated no aggregating phenotype (**Fig. 4.1 and 4.2**). This finding reinforced the proposed acetate-sharing hypothesis, however, no current was produced by *G. sulfurreducens* through acetate sharing from *R. palustris* CGA009 under either $+HCO_3^-$ or $-HCO_3^-$ conditions within the BES. Although CGA009 was capable of complete metabolism of the alkyl side chain of *p*-coumarate under the restrictive $-HCO_3^-$ conditions, metabolism of the aromatic group yielded too many electrons and quickly inhibited growth. Because *G. sulfurreducens* functioned as the sole electron sink for oxidizing excess reducing equivalents by conversion of acetate to CO_2 with an electrode in the $-HCO_3^-$ conditions, this further verified that *R. palustris* did not secrete acetate to maintain redox balance. However, the observation that a transient increase in current occurred with the introduction of dark conditions in the $-HCO_3^-$ experiment suggests that acetate may be released

under low-light conditions, though insufficient evidence was attained to conclusively demonstrate this.

4.6 Acknowledgements

We would like to thank Bahareh Guilvaiee and Dr. Tammo Steenhuis for training and use of their digital microscope. This project was funded in part by the US DOE Advanced Research Projects Agency – Energy (ARPA-E) Open 2012 program project number DE-AR0000312.

CHAPTER 5

TOWARDS ELECTROSYNTHESIS WITH UNCOUPLED EXTRACELLULAR ELECTRON UPTAKE AND METABOLIC GROWTH: CURRENT INCREASE WITH *RHODOPSEUDOMONAS PALUSTRIS*

Adapted from: Devin F. R. Doud, and Largus T. Angenent. Submitted to *Environmental Science and Technology Letters*, July 2014

5.1 Abstract

Metabolite production from CO_2 with microbes at cathodes (*i.e.*, microbial electrosynthesis) is an attractive application of microbial electrochemistry. However, processes for the uptake of electrons from electrodes remain elusive and microbial conservation of energy does often not occur at the cathode. One mechanism known for the uptake of electrons from electrodes is iron-mediated electron transfer to iron-oxidizing bacteria such as obligate aerobic chemolithotrophs and anaerobic photoautotrophs. However, for photoautotrophs this requires an illuminated cathode to provide metabolic energy for growth. Here, we increased published iron-mediated electron uptake rates by *Rhodopseudomonas palustris* TIE-1 by uncoupling the electrochemical from the biological environment in a photobioelectrochemical system consisting of an electrochemical system and a photobioreactor. This uncoupled system resulted in a 56 times higher volumetric iron-mediated electron uptake rate (electric current) than in a single photobioelectrochemical system.

5.2 Introduction

Microbial electrosynthesis focuses on the production of desirable chemicals from inorganic substrates, such as CO_2, with electrons provided from a cathode. Central to this is the ability of a microbe to extract electrons from solid-state materials such as electrodes. This activity has been observed in acetogens (Nevin et al. 2011), methanogens (Cheng et al. 2009), and both aerobic (Summers, Gralnick, and Bond 2013) and anaerobic iron oxidizers (Bose et al. 2014). While the mechanism(s) allowing electron transfer to acetogens and methanogens remain elusive, there is also often no evidence that microbes conserve energy during electrosynthesis at the cathode (Rosenbaum et al. 2011). One known mechanism for the extraction of electrons from a cathode that can proceed with conservation of metabolic energy and growth of the microbe that has previously been demonstrated is iron mediated from cathodes to iron-oxidizing bacteria (Matsumoto et al. 2000, Kinsel and Umbreit 1964).

Rhodopseudomonas palustris TIE-1, which can act as an iron oxidizer, has been identified as being capable of extracting electrons from a poised electrode at + 0.1 V *vs*. standard hydrogen electrode (SHE) (Bose et al. 2014). This is a potential more positive than previously described for activity of any pure culture at a cathode. Under these conditions, *R. palustris* oxidizes iron as a source of electrons, but requires light to obtain energy for carbon fixation and growth through cyclic anoxygenic photosynthesis (Larimer et al. 2004). This enables *R. palustris* to utilize electrons at more positive potentials compared to aerobic iron-oxidizing bacteria that must conserve energy from this oxidation (Weber, Achenbach, and Coates 2006). However, the published activity of ~ 27 μA in a 350-mL reactor (Bose et al. 2014) was facilitated by mediated electron transfer of approximately 4 μM Fe, resulting in an average cycling time of 43 min per molecule of Fe(II) to sustain this current. This suggests that volumetric productivity was limited

by either low concentrations of iron within the system or suboptimal illumination of *R. palustris*. Because abiotic reduction and diffusion rates are expected to occur on a shorter time scale, the slow turnover rate of iron through biological oxidation in this system is likely linked to slow metabolism due to insufficient illumination.

When growing on Fe(II) in batch conditions in serum bottles, *R. palustris* TIE-1 has been found to have a maximum rate of iron oxidation around 33 μM/h before becoming substrate limited (Bose and Newman 2011). Comparing this rate to that achieved in a bioelectrochemical system (BES), which regenerated Fe(II) continuously, only 8.8% of this volumetric activity (2.88 μM/h) was maintained. This suggests that while the cathode may be capable of regenerating iron and that *R. palustris* can utilize Fe(II) at micromolar concentrations, the conventional BES was not capable of supporting maximal Fe(II) growth rates of *R. palustris*. To improve the rate of electron utilization by *R. palustris* at a cathode, limitations of both iron and illumination were investigated, resulting in the design and operation of a novel photobioelectrochemical system (photoBES) featuring 56x higher iron oxidation rates per illuminated volume compared to a conventional BES. The utilization of iron-mediated electron transfer may hold consequences for microbial electrosynthesis.

5.3 Materials and methods

5.3.1 Growth

Rhodopseudomonas palustris TIE-1 and Δpio (a mutant incapable of growth by iron oxidation) were routinely pre-cultured in modified anaerobic *Rhodospirillaceae* medium (Lee et al. 2002) consisting of 2.0 g $NaCH_3CO_2$, 0.5 g KH_2PO_4, 0.5 g K_2HPO_4, 0.2 g $MgSO_4$ x 7 H_2O, 0.4 g NaCl,

0.05g $CaCl_2$ x 2 H_2O, 0.01g Fe-Citrate, 1.0 g $(NH_4)_2SO_4$, and 1 mL trace metals per 949 mL. After autoclaving, 50 mL of 400 mM sterile $NaHCO_3$, and 1 ml sterile trace vitamins were added to the medium. The trace metal solution consisted of 1 mL 25% HCl (v/v), 70.0 mg $ZnCl_2$, 100.0 mg $MnCl_2$ x 4 H_2O, 60.0 mg H_3BO_3, 200.0 mg $CoCl_2$ x 6 H_2O, 20.0 mg $CuCl_2$ x 2 H_2O, 20.0 mg $NiCl_2$ x 6 H_2O, and 40.0 mg Na_2MoO_4 x 2 H_2O per liter. The trace vitamin solution consisted of 1.0 g *p*-aminobenzoic acid, 1.0 g thiamine, and 0.1 g biotin per liter. Sterile media was added to autoclaved serum bottles and sparged for 20 min with sterile filtered 80:20 N_2/CO_2 gas.

5.3.2 Photobioelectrochemical systems

5.3.2.1 Conventional H-type bioelectrochemical system

We utilized a glass two-chamber, H-type BES (referred to here as a single photoBES) where electrochemical and microbial processes occurred at the same location. This BES was equipped with water jackets for temperature control and ports for electrochemical components (TerAvest et al. 2014). We autoclaved the single photoBES and added sterile components prior to the operating run. Both the working chamber and counter chamber were each filled with 300 mL *Rhodospirillaceae* medium with sodium acetate omitted, and were operated in a batch mode. We used a total of 40 μM Fe-Citrate in the working chamber of the single photoBES. The working electrode consisted of 9 cm x 9 cm carbon cloth (PANEX ® 30 – PW06, Zoltek Corp, St Louis, MO) that was attached to a carbon rod with carbon cement (CCC Carbon Adhesive, EMS, Hatfield, PA). The working electrode was potentiostatically controlled (VSP, BioLogic USA, Knoxville, TN) at -0.220 V *vs*. Ag/AgCl using an in-house made Ag/AgCl (sat'd) reference electrode. The counter electrode consisted of a 2 x 7 x 1 cm carbon block (Poco graphite, Decatur, TX) that was attached to a carbon rod with carbon cement (CCC Carbon Adhesive) and was separated from the working chamber by an anion exchange membrane (Membranes

International, Ringwood, NJ). We provided anaerobic conditions by sparging reactors with 80:20 N_2/CO_2 through sterile filters and the single photoBES was maintained at 30°C *via* water jackets and a recirculating water heater (Model 1104, VWR Scientific, Radnor, PA). The working chamber was illuminated externally with ~ 40 W/m^2 from a single 60-W incandescent lamp, as used in the previous study (Bose et al. 2014), and the reactor was continuously stirred *via* a magnetic stir bar. Iron(II) under dark *vs*. light conditions was detected *via* the Ferrozine assay (Riemer et al. 2004).

5.3.3 Uncoupled photoBES

5.3.3.1 10-Stack photobioreactor

We utilized a 10-stack photobioreactor for the illuminated portion of the uncoupled photoBES. The bioreactor frame was 3D printed using VeroClear photocurable resin (Stratasys, Edina, MN) (**Fig. 5.1**). Waveguides were fabricated from borosilicate glass slides (VistaVisio Microscope Slides, VWR, Radnor, PA) and treated with Armour Etch glass etching cream (Armour Products, Hawthorne, NJ) for 7 h after which the glass slide was soaked in water and the etching cream was washed away. Waveguides were inserted into the printed bioreactor frame and polydimethylsiloxane (PDMS) (Dow Chemicals, Midland, MI) was added to all joints and cured at 80°C for 30 min to seal the bioreactor. The assembled bioreactor was then coated with parylene C to prevent oxygen penetration. The active volume of the 10-stack photobioreactor was 17 mL (**Fig. 5.1**). During the experimental period, the 10-stack photobioreactor was illuminated from either side with 470-nm high power blue LEDs (BY-HP100BL, TopLEDLight, ShenZhen China) at a distance of 4 cm and a forward current of 0.75 A. This resulted in an intensity of ~ 27.5 μmol photons/s delivered to the surface area of the exposed waveguide edges.

The LEDs were mounted on heatsinks and fans were used to maintain a continuous temperature on the LEDs and reactors (**Fig 5.1B**).

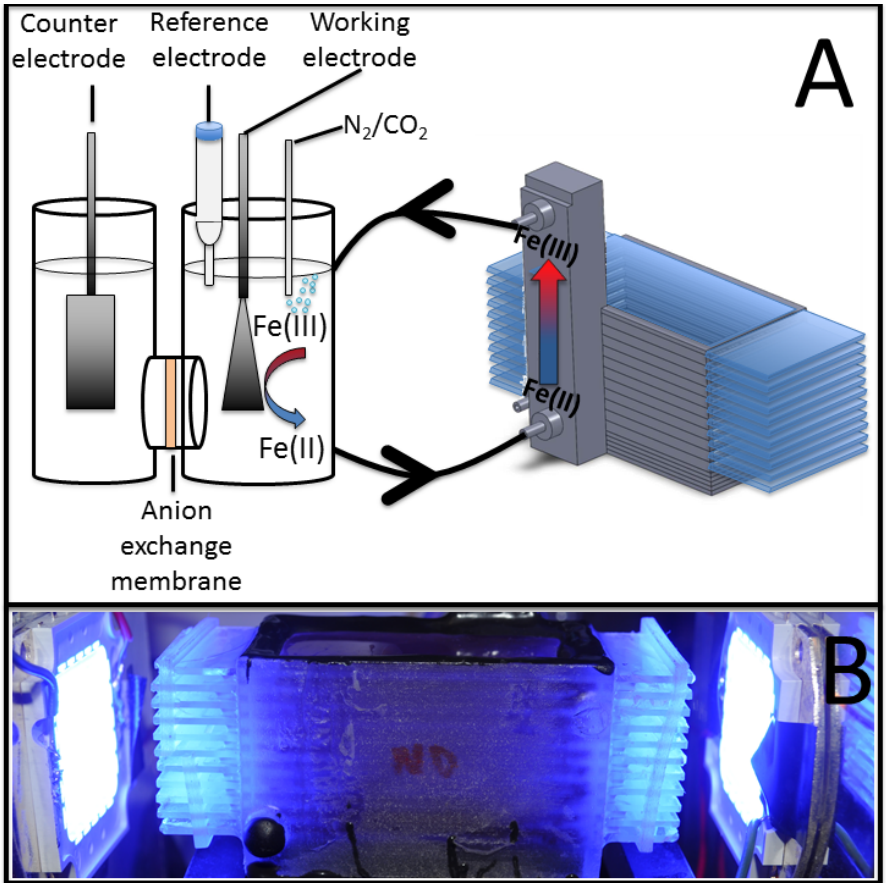

Figure 5.1. System setup: A) Schematic of an uncoupled photoBES that consisted of an abiotic electrochemical system (left) and a 10-stack waveguide photobioreactor (right) to utilize closed-loop recirculation with an iron-mediated system to transfer electrons from the working electrode to *R. palustris* for Fe(II) oxidation; and B) LED lights were utilized to illuminate the waveguides from both sides.

5.3.3.2 Uncoupled PhotoBES Operation

The complete uncoupled photobioelectrochemical system (uncoupled photoBES) utilized a glass electrochemical system, with similar electrode design as specified previously but without water jackets and temperature control, together with the 10-stack photobioreactor. Ports at the bottom

and top of the 10-stack photobioreactor were used to connect tubing to the working chamber of the 2-chamber electrochemical system **(Fig. 5.1)**. This uncoupled photoBES, with an active volume of 83 mL for the electrochemical working chamber and 17 mL for the 10-stack photobioreactor, was used to electrochemically regenerate and deliver Fe(II) to the optimally illuminated culture of *R. palustris*. The electrochemical chamber was darkened to prevent growth of *R. palustris* in the working chamber. The uncoupled photoBES was operated in batch with no addition or removal of substrate or effluent. *R. palustris* TIE-1 was resuspended in a total of 100 mL of *Rhodospirillaceae* medium with 9 mM iron nitrilotriacetate (Fe-NTA) to an OD_{600} of 1.0, which was then added to the system. An increased starting OD was used to reduce startup time of the reactor, and iron concentrations were increased to prevent limitations in current uptake that may occurr due to limitations in recirculations between chambers. This solution was pumped between the 10-stack photobioreactor and the working chamber of the electrochemical system using a Masterflex® L/S® Precision Variable-Speed Drive peristaltic pump (Cole Parmer, Vernon Hills, IL) at a flow rate of 3.2 mL/min. The working chamber of the electrochemical system was sparged with 80:20 N_2/CO_2 to maintain anaerobic conditions throughout the system to prevent spontaneous oxidation of Fe(II) by O_2 at circumneutral pH and provide CO_2 for growth by carbon fixation in the photobioreactor. Prior to operation, we autoclaved the electrochemical system and all tubing, while we disinfected the photobioreactors with a 70% ethanol wash, rinsed with sterile DI water, and allowed to dry in a biosafety cabinet.

5.4 Results and discussion

5.4.1 Electron uptake is mediated by a light-dependent Fe(II)/Fe(III) system

R. palustris TIE-1 is capable of growth by photolithoautotrophy with Fe(II) as a sole electron source. Using a poised electrode, Fe(II) can be regenerated within an electrochemical system with electric current functioning as a proxy for the biological rate of oxidation. This was already demonstrated for both a WT *R. palustris* TIE-1 and Δpio; however, maximum volumetric rates of electron uptake were very low (~0.077 μA/mL) (Bose et al. 2014). Here, we verified these published results under similar conditions with *R. palustris* TIE-1 in single photoBESs.

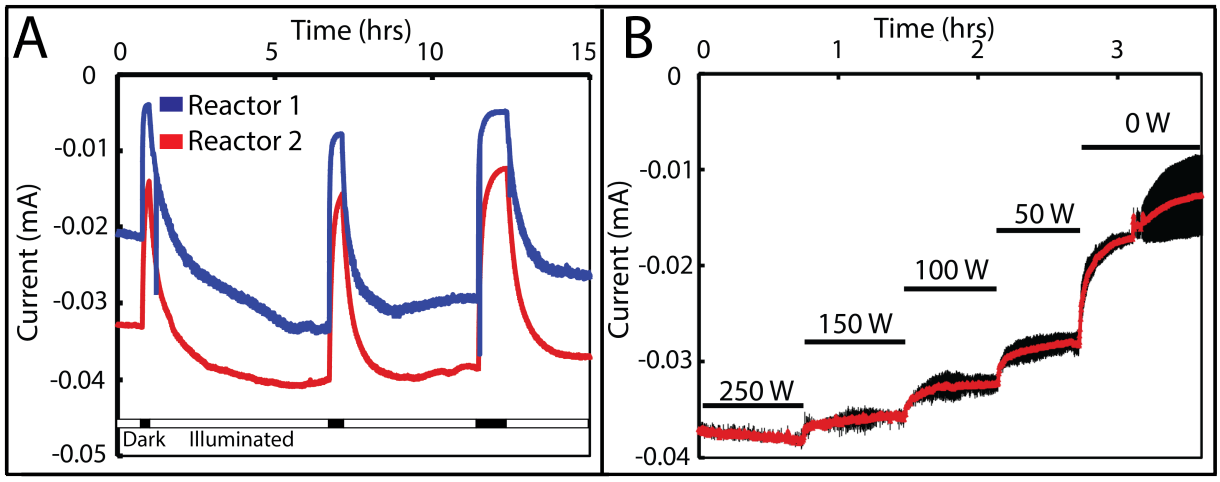

Figure 5.2. Performance of *R. palustris* TIE-1 that was grown at the cathode of an H-type BES (single photoBESs): A) light removed and reintroduced three times showed light-dependent electron uptake from the electrode in duplicate cultures; B) decreased illumination intensity resulted in a decreased electric current (red represents average; black standard deviation).

While recreating previously reported experimental conditions, we observed electron uptake for *R. palustris* TIE-1 to be linked to illumination and found that terminating illumination altogether considerably reduced the electric current (72 ± 11%; n = 12) (**Fig. 5.2A**). Reduction in current was attained immediately following the removal of light, and although slower to recover,

the return of current occurred immediately with reintroduction of light. Therefore, a dark/illuminated electron uptake ratio of ~0.28 was observed for the single photoBES. No light-dependent response was observed for abiotic controls and their background abiotic current densities remained low. Even at the low planktonic culture densities achieved in a mature single photoBES ($OD_{600} < 0.01$), decreasing the illumination of single photoBESs resulted in decreasing rates of electron uptake (**Fig. 5.2B**). When illumination was terminated altogether, a significant increase in Fe(II) was measured compared to illuminated conditions (40.5 ± 1.8 μM in dark vs. 33.6 ± 2.8 μM in light, $p < 0.05$, $n = 3$); however, even under fully illuminated conditions Fe(II) was always present and nonlimiting. Our findings agree with the magnitude of electron uptake rates that were previously published for *R. palustris* TIE-1 (Bose et al. 2014), even though our total iron concentration was 10x higher (40 μM *vs.* 4 μM). In addition, our findings also agreed with their dark/illuminated electron uptake ratio (Bose et al. 2014), suggesting that *R. palustris* uses: 1) energy reserves for the uptake of electrons in the dark; or 2) an uncharacterized light-independent route for electron uptake under these conditions. Contrary to the published findings (Bose et al. 2014), however, inoculation of *R. palustris* TIE-1 Δpio in our single photoBES did not result in electron uptake, which is in accordance with the known cellular mechanisms of iron mediation of *R. palustris* (Jiao and Newman 2007).

5.4.2 Increased volumetric rates of microbial iron oxidation are supported by improved illumination

For future utilization of microbial electrosynthesis *via* anaerobic iron-oxidizing bacteria we postulated that improved volumetric rates of electron uptake must be achieved. We also observed that increasing illumination improved current uptake rates for TIE-1 and that Fe(II) was always available, suggesting that at iron concentrations of 40 μM, the limiting factor was the delivery of

light. In an attempt to improve volumetric electron uptake rates for *R. palustris* TIE-1, we decided to uncouple the electrochemical iron(III) reduction from the microbial metabolism.

Waveguide-based photobioreactors have been used for high-density cultivation of photosynthetic microbes to ensure high volumetric productivities because they allow for the delivery of light to internal portions of photobioreactors that would otherwise receive suboptimal intensities due to self shading (Jung et al. 2012). In an attempt to cultivate *R. palustris* with improved volumetric productivities of mediated electron uptake, *R. palustris* was grown inside a waveguide-based photobioreactor with abundant illumination and surface area for microbial attachment. To provide the culture in the waveguide reactor with a continuous supply of Fe(II), the photobioreactor was connected in a closed-loop to a darkened electrochemical system, where Fe(III) was reduced at a poised electrode (**Fig. 5.1**). We also increased the total iron concentration to 9 mM (supplied as Fe-NTA) to circumvent a possible limitation of Fe(II) from uncoupling the environments.

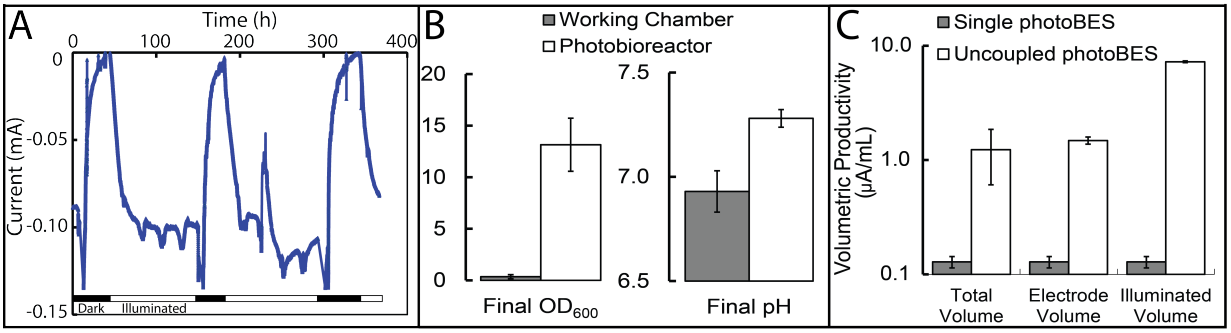

Figure 5.3. Operating performance of an uncoupled photoBES with an abiotic electrochemical system and a 10-stack waveguide-based photobioreactor and a comparison to the single photoBES: A) light-dependent electron uptake (electric current) as measured with the abiotic electrochemical system; B) final optical density and pH in the darkened electrochemical working chamber and 10-stack photobioreactor; and C) operating performance comparison between the single photoBES and the uncoupled photoBES for biological triplicates.

As anticipated, the electron uptake, which was measured with the electrochemical system, was still dependent on the illumination of the photobioreactor (**Fig. 5.3A**). Although the illumination experiments took longer to perform compared to the single photoBES reactor (400 h *vs*. 15 h) due to the longer equilibration caused by recirculation, both systems were operated for similar lengths of time demonstrating that the improved performance was not due simply to longer incubation. Following operation, the liquid and all biomass from the waveguide and electrochemical chambers was extracted. The increased optical density (OD) and pH in the illuminated waveguide-based photobioreactor compared to the dark working chamber of the electrochemical system suggest that growth of *R. palustris* was confined to the photobioreactor (**Fig. 5.3B**). Photoelectroautotrophic growth of *R. palustris* in the photobioreactor of the uncoupled photoBES resulted in 56 times higher volumetric current densities per illuminated volume than the single photoBES (7.23 ± 0.62 *vs*. 0.13 ± .01 μA/mL; n = 3) (**Fig. 5.3C**). Looking closer at the results from **Fig. 3A**, when illumination was terminated we observed a 94 ± 4.0% decrease in the electron uptake rate (n = 9) and a resulting dark/illuminated electron uptake ratio of ~0.06. This ratio was considerably lower than we had observed for the single photoBES (0.06 *vs*. 0.28). No change in current was observed for the abiotic control. Thus, the dark electron uptake without illumination almost disappeared for the uncoupled system, possibly due to the physical separation of the electrode from the metabolically active microbial culture.

To verify that the physical separation of the electrode from the microbial culture was the cause for the lower dark/illuminated electron uptake ratio in the single *vs*. uncoupled photoBES, indium tin oxide (ITO) electrodes were integrated in the waveguide-based photobioreactor. We refer to this here as an integrated photoBES (**Supplementary Materials**). This allowed for photoelectroautotrophic growth of *R. palustris* under identical conditions in the photobioreactor

of the uncoupled photoBES, but with the physical presence of a poised electrode (**Fig. A3.1**). Illumination termination experiments for the integrated photoBES demonstrated a similar decrease in the electron uptake compared to the single photoBES (69 ± 12%; n = 3) with a dark/illuminated electron uptake ratio of ~0.31. This suggests that that the physical localization of the electrode and the microbe is a responsible factor in the difference in dark/illuminated electron uptake ratios.

5.5 Conclusions

In summary, we found that efficient illumination, while providing for nonlimiting Fe(II) concentrations to a culture of *R. palustris,* increased electron uptake rates by 56 times. This occurred in a photoBES where the electrochemistry was uncoupled from the metabolic processes of the photosynthetic culture by using mediated electron transfer with iron. Even though this result was found for a wild-type microbe that at this point cannot produce a chemical from CO_2, this finding may hold important consequences for the field of microbial electrosynthesis. Currently, microbial electrosynthesis is plagued by very low current densities, and uncoupling a high-rate electrochemical system from an optimized bioprocess for bacterial growth is a promising strategy. Our current objective is to genetically engineer *R. palustris* as an iron-oxidizing bacterium that can generate products from CO_2 with electrons from a cathode.

5.6 Acknowledgements

We would like to thank Dr. David Erickson and his research lab at Cornell University for the collaboration in designing the 10-stack waveguide reactor. We would also like to thank Dr.

Dianne Newman for providing the TIE-1 and Δpio strains. This project was funded in part by the US DOE Advanced Research Projects Agency – Energy (ARPA-E) Open 2012 program project number DE-AR0000312.

CHAPTER 6

SUMMARY AND RECOMMENDATIONS FOR FUTURE WORK

6.1 Summary

The innate redox imbalance of *R. palustris* under photoheterotrophic conditions presents an ideal resource for the production of bioenergy from the metabolism of a wide range of organic waste streams. Because the production of ATP from photosynthesis is uncoupled from the metabolism of organic substrates, numerous endergonic pathways for the production of desirable chemicals requiring reduction steps could be developed. Here we demonstrated this proof-of-concept utilizing light to power the conversion of *n*-butyrate to *n*-butanol (Chapter 3). Though this engineered activity resulted in inhibited rates of growth, the amount of *n*-butanol produced from *n*-butyrate suggested that all of the reducing equivalents predicted to be in excess based on previous empirical observations were diverted into this route. Directing reducing equivalents into metabolites is not the only strategy that has been proposed for maintaining redox balance. The hypothesis that *R. palustris* secretes acetate to reduce the redox burden while growing in pure culture was tested by culturing *R. palustris* with *G. sulfurreducens* in a bioelectrochemical system with *p*-coumarate as the sole carbon source under anaerobic conditions (Chapter 4). Using current production as a proxy for metabolite sharing of acetate from *R. palustris* CGA009, this system was used to verify that *R. palustris* does not secrete acetate as a redox strategy when consuming *p*-coumarate under fully illuminated conditions. Finally, by inverting the potential of the electrochemical system, we were able to characterize growth of *R. palustris* using the electrode as the sole electron acceptor (Chapter 5). It was found that levels of growth much lower than expected from iron oxidation were observed in the electrochemical system. To address these limitations and help further the foundation for microbial electrosynthesis

technologies, we focused on improving rates of electron uptake by improving suboptimal illumination. For this, we constructed a new photobioelectrochemical reactor to uncouple the electrochemical and biological environments. This effort resulted in 56 x higher rates of iron oxidation by *R. palustris* in the illuminated volume of the reactor.

6.2 Future work

The results presented here demonstrate that the innate redox environment of *R. palustris* can be harnessed in non-conventional ways for applications in bioenergy. However, this demonstration is far from being mature enough to be considered a viable application for bioenergy. Additional work developing the concepts introduced in Chapters 3, 4, and 5 is presented here.

Chapter 3 demonstrates that engineered pathways for the production of reduced compounds can be used as an obligate strategy for growth. In addition, due to ATP production from photosynthesis, there are no energy constrains on the pathways that can be introduced. With that said, the rates and efficiencies of the introduced butyrate to butanol pathway remain low. However, because growth is linked directly with the ability to produce butanol, it is anticipated that any spontaneous changes to cells that enable better butanol production will also be able to grow faster than bulk cells. To harness this, directed evolution while monitoring performance between subsequent cultures may be one way of improving the slow growth and butanol production rates that are currently demonstrated by the engineered strain. In addition, while the current strain is producing butanol with the anticipated carbon conversion efficiency of ~45%, introducing this pathway into a ΔRuBisCO strain of *R. palustris* would likely increase the carbon conversion efficiency to 65%, although this strain may demonstrate a further reduction in rates of growth and butanol production.

We observed in Chapter 4 that *R. palustris* did not secrete acetate to *G. sulfurreducens* while consuming *p*-coumarate as a carbon source in a bioelectrochemical system. Although *G. sulfurreducens* on the electrode did not enable growth of *R. palustris* CGA009 under restrictive -HCO_3^- conditions, utilization of this approach could be useful for measuring the extent of acetate syntrophy for other microbial interactions. In addition, investigating the observation of a potential light/dark acetate release that was seen under the -HCO_3^- conditions could further test if acetate sharing requires certain environmental triggers, such as short light/dark cycles, to proceed.

Our results from Chapter 5 suggest that reactor engineering can be one approach used to improve performance of electron uptake, which is a largely new concept, in a bioelectrochemical system. Uncoupling the biological and electrochemical environments, a finding that may have important future implications in microbial electrosynthesis, enabled the improved reactor performance we observed. Although this was an advance in the direction toward realizing microbial electrosynthesis, no actual production of a desirable chemical occurred within our system. To further develop the full potential of high-rate iron-mediated electron transfer to *R. palustris*, we envision metabolically engineering a route to couple the uptake of electrons from iron with production of a chemical such as butanol. Because this approach will require integrating iron oxidation as a metabolic route for growth in an environment where organic substrates are readily available, considerable manipulations to regulation and central metabolism would likely be required to achieve this result.

REFERENCES

Abarnou, A., and L. Miossec. 1992. "Chlorinated waters discharged to the marine environment chemistry and environmental impact. An overview." *Science of the Total Environment* 126 (1-2):173-197.

Alsaker, K. V., and E. T. Papoutsakis. 2005. "Transcriptional program of early sporulation and stationary-phase events in *Clostridium acetobutylicum*." *Journal of Bacteriology* 187 (20):7103-7118.

An, J. Y., and B. W. Kim. 2000. "Biological desulfurization in an optical-fiber photobioreactor using an automatic sunlight collection system." *Journal of Biotechnology* 80 (1):35-44.

Atsumi, S., A. F. Cann, M. R. Connor, C. R. Shen, K. M. Smith, M. P. Brynildsen, K. J. Chou, T. Hanai, and J. C. Liao. 2008. "Metabolic engineering of *Escherichia coli* for 1-butanol production." *Metabolic Engineering* 10 (6):305-11.

Barbosa, M. J., J. M. S. Rocha, J. Tramper, and R. H. Wijffels. 2001. "Acetate as a carbon source for hydrogen production by photosynthetic bacteria." *Journal of Biotechnology* 85 (1):25-33.

Baron, D., E. LaBelle, D. Coursolle, J. A. Gralnick, and D. R. Bond. 2009. "Electrochemical measurement of electron transfer kinetics by *Shewanella oneidensis* MR-1." *Journal of Biological Chemistry* 284 (42):28865-28873.

Behrenfeld, M. J., and Z. S. Kolber. 1999. "Widespread iron limitation of phytoplankton in the South Pacific Ocean." *Science* 283 (5403):840-843.

Belchik, S. M., D. W. Kennedy, A. C. Dohnalkova, Y. M. Wang, P. C. Sevinc, H. Wu, Y. H. Lin, H. P. Lu, J. K. Fredrickson, and L. Shi. 2011. "Extracellular reduction of hexavalent chromium by cytochromes MtrC and OmcA of *Shewanella oneidensis* MR-1." *Applied and Environmental Microbiology* 77 (12):4035-4041.

Beliaev, A. S., D. A. Saffarini, J. L. McLaughlin, and D. Hunnicutt. 2001. "MtrC, an outer membrane decahaem *c* cytochrome required for metal reduction in *Shewanella putrefaciens* MR-1." *Molecular Microbiology* 39 (3):722-730.

Bintsis, T., E. Litopoulou-Tzanetaki, and R. K. Robinson. 2000. "Existing and potential applications of ultraviolet light in the food industry - a critical review." *Journal of the Science of Food and Agriculture* 80 (6):637-645.

Bird, L. J., V. Bonnefoy, and D. K. Newman. 2011. "Bioenergetic challenges of microbial iron metabolisms." *Trends in Microbiology* 19 (7):330-340.

Bond-Watts, B. B., R. J. Bellerose, and M. C. Y. Chang. 2011. "Enzyme mechanism as a kinetic control element for designing synthetic biofuel pathways." *Nature Chemical Biology* 7 (4):222-227.

Bond, D. R., and D. R. Lovley. 2003. "Electricity production by *Geobacter sulfurreducens* attached to electrodes." *Applied and Environmental Microbiology* 69 (3):1548-55.

Bose, A., E. J. Gardel, C. Vidoudez, E. A. Parra, and P. R. Girguis. 2014. "Electron uptake by iron-oxidizing phototrophic bacteria." *Nature Communications* 5.

Bose, A., and D. K. Newman. 2011. "Regulation of the phototrophic iron oxidation (pio) genes in *Rhodopseudomonas palustris* TIE-1 is mediated by the global regulator, FixK." *Molecular Microbiology* 79 (1):63-75.

Boynton, Z. L., G. N. Bennett, and F. B. Rudolph. 1996. "Cloning, sequencing, and expression of clustered genes encoding beta-hydroxybutyryl-coenzyme A (CoA) dehydrogenase,

crotonase, and butyryl-CoA dehydrogenase from *Clostridium acetobutylicum* ATCC 824." *Journal of Bacteriology* 178 (11):3015-3024.
Bukhari, Z., T. M. Hargy, J. R. Bolton, B. Dussert, and J. L. Clancy. 1999. "Medium-pressure UV for oocyst inactivation." *Journal American Water Works Association* 91 (3):86-94.
Carpentier, W., K. Sandra, I. De Smet, A. Brige, L. De Smet, and J. Van Beeumen. 2003. "Microbial reduction and precipitation of vanadium by *Shewanella oneidensis*." *Applied and Environmental Microbiology* 69 (6):3636-3639.
Chang, J. C. H., S. F. Ossoff, D. C. Lobe, M. H. Dorfman, C. M. Dumais, R. G. Qualls, and J. D. Johnson. 1985. "UV inactivation of pathogenic and indicator microorganisms." *Applied and Environmental Microbiology* 49 (6):1361-1365.
Chauvatcharin, S., C. Siripatana, T. Seki, M. Takagi, and T. Yoshida. 1998. "Metabolism analysis and on-line physiological state diagnosis of acetone-butanol fermentation." *Biotechnology and Bioengineering* 58 (6):561-571.
Chen, C. Y., G. D. Saratale, C. M. Lee, P. C. Chen, and J. S. Chang. 2008. "Phototrophic hydrogen production in photobioreactors coupled with solar-energy-excited optical fibers." *International Journal of Hydrogen Energy* 33 (23):6886-6895.
Cheng, S., D. Xing, D. F. Call, and B. E. Logan. 2009. "Direct biological conversion of electrical current into methane by electromethanogenesis." *Environmental Science & Technology* 43 (10):3953-3958.
Colberg, P. J., and L. Y. Young. 1982. "Biodegradation of lignin-derived molecules under anaerobic conditions." *Canadian Journal of Microbiology* 28 (7):886-889.
Cormack, B. P., R. H. Valdivia, and S. Falkow. 1996. "FACS-optimized mutants of the green fluorescent protein (GFP)." *Gene* 173 (1 Spec No):33-8.
Cornillot, E., R. V. Nair, E. T. Papoutsakis, and P. Soucaille. 1997. "The genes for butanol and acetone formation in *Clostridium acetobutylicum* ATCC 824 reside on a large plasmid whose loss leads to degeneration of the strain." *Journal of Bacteriology* 179 (17):5442-5447.
DeLisa, M. P., and R. J. Conrado. 2009. "Synthetic metabolic pipelines." *Nature Biotechnology* 27 (8):728-9.
Dellomonaco, C., J. M. Clomburg, E. N. Miller, and R. Gonzalez. 2011. "Engineered reversal of the beta-oxidation cycle for the synthesis of fuels and chemicals." *Nature* 476 (7360):355-9.
Desai, R. P., L. M. Harris, N. E. Welker, and E. T. Papoutsakis. 1999. "Metabolic flux analysis elucidates the importance of the acid-formation pathways in regulating solvent production by *Clostridium acetobutylicum*." *Metabolic Engineering* 1 (3):206-13.
Durre, P., R. J. Fischer, A. Kuhn, K. Lorenz, W. Schreiber, B. Sturzenhofecker, S. Ullmann, K. Winzer, and U. Sauer. 1995. "Solventogenic enzymes of *Clostridium acetobutylicum*: catalytic properties, genetic organization, and transcriptional regulation." *FEMS Microbiology Reviews* 17 (3):251-62.
Eady, R. R. 1996. "Structure-function relationships of alternative nitrogenases." *Chemical Reviews* 96 (7):3013-3030.
Evans, W. C. 1963. "The microbiological degradation of aromatic compounds." *Journal of General Microbiology* 32:177-84.
Fontaine, L., I. Meynial-Salles, L. Girbal, X. Yang, C. Croux, and P. Soucaille. 2002. "Molecular characterization and transcriptional analysis of *adhE2*, the gene encoding the NADH-dependent aldehyde/alcohol dehydrogenase responsible for butanol production in

alcohologenic cultures of *Clostridium acetobutylicum* ATCC 824." *Journal of Bacteriology* 184 (3):821-830.
Fornero, J. J., M. Rosenbaum, and L. T. Angenent. 2010. "Electric power generation from municipal, food, and animal wastewaters using microbial fuel cells." *Electroanalysis* 22 (7-8):832-843.
Gabriel, C. L. 1928. "Butanol fermentation process." *Industrial and Engineering Chemistry* 20:1063-1067.
Garrity, G. M., ed. 2007 *Bergey's manual of systematic bacteriology: second edition*. Edited by Noel R. Krieg Don J. Brenner, James T. Staley. Vol. 2, *Bergey's Manual of Systematic Bacteriology*. Lansing MI: Springer.
Golimowski, J., and K. Golimowska. 1996. "UV-photooxidation as pretreatment step in inorganic analysis of environmental samples." *Analytica Chimica Acta* 325 (3):111-133.
Gorby, Y. A., S. Yanina, J. S. McLean, K. M. Rosso, D. Moyles, A. Dohnalkova, T. J. Beveridge, I. S. Chang, B. H. Kim, K. S. Kim, D. E. Culley, S. B. Reed, M. F. Romine, D. A. Saffarini, E. A. Hill, L. Shi, D. A. Elias, D. W. Kennedy, G. Pinchuk, K. Watanabe, S. Ishii, B. Logan, K. H. Nealson, and J. K. Fredrickson. 2006. "Electrically conductive bacterial nanowires produced by *Shewanella oneidensis* strain MR-1 and other microorganisms." *Proceedings of the National Academy of Sciences of the United States of America* 103 (30):11358-11363.
Gordon, J. M. 2002. "Tailoring optical systems to optimized photobioreactors." *International Journal of Hydrogen Energy* 27 (11-12):1175-1184.
Gosse, J. L., B. J. Engel, F. E. Rey, C. S. Harwood, L. E. Scriven, and M. C. Flickinger. 2007. "Hydrogen production by photoreactive nanoporous latex coatings of nongrowing *Rhodopseudomonas palustris* CGA009." *Biotechnology Progress* 23 (1):124-30.
Gottwald, M., and G. Gottschalk. 1985. "The internal pH of *Clostridium acetobutylicum* and its effect on the shift from acid to solvent formation." *Archives of Microbiology* 143 (1):42-46.
Grimmler, C., H. Janssen, D. Krausse, R. J. Fischer, H. Bahl, P. Durre, W. Liebl, and A. Ehrenreich. 2011. "Genome-wide gene expression analysis of the switch between acidogenesis and solventogenesis in continuous cultures of *Clostridium acetobutylicum*." *Journal of Molecular Microbiology and Biotechnology* 20 (1):1-15.
Guex, N., and M. C. Peitsch. 1997. "SWISS-MODEL and the Swiss-PdbViewer: an environment for comparative protein modeling." *Electrophoresis* 18 (15):2714-23.
Gustafsson, C., S. Govindarajan, and J. Minshull. 2004. "Codon bias and heterologous protein expression." *Trends in Biotechnology* 22 (7):346-53.
Hadicke, O., H. Grammel, and S. Klamt. 2011. "Metabolic network modeling of redox balancing and biohydrogen production in purple nonsulfur bacteria." *BMC Systems Biology* 5.
Harris, L. M., N. E. Welker, and E. T. Papoutsakis. 2002. "Northern, morphological, and fermentation analysis of *spo0A* inactivation and overexpression in *Clostridium acetobutylicum* ATCC 824." *Journal of Bacteriology* 184 (13):3586-3597.
Hartmanis, M. G. N., T. Klason, and S. Gatenbeck. 1984. "Uptake and activation of acetate and butyrate in *Clostridium acetobutylicum*." *Applied Microbiology and Biotechnology* 20 (1):66-71.
Hartshorne, R. S., B. N. Jepson, T. A. Clarke, S. J. Field, J. Fredrickson, J. Zachara, L. Shi, J. N. Butt, and D. J. Richardson. 2007. "Characterization of *Shewanella oneidensis* MtrC: a cell-surface decaheme cytochrome involved in respiratory electron transport to

extracellular electron acceptors." *Journal of Biological Inorganic Chemistry* 12 (7):1083-1094.

Hartshorne, R. S., C. L. Reardon, D. Ross, J. Nuester, T. A. Clarke, A. J. Gates, P. C. Mills, J. K. Fredrickson, J. M. Zachara, L. Shi, A. S. Beliaev, M. J. Marshall, M. Tien, S. Brantley, J. N. Butt, and D. J. Richardson. 2009. "Characterization of an electron conduit between bacteria and the extracellular environment." *Proceedings of the National Academy of Sciences of the United States of America* 106 (52):22169-22174.

Harwood, C. S., and J. Gibson. 1986. "Uptake of benzoate by *Rhodopseudomonas palustris* grown anaerobically in light." *Journal of Bacteriology* 165 (2):504-9.

Hassen, A., M. Mahrouk, H. Ouzari, M. Cherif, A. Boudabous, and J. J. Damelincourt. 2000. "UV disinfection of treated wastewater in a large-scale pilot plant and inactivation of selected bacteria in a laboratory UV device." *Bioresource Technology* 74 (2):141-150.

He, Z., S. D. Minteer, and L. T. Angenent. 2005. "Electricity generation from artificial wastewater using an upflow microbial fuel cell." *Environmental Science & Technology* 39 (14):5262-5267.

Healy, J. B., and L. Y. Young. 1979. "Anaerobic biodegradation of eleven aromatic compounds to methane." *Applied and Environmental Microbiology* 38 (1):84-9.

Hillmer, P., and H. Gest. 1977. "H_2 metabolism in the photosynthetic bacterium *Rhodopseudomonas capsulata*: H_2 production by growing cultures." *Journal of Bacteriology* 129 (2):724-31.

Hirakawa, H., A. L. Schaefer, E. P. Greenberg, and C. S. Harwood. 2012. "Anaerobic *p*-coumarate degradation by *Rhodopseudomonas palustris* and identification of CouR, a MarR repressor protein that binds *p*-coumaroyl coenzyme A." *Journal of Bacteriology* 194 (8):1960-7.

Honicke, D., H. Janssen, C. Grimmler, A. Ehrenreich, and T. Lutke-Eversloh. 2012. "Global transcriptional changes of *Clostridium acetobutylicum* cultures with increased butanol:acetone ratios." *New Biotechnology* 29 (4):485-93.

Inglesby, A. E., D. A. Beatty, and A. C. Fisher. 2012. "*Rhodopseudomonas palustris* purple bacteria fed *Arthrospira maxima* cyanobacteria: demonstration of application in microbial fuel cells." *RSC Advances* 2 (11):4829-4838.

Inui, M., K. Nakata, J. H. Roh, K. Zahn, and H. Yukawa. 1999. "Molecular and functional characterization of the *Rhodopseudomonas palustris* no. 7 phosphoenolpyruvate carboxykinase gene." *Journal of Bacteriology* 181 (9):2689-96.

Inui, M., J. H. Roh, K. Zahn, and H. Yukawa. 2000. "Sequence analysis of the cryptic plasmid pMG101 from *Rhodopseudomonas palustris* and construction of stable cloning vectors." *Applied and Environmental Microbiology* 66 (1):54-63.

Inui, M., M. Suda, S. Kimura, K. Yasuda, H. Suzuki, H. Toda, S. Yamamoto, S. Okino, N. Suzuki, and H. Yukawa. 2008. "Expression of *Clostridium acetobutylicum* butanol synthetic genes in *Escherichia coli*." *Applied Microbiology and Biotechnology* 77 (6):1305-16.

Janssen, H., C. Doring, A. Ehrenreich, B. Voigt, M. Hecker, H. Bahl, and R. J. Fischer. 2010. "A proteomic and transcriptional view of acidogenic and solventogenic steady-state cells of *Clostridium acetobutylicum* in a chemostat culture." *Applied Microbiology and Biotechnology* 87 (6):2209-2226.

Javanmardian, M., and B. O. Palsson. 1991. "High-density photoautotrophic algal cultures - design, construction, and operation of a novel photobioreactor system." *Biotechnology and Bioengineering* 38 (10):1182-1189.

Jensen, H. M., A. E. Albers, K. R. Malley, Y. Y. Londer, B. E. Cohen, B. A. Helms, P. Weigele, J. T. Groves, and C. M. Ajo-Franklin. 2010. "Engineering of a synthetic electron conduit in living cells." *Proceedings of the National Academy of Sciences of the United States of America* 107 (45):19213-19218.

Jiao, Y., and D. K. Newman. 2007. "The pio operon is essential for phototrophic Fe(II) oxidation in *Rhodopseudomonas palustris* TIE-1." *Journal of Bacteriology* 189 (5):1765-1773.

Jickells, T. D., Z. S. An, K. K. Andersen, A. R. Baker, G. Bergametti, N. Brooks, J. J. Cao, P. W. Boyd, R. A. Duce, K. A. Hunter, H. Kawahata, N. Kubilay, J. laRoche, P. S. Liss, N. Mahowald, J. M. Prospero, A. J. Ridgwell, I. Tegen, and R. Torres. 2005. "Global iron connections between desert dust, ocean biogeochemistry, and climate." *Science* 308 (5718):67-71.

Jones, D. T., and D. R. Woods. 1986. "Acetone-butanol fermentation revisited." *Microbiological Reviews* 50 (4):484-524.

Joshi, G. S., S. Romagnoli, N. C. VerBerkmoes, R. L. Hettich, D. Pelletier, and F. R. Tabita. 2009. "Differential accumulation of form I RubisCO in *Rhodopseudomonas palustris* CGA010 under photoheterotrophic growth conditions with reduced carbon sources." *Journal of Bacteriology* 191 (13):4243-4250.

Jung, E. E., M. Kalontarov, D. F. R. Doud, M. D. Ooms, L. T. Angenent, D. Sinton, and D. Erickson. 2012. "Slab waveguide photobioreactors for microalgae based biofuel production." *Lab on a Chip* 12 (19):3740-3745.

Karpinets, T. V., D. A. Pelletier, C. L. Pan, E. C. Uberbacher, G. V. Melnichenko, R. L. Hettich, and N. F. Samatova. 2009. "Phenotype fingerprinting suggests the involvement of single-genotype consortia in degradation of aromatic compounds by *Rhodopseudomonas palustris*." *PLoS ONE* 4 (2):-.

Kinsel, N. A., and W. W. Umbreit. 1964. "Method for electrolysis of culture medium to increase growth of the sulfur-oxidizing iron bacterium *Ferrobacillus sulfooxidans*." *Journal of Bacteriology* 87 (5):1243-4.

Kirk, T. K., and R. L. Farrell. 1987. "Enzymatic "combustion": the microbial degradation of lignin." *Annual Review of Microbiology* 41:465-505.

Koebnik, R., K. P. Locher, and P. Van Gelder. 2000. "Structure and function of bacterial outer membrane proteins: barrels in a nutshell." *Molecular Microbiology* 37 (2):239-253.

Kovach, M. E., P. H. Elzer, Steven H. D., G. T. Robertson, M. A. Farris, R. M. Roop Ii, and K. M. Peterson. 1995. "Four new derivatives of the broad-host-range cloning vector pBBR1MCS, carrying different antibiotic-resistance cassettes." *Gene* 166 (1):175-176.

Larimer, F. W., P. Chain, L. Hauser, J. Lamerdin, S. Malfatti, L. Do, M. L. Land, D. A. Pelletier, J. T. Beatty, A. S. Lang, F. R. Tabita, J. L. Gibson, T. E. Hanson, C. Bobst, J. L. T. Y. Torres, C. Peres, F. H. Harrison, J. Gibson, and C. S. Harwood. 2004. "Complete genome sequence of the metabolically versatile photosynthetic bacterium *Rhodopseudomonas palustris*." *Nature Biotechnology* 22 (1):55-61.

Lazarova, V., P. Savoye, M. L. Janex, E. R. Blatchley, and M. Pommepuy. 1999. "Advanced wastewater disinfection technologies: state of the art and perspectives." *Water Science and Technology* 40 (4-5):203-213.

Leang, C., X. L. Qian, T. Mester, and D. R. Lovley. 2010. "Alignment of the *c*-type cytochrome OmcS along pili of *Geobacter sulfurreducens*." *Applied and Environmental Microbiology* 76 (12):4080-4084.

Lee, C. M., P. C. Chen, C. C. Wang, and Y. C. Tung. 2002. "Photohydrogen production using purple nonsulfur bacteria with hydrogen fermentation reactor effluent." *International Journal of Hydrogen Energy* 27 (11–12):1309-1313.

Li, Z., A. Venkataraman, M. A. Rosenbaum, and L. T. Angenent. 2012. "A laminar-flow microfluidic device for quantitative analysis of microbial electrochemical activity." *ChemSusChem* 5 (6):1119-23.

Little, J. W., and D. W. Mount. 1982. "The SOS regulatory system of *Escherichia coli*." *Cell* 29 (1):11-22.

Lloyd, J. R., V. A. Sole, C. V. G. Van Praagh, and D. R. Lovley. 2000. "Direct and Fe(II)-mediated reduction of technetium by Fe(III)-reducing bacteria." *Applied and Environmental Microbiology* 66 (9):3743-3749.

Lovley, D. R. 1991. "Dissimilatory Fe(III) and Mn(IV) Reduction." *Microbiological Reviews* 55 (2):259-287.

Lovley, D. R. 2011. "Powering microbes with electricity: direct electron transfer from electrodes to microbes." *Environmental Microbiology Reports* 3 (1):27-35.

Lovley, D. R., and E. J. Phillips. 1988. "Novel mode of microbial energy metabolism: organic carbon oxidation coupled to dissimilatory reduction of iron or manganese." *Applied and Environmental Microbiology* 54 (6):1472-80.

Lower, B. H., R. Yongsunthon, L. Shi, L. Wildling, H. J. Gruber, N. S. Wigginton, C. L. Reardon, G. E. Pinchuk, T. C. Droubay, J. F. Boily, and S. K. Lower. 2009. "Antibody recognition force microscopy shows that outer membrane cytochromes OmcA and MtrC are expressed on the exterior surface of *Shewanella oneidensis* MR-1." *Applied and Environmental Microbiology* 75 (9):2931-2935.

Marsili, E., D. B. Baron, I. D. Shikhare, D. Coursolle, J. A. Gralnick, and D. R. Bond. 2008. "*Shewanella* secretes flavins that mediate extracellular electron transfer." *Proceedings of the National Academy of Sciences of the United States of America* 105 (10):3968-3973.

Matsumoto, N., H. Yoshinaga, N. Ohmura, A. Ando, and H. Saiki. 2000. "High density cultivation of two strains of iron-oxidizing bacteria through reduction of ferric iron by intermittent electrolysis." *Biotechnology and Bioengineering* 70 (4):464-6.

McFadden, B. A. 1973. "Autotrophic CO_2 assimilation and the evolution of ribulose diphosphate carboxylase." *Bacteriology Reviews* 37 (3):289-319.

McKinlay, J. B., and C. S. Harwood. 2010. "Carbon dioxide fixation as a central redox cofactor recycling mechanism in bacteria." *Proceedings of the National Academy of Sciences of the United States of America* 107 (26):11669-11675.

McKinlay, J. B., and C. S. Harwood. 2011. "Calvin cycle flux, pathway constraints, and substrate oxidation state together determine the H_2 biofuel yield in photoheterotrophic bacteria." *Mbio* 2 (2).

McKinlay, J. B., Y. Oda, M. Ruhl, A. L. Posto, U. Sauer, and C. S. Harwood. 2014. "Non-growing *Rhodopseudomonas palustris* increases the hydrogen gas yield from acetate by shifting from the glyoxylate shunt to the tricarboxylic acid cycle." *Journal of Biological Chemistry* 289 (4):1960-70.

Meitl, L. A., C. M. Eggleston, P. J. S. Colberg, N. Khare, C. L. Reardon, and L. Shi. 2009. "Electrochemical interaction of *Shewanella oneidensis* MR-1 and its outer membrane

cytochromes OmcA and MtrC with hematite electrodes." *Geochimica Et Cosmochimica Acta* 73 (18):5292-5307.
Meulemans, C. C. E. 1987. "The basic principles of UV-disinfection of water." *Ozone-Science & Engineering* 9 (4):299-313.
Morishima, K., M. Yoshida, A. Furuya, T. Moriuchi, M. Ota, and Y. Furukawa. 2007. "Improving the performance of a direct photosynthetic/metabolic bio-fuel cell (DPBFC) using gene manipulated bacteria." *Journal of Micromechanics and Microengineering* 17 (11):2391-2391.
Muller, F. M. 1933. "On the metabolism of the purple sulphur bacteria in organic media." *Archives of Microbiology* 4 (1):131-166.
Myers, C. R., and K. H. Nealson. 1988. "Bacterial manganese reduction and growth with manganese oxide as the sole electron acceptor." *Science* 240 (4857):1319-1321.
Myers, J. M., and C. R. Myers. 2000. "Role of the tetraheme cytochrome CymA in anaerobic electron transport in cells of *Shewanella putrefaciens* MR-1 with normal levels of menaquinone." *Journal of Bacteriology* 182 (1):67-75.
Nair, R. V., G. N. Bennett, and E. T. Papoutsakis. 1994. "Molecular characterization of an aldehyde/alcohol dehydrogenase gene from *Clostridium acetobutylicum* ATCC 824." *Journal of Bacteriology* 176 (3):871-885.
Nakamura, Y., T. Gojobori, and T. Ikemura. 2000. "Codon usage tabulated from international DNA sequence databases: status for the year 2000." *Nucleic Acids Research* 28 (1):292.
Nevin, K. P., S. A. Hensley, A. E. Franks, Z. M. Summers, J. H. Ou, T. L. Woodard, O. L. Snoeyenbos-West, and D. R. Lovley. 2011. "Electrosynthesis of organic compounds from carbon dioxide Is catalyzed by a diversity of acetogenic microorganisms." *Applied and Environmental Microbiology* 77 (9):2882-2886.
Nevin, K. P., and D. R. Lovley. 2000. "Lack of production of electron-shuttling compounds or solubilization of Fe(III) during reduction of insoluble Fe(III) oxide by *Geobacter metallireducens*." *Applied and Environmental Microbiology* 66 (5):2248-2251.
Nevin, K. P., T. L. Woodard, A. E. Franks, Z. M. Summers, and D. R. Lovley. 2010. "Microbial electrosynthesis: feeding microbes electricity to convert carbon dioxide and water to multicarbon extracellular organic compounds." *Mbio* 1 (2).
Nolling, J., G. Breton, M. V. Omelchenko, K. S. Makarova, Q. D. Zeng, R. Gibson, H. M. Lee, J. Dubois, D. Y. Qiu, J. Hitti, Y. I. Wolf, R. L. Tatusov, F. Sabathe, L. Doucette-Stamm, P. Soucaille, M. J. Daly, G. N. Bennett, E. V. Koonin, and D. R. Smith. 2001. "Genome sequence and comparative analysis of the solvent-producing bacterium *Clostridium acetobutylicum*." *Journal of Bacteriology* 183 (16):4823-4838.
Oda, Y., S. K. Samanta, F. E. Rey, L. Wu, X. Liu, T. Yan, J. Zhou, and C. S. Harwood. 2005. "Functional genomic analysis of three nitrogenase isozymes in the photosynthetic bacterium *Rhodopseudomonas palustris*." *Journal of Bacteriology* 187 (22):7784-94.
Pan, C., Y. Oda, P. K. Lankford, B. Zhang, N. F. Samatova, D. A. Pelletier, C. S. Harwood, and R. L. Hettich. 2008. "Characterization of anaerobic catabolism of *p*-coumarate in *Rhodopseudomonas palustris* by integrating transcriptomics and quantitative proteomics." *Molecular & Cellular Proteomics* 7 (5):938-948.
Pasteur, L. 1861a. "Experiences et vues nouvelles sur la nature des fermentations." *Comptes rendus de l'Academie des sciences* 52:1260-1264.
Pasteur, L. 1861b. "Animacules infusoires vivant sans gaz oxyge libre et deÂterminant des fermentations." *Comptes rendus de l'Academie des sciences* 52:344-347.

Pasteur, Louis. 1862. "Quelques résultats nouveaux relatifs aux fermentations acétique et butyrique." *Bulletin de la Société Chimique de Paris*:pp. 52-53.

Pereira, V. J., K. G. Linden, and H. S. Weinberg. 2007. "Evaluation of UV irradiation for photolytic and oxidative degradation of pharmaceutical compounds in water." *Water Research* 41 (19):4413-4423.

Petersen, D. J., R. W. Welch, F. B. Rudolph, and G. N. Bennett. 1991. "Molecular cloning of an alcohol (butanol) dehydrogenase gene cluster from *Clostridium acetobutylicum* ATCC 824." *Journal of Bacteriology* 173 (5):1831-1834.

Pham, H. T., N. Boon, P. Aelterman, P. Clauwaert, L. De Schamphelaire, P. van Oostveldt, K. Verbeken, K. Rabaey, and W. Verstraete. 2008. "High shear enrichment improves the performance of the anodophilic microbial consortium in a microbial fuel cell." *Microbial Biotechnology* 1 (6):487-496.

Phattarasukol, S., M. C. Radey, C. R. Lappala, Y. Oda, H. Hirakawa, M. J. Brittnacher, and C. S. Harwood. 2012. "Identification of a *p*-coumarate degradation regulon in *Rhodopseudomonas palustris* by Xpression, an integrated tool for prokaryotic RNA-seq data processing." *Applied and Environmental Microbiology* 78 (19):6812-8.

Protocols, Cold Spring Harbor. 2006. "Laemmli sample buffer (2X)." *Cold Spring Harbor Protocols* 2006 (1):pdb.rec10424.

Rabaey, K., P. Girguis, and L. K. Nielsen. 2011. "Metabolic and practical considerations on microbial electrosynthesis." *Current Opinion in Biotechnology* 22 (3):371-377.

Rabaey, K., G. Lissens, S. D. Siciliano, and W. Verstraete. 2003. "A microbial fuel cell capable of converting glucose to electricity at high rate and efficiency." *Biotechnology Letters* 25 (18):1531-1535.

Rabaey, K., and R. A. Rozendal. 2010. "Microbial electrosynthesis - revisiting the electrical route for microbial production." *Nature Reviews Microbiology* 8 (10):706-716.

Reguera, G., K. D. McCarthy, T. Mehta, J. S. Nicoll, M. T. Tuominen, and D. R. Lovley. 2005. "Extracellular electron transfer *via* microbial nanowires." *Nature* 435 (7045):1098-1101.

Richardson, D. J., G. F. King, D. J. Kelly, A. G. Mcewan, S. J. Ferguson, and J. B. Jackson. 1988. "The role of auxiliary oxidants in maintaining redox balance during phototrophic growth of *Rhodobacter capsulatus* on propionate or butyrate." *Archives of Microbiology* 150 (2):131-137.

Riemer, J., H. H. Hoepken, H. Czerwinska, S. R. Robinson, and R. Dringen. 2004. "Colorimetric ferrozine-based assay for the quantitation of iron in cultured cells." *Analytical Biochemistry* 331 (2):370-5.

Rosano, G. L., and E. A. Ceccarelli. 2009. "Rare codon content affects the solubility of recombinant proteins in a codon bias-adjusted *Escherichia coli* strain." *Microbial Cell Factories* 8:41.

Rosenbaum, M. A., H. Y. Bar, Q. K. Beg, D. Segre, J. Booth, M. A. Cotta, and L. T. Angenent. 2012. "Transcriptional analysis of *Shewanella oneidensis* MR-1 with an electrode compared to Fe(III)citrate or oxygen as terminal electron acceptor." *PLoS ONE* 7 (2).

Rosenbaum, M., F. Aulenta, M. Villano, and L. T. Angenent. 2011. "Cathodes as electron donors for microbial metabolism: which extracellular electron transfer mechanisms are involved?" *Bioresource Technology* 102 (1):324-33.

Ross, D. E., J. M. Flynn, D. B. Baron, J. A. Gralnick, and D. R. Bond. 2011. "Towards electrosynthesis in *Shewanella*: energetics of reversing the Mtr pathway for reductive metabolism." *PLoS ONE* 6 (2).

Ross, D. E., S. S. Ruebush, S. L. Brantley, R. S. Hartshorne, T. A. Clarke, D. J. Richardson, and M. Tien. 2007. "Characterization of protein-protein interactions involved in iron reduction by *Shewanella oneidensis* MR-1." *Applied and Environmental Microbiology* 73 (18):5797-5808.

Russell, J. B. 1992. "Another explanation for the toxicity of fermentation acids at low pH: anion accumulation versus uncoupling." *Journal of Applied Bacteriology* 73 (5):363-370.

Sani, R. K., B. M. Peyton, and A. Dohnalkova. 2008. "Comparison of uranium(VI) removal by *Shewanella oneidensis* MR-1 in flow and batch reactors." *Water Research* 42 (12):2993-3002.

Sauer, U., and P. Durre. 1995. "Differential induction of genes related to solvent formation during the shift from acidogenesis to solventogenesis in continuous culture of *Clostridium acetobutylicum*." *FEMS Microbiology Letters* 125 (1):115-120.

Schulz, G. E. 2002. "The structure of bacterial outer membrane proteins." *Biochimica Et Biophysica Acta-Biomembranes* 1565 (2):308-317.

Shelobolina, E. S., H. A. Vrionis, R. H. Findlay, and D. R. Lovley. 2008. "*Geobacter uraniireducens* sp. nov., isolated from subsurface sediment undergoing uranium bioremediation." *International Journal of Systematic and Evolutionary Microbiology* 58:1075-1078.

Shen, C. R., E. I. Lan, Y. Dekishima, A. Baez, K. M. Cho, and J. C. Liao. 2011. "Driving forces enable high-titer anaerobic 1-butanol synthesis in *Escherichia coli*." *Applied and Environmental Microbiology* 77 (9):2905-2915.

Sillers, R., M. A. A-Hinai, and E. T. Papoutsakis. 2009. "Aldehyde-alcohol dehydrogenase and/or thiolase overexpression coupled with CoA transferase downregulation lead to higher alcohol titers and selectivity in *Clostridium acetobutylicum* fermentations." *Biotechnology and Bioengineering* 102 (1):38-49.

Sommer, R., T. Haider, A. Cabaj, W. Pribil, and M. Lhotsky. 1998. "Time dose reciprocity in UV disinfection of water." *Water Science and Technology* 38 (12):145-150.

Stolz, J. E., P. Basu, J. M. Santini, and R. S. Oremland. 2006. "Arsenic and selenium in microbial metabolism." *Annual Review of Microbiology* 60:107-130.

Suhas, P. J. Carrott, and M. M. Ribeiro Carrott. 2007. "Lignin - from natural adsorbent to activated carbon: a review." *Bioresource Technology* 98 (12):2301-12.

Summers, Z. M., J. A. Gralnick, and D. R. Bond. 2013. "Cultivation of an obligate Fe(II)-oxidizing lithoautotrophic bacterium using electrodes." *Mbio* 4 (1).

TerAvest, M. A., M. A. Rosenbaum, N. J. Kotloski, J. A. Gralnick, and L. T. Angenent. 2014. "Oxygen allows *Shewanella oneidensis* MR-1 to overcome mediator washout in a continuously fed bioelectrochemical system." *Biotechnology Bioengineering* 111 (4):692-9.

Thauer, R. K., K. Jungermann, and K. Decker. 1977. "Energy conservation in chemotrophic anaerobic bacteria." *Bacteriology Reviews* 41 (1):100-80.

Torres, C. I., A. K. Marcus, H. S. Lee, P. Parameswaran, R. Krajmalnik-Brown, and B. E. Rittmann. 2010. "A kinetic perspective on extracellular electron transfer by anode-respiring bacteria." *FEMS Microbiology Reviews* 34 (1):3-17.

Turick, C. E., W. A. Apel, and N. S. Carmiol. 1996. "Isolation of hexavalent chromium-reducing anaerobes from hexavalent-chromium-contaminated and noncontaminated environments." *Applied Microbiology and Biotechnology* 44 (5):683-688.

Venkataraman, A., M. A. Rosenbaum, S. D. Perkins, J. J. Werner, and L. T. Angenent. 2011. "Metabolite-based mutualism between *Pseudomonas aeruginosa* PA14 and *Enterobacter aerogenes* enhances current generation in bioelectrochemical systems." *Energy & Environmental Science* 4 (11):4550-4559.

Venkataraman, A., M. Rosenbaum, J. B. A. Arends, R. Halitschke, and L. T. Angenent. 2010. "Quorum sensing regulates electric current generation of *Pseudomonas aeruginosa* PA14 in bioelectrochemical systems." *Electrochemistry Communications* 12 (3):459-462.

Walter, K. A., G. N. Bennett, and E. T. Papoutsakis. 1992. "Molecular characterization of two *Clostridium acetobutylicum* ATCC 824 butanol dehydrogenase isozyme genes." *Journal of Bacteriology* 174 (22):7149-58.

Weber, K. A., L. A. Achenbach, and J. D. Coates. 2006. "Microorganisms pumping iron: anaerobic microbial iron oxidation and reduction." *Nature Reviews Microbiology* 4 (10):752-764.

Xing, D., Y. Zuo, S. Cheng, J. M. Regan, and B. E. Logan. 2008. "Electricity generation by *Rhodopseudomonas palustris* DX-1." *Environmental Science & Technology* 42 (11):4146-51.

Yi, H. N., K. P. Nevin, B. C. Kim, A. E. Franks, A. Klimes, L. M. Tender, and D. R. Lovley. 2009. "Selection of a variant of *Geobacter sulfurreducens* with enhanced capacity for current production in microbial fuel cells." *Biosensors & Bioelectronics* 24 (12):3498-3503.

Yokoyama, S., R. Yokoyama, C. S. Kinlaw, and D. E. Harry. 1990. "Molecular evolution of the zinc-containing long-chain alcohol-dehydrogenase genes." *Molecular Biology and Evolution* 7 (2):143-154.

Zimmer, J. L., and R. M. Slawson. 2002. "Potential repair of *Escherichia coli* DNA following exposure to UV radiation from both medium- and low-pressure UV sources used in drinking water treatment." *Applied and Environmental Microbiology* 68 (7):3293-3299.

APPENDIX

8.1 APPENDIX 1

SUPPLEMENTAL INFORMATION FOR: METABOLIC ENGINEERING OF *RHODOPSEUDOMONAS PALUSTRIS* FOR THE OBLIGATE REDUCTION OF *N*-BUTYRATE TO *N*-BUTANOL

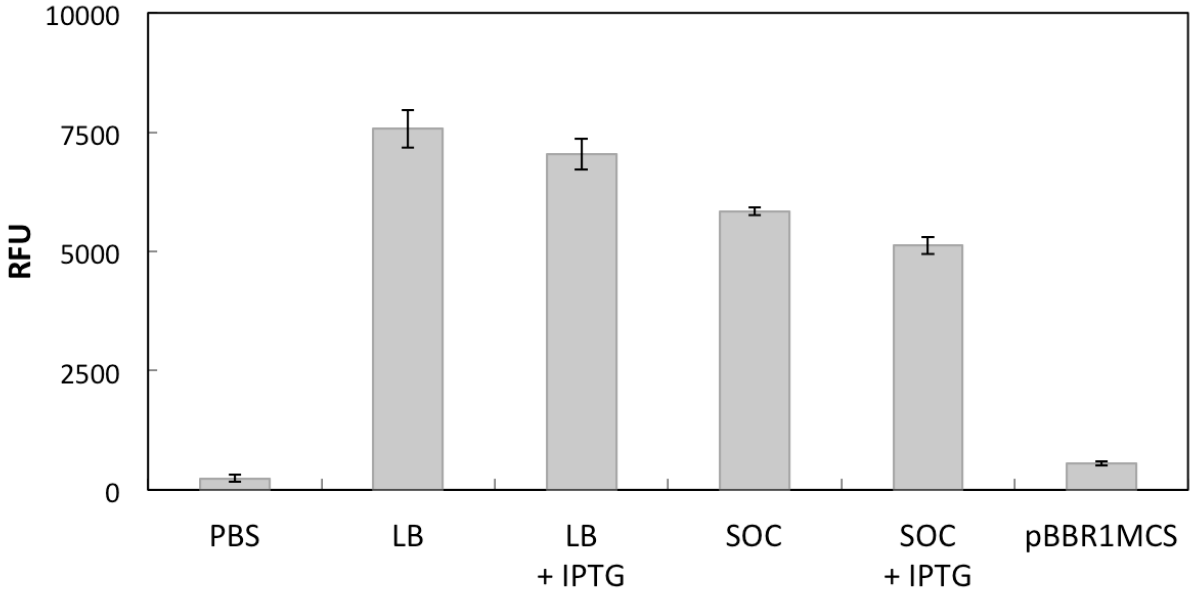

Figure A1.1. Response of pBBR1MCS-2 expression vector to IPTG induction and catabolite repression in *R. palustris* CGA009. Fluorescence is expressed as RFU (relative fluorescence per 1 unit of OD_{600})

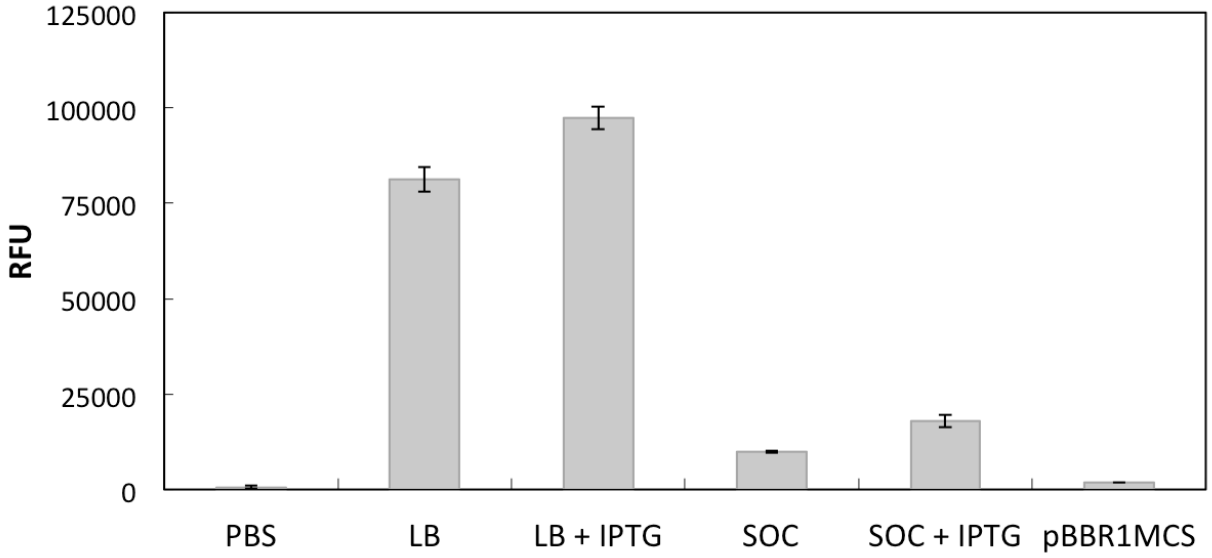

Figure A1.2. Response of pBBR1MCS-2 expression vector to IPTG induction and catabolite repression in *E. coli* DH5α. Fluorescence is expressed as RFU (relative fluorescence per 1 unit of OD_{600})

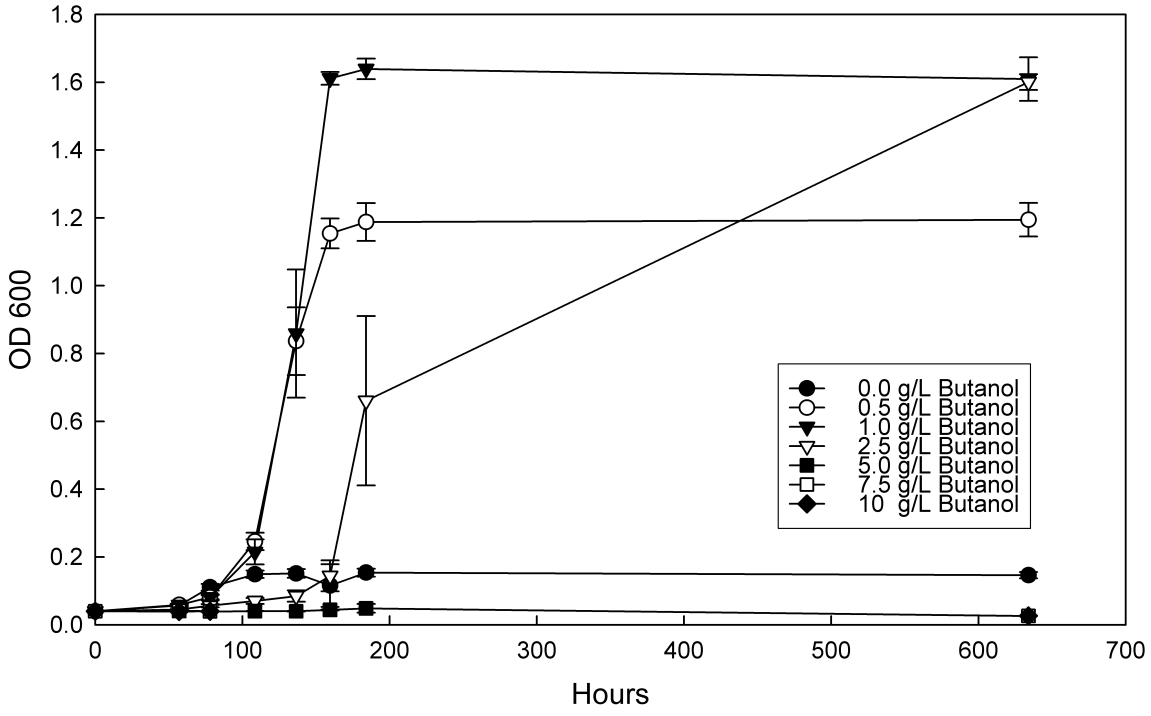

Figure A1.3. Triplicate growth of *R. palustris* CGA009 with butanol as a substrate. Minor lag phase observed for 2.5 g/L butanol, but maximum growth was ultimately achieved. Small growth later observed for 5.0 and 7.5 g/L butanol, but on much longer time scale.

Sequence of codon optimized 824 *adhE2*: Restriction sites for cloning are underlined. Coding sequence of gene indicated by upper case. 6X His tag used for western blot detection is indicated in red.

ctcgaggaaataaggcaacgtacgaaggaggtaaataATGAAGGTCACCAACCAGAAGGAACTGAAGCA
GAAGCTGAACGAGCTGCGGGAAGCCCAGAAGAAGTTCGCCACCTACACCCAGGAGC
AGGTGGACAAGATCTTCAAGCAGTGCGCCATCGCGGCCGCGAAGGAACGCATCAAC
CTGGCCAAGCTGGCGGTGGAGGAAACCGGCATCGGCCTGGTCGAGGACAAGATCAT
CAAGAACCACTTCGCCGCGGAATACATCTATAACAAGTACAAGAACGAGAAGACCT
GCGGCATCATCGACCATGACGACAGCCTGGGCATCACCAAGGTGGCCGAGCCGATC
GGCATCGTGGCCGCGATCGTCCCGACCACCAACCCGACCTCGACCGCGATCTTCAAG
AGCCTGATCTCCCTGAAGACCCGCAACGCGATCTTCTTCAGCCCGCACCCGCGGGCC
AAGAAGTCCACCATCGCCGCGGCCAAGCTGATCCTGGACGCGGCCGTCAAGGCGGG
CGCCCCGAAGAACATCATCGGCTGGATCGACGAACCGTCCATCGAGCTGTCGCAGG
ACCTGATGTCGGAGGCCGACATCATCCTGGCGACCGGCGGCCCGAGCATGGTGAAG
GCGGCCTACTCGTCGGGCAAGCCGGCCATCGGCGTCGGCGCGGGCAACACCCCGGC
CATCATCGACGAGTCCGCGGACATCGACATGGCCGTGTCCTCGATCATCCTGTCGAA
GACCTATGACAACGGCGTGATCTGCGCCTCGGAACAGAGCATCCTGGTCATGAACA
GCATCTACGAGAAGGTGAAGGAGGAATTCGTCAAGCGCGGCTCGTATATCCTGAAC
CAGAACGAAATCGCCAAGATCAAGGAGACCATGTTCAAGAACGGCGCCATCAACGC
GGACATCGTGGGCAAGAGCGCGTACATCATCGCCAAGATGGCGGGCATCGAAGTCC
CGCAGACCACCAAGATCCTGATCGGCGAGGTGCAGAGCGTCGAAAAGTCCGAGCTG
TTCTCGCACGAGAAGCTGTCGCCGGTGCTGGCGATGTACAAGGTCAAGGACTTCGA
CGAAGCCCTGAAGAAGGCGCAGCGCCTGATCGAGCTGGGCGGCTCGGGCCATACCA
GCTCCCTGTATATCGACAGCCAGAACAACAAGGACAAGGTGAAGGAGTTCGGCCTG
GCCATGAAGACCTCGCGGACCTTCATCAACATGCCGTCGAGCCAGGGCGCGTCCGG
CGACCTGTATAACTTCGCGATCGCCCCGTCGTTCACCCTGGGCTGCGGCACCTGGGG
CGGCAACTCCGTGTCGCAGAACGTCGAGCCGAAGCATCTGCTGAACATCAAGTCGG
TGGCCGAACGCCGGGAGAACATGCTGTGGTTCAAGGTCCCGCAGAAGATCTACTTC
AAGTATGGCTGCCTGCGCTTCGCCCTGAAGGAACTGAAGGACATGAACAAGAAGCG
GGCGTTCATCGTCACCGACAAGGACCTGTTCAAGCTGGGCTACGTGAACAAGATCA
CCAAGGTCCTGGACGAGATCGACATCAAGTATTCGATCTTCACCGACATCAAGTCGG
ACCCGACCATCGACAGCGTGAAGAAGGGCGCGAAGGAAATGCTGAACTTCGAGCCG
GACACCATCATCAGCATCGGCGGCGGCTCCCCGATGGACGCGGCCAAGGTCATGCA
CCTGCTGTACGAGTATCCGGAGGCGGAAATCGAGAACCTGGCCATCAACTTCATGG
ACATCCGCAAGCGGATCTGCAACTTCCCGAAGCTGGGCACCAAGGCCATCAGCGTG
GCGATCCCGACCACCGCCGGCACCGGCTCCGAAGCCACCCCGTTCGCGGTCATCACC
AACGACGAGACCGGCATGAAGTACCCGCTGACCAGCTATGAACTGACCCCGAACAT
GGCGATCATCGACACCGAGCTGATGCTGAACATGCCGCGCAAGCTGACCGCGGCCA
CCGGCATCGACGCCCTGGTGCATGCCATCGAAGCGTACGTGTCGGTCATGGCGACC
GACTATACCGACGAGCTGGCCCTGCGCGCGATCAAGATGATCTTCAAGTACCTGCCG
CGTGCGTATAAGAACGGCACCAACGACATCGAAGCGCGGGAGAAGATGGCGCACG
CCAGCAACATCGCGGGCATGGCGTTCGCCAACGCGTTCCTGGGCGTGTGCCACTCGA

TGGCGCATAAGCTGGGCGCCATGCACCATGTCCCGCATGGCATCGCCTGCGCGGTGC
TGATCGAGGAAGTCATCAAGTACAACGCGACCGACTGCCCGACCAAGCAGACCGCC
TTCCCGCAGTATAAGTCGCCGAACGCGAAGCGCAAGTACGCCGAAATCGCGGAGTA
TCTGAACCTGAAGGGCACCAGCGACACCGAAAAGGTCACCGCCCTGATCGAGGCGA
TCTCCAAGCTGAAGATCGACCTGTCCATCCCGCAGAACATCTCGGCGGCCGGCATCA
ACAAGAAGGACTTCTACAACACCCTGGACAAGATGTCGGAGCTGGCGTTCGACGAC
CAGTGCACCACCGCCAACCCGCGCTATCCGCTGATCTCCGAGCTGAAGGACATCTAC
ATCAAGTCGTTCCACCACCATCACCATCACTAAtctaga

8.2 APPENDIX 2

SUPPLEMENTAL INFORMATION FOR: SYNTROPHIC ACETATE SHARING BETWEEN *RHODOPSEUDOMONAS PALUSTRIS* CELLS WHILE DEGRADING THE LIGNIN MOLECULE *P*-COUMARATE IS NOT A STRATEGY USED TO AID REDOX BALANCE

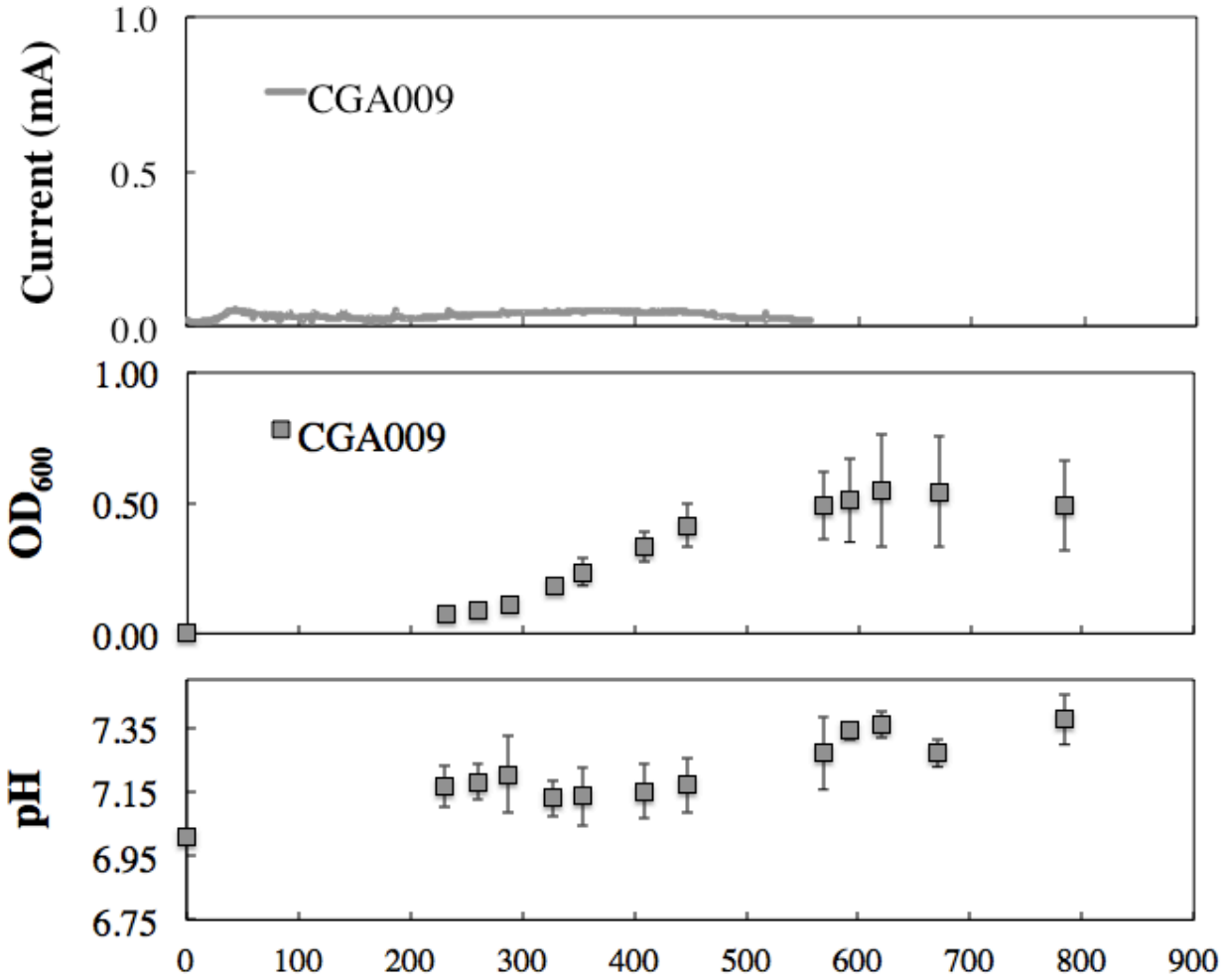

Figure A2.1. Growth of *R. palustris* CGA009 alone in BES with FW 5 mM *p*-coumarate for no *G. sulfurreducens* control. Standard deviation of duplicate reactors is plotted.

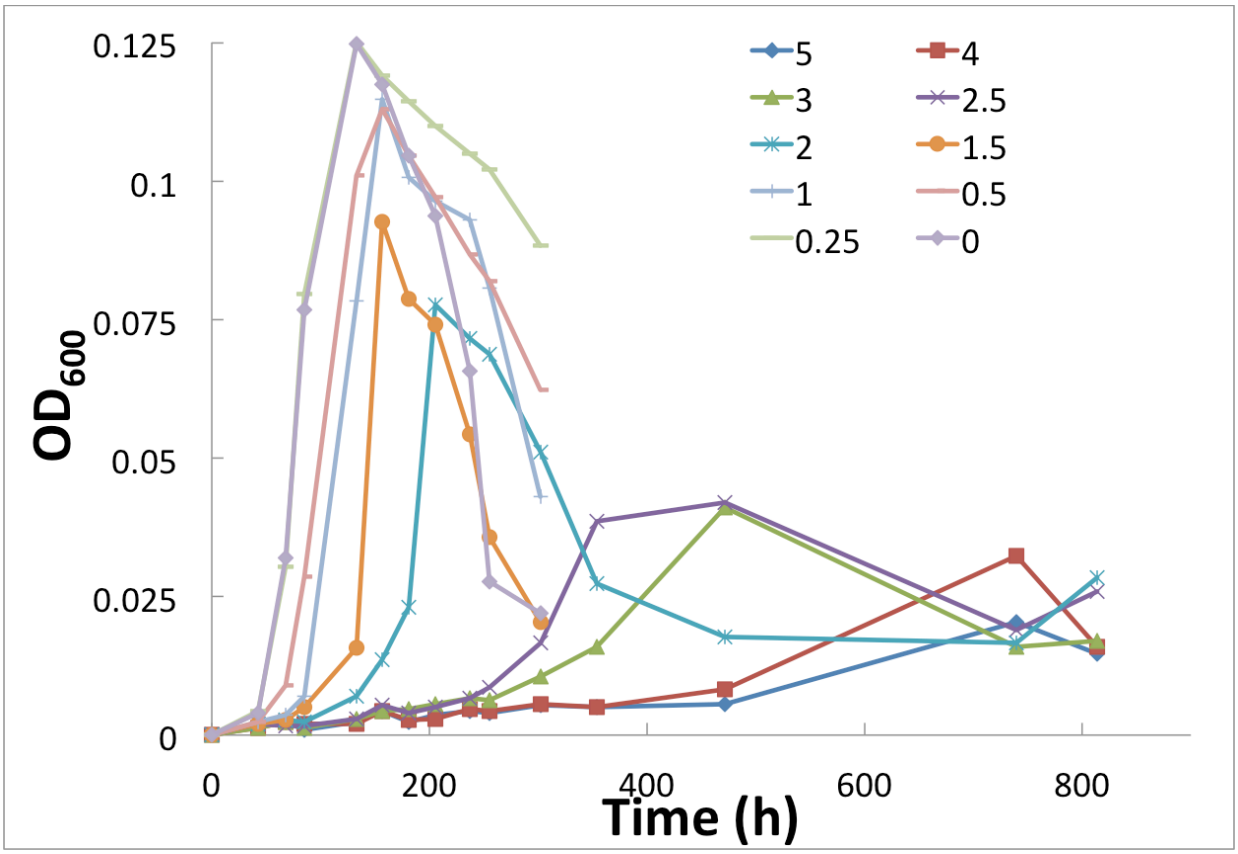

Figure A2.2. Toxicity assay of *G. sulfurreducens* grown in FW medium with 10 mM acetate 20 mM fumarate with increasing concentrations of *p*-coumarate [mM].

8.3 APPENDIX 3

SUPPLEMENTAL INFORMATION FOR: TOWARDS ELECTROSYNTHESIS WITH UNCOUPLED EXTRACELLULAR ELECTRON UPTAKE AND METABOLIC GROWTH: CURRENT INCREASE WITH *RHODOPSEUDOMONAS PALUSTRIS*

Reactor volumes:

The volume of 300 mL for the single photoBES system was chosen in an attempt to replicate the exact conditions of the previously reported from Bose growing *R. palustris* with an electrode. The low reported *R. palustris* OD attained (~0.01) was due to the limited support for growth that the traditional electrochemical system provided. The difference in working volume from the benchmark single photoBES system and the uncoupled system (17 mL for the 10-stack waveguide reactor) was restricted by the scale of the prototype 10-stack waveguide reactor that has been developed. Although the geometry of the 10-stack reactor (distance between waveguides) is optimized for light delivery and fixed at this distance, we envision that the waveguide reactor could be scaled up in the future (additional layers, increased width and length) to volumes comparable with the single photoBES. The higher OD in the uncoupled photoBES demonstrate that growth is supported to a higher level than in the single photoBES where OD levels of this magnitude were never observed, even with comparable operation times.

Integrated PhotoBES:

The integrated photoBES was constructed using ITO film (Bayview Optics, Dover-Foxcroft, ME), which was cut to the same dimensions as the chemical etched waveguide and bonded to the etched surface using polydimethylsiloxane (PDMS) (Dow Chemicals, Midland, MI) before insertion into the reactor frame. The different layers of ITO electrode were bonded to a carbon rod current collector using conductive silver epoxy (MG Chemicals, Surrey, B.C.). A port was created at the top of the reactor for the Ag/AgCl/sat'd KCl reference electrode (**Fig. S1**). An anion exchange membrane (Membranes International, Ringwood, NJ) was integrated (**Fig. S1**). This was a batch process and no eflow was required since the ITO electrodes functioned to regenerate the Fe(II) *in situ*, and thus the total volume was only the 17 mL of photobioreactor working volume. Hydrated sterile N_2/CO_2 was slowly sparged through the reactor to supply CO_2 and maintain pH, but this caused experimental problems and further development is required. The total iron concentration was 40 μM Fe-NTA, which was similar compated to the single PhotoBES.

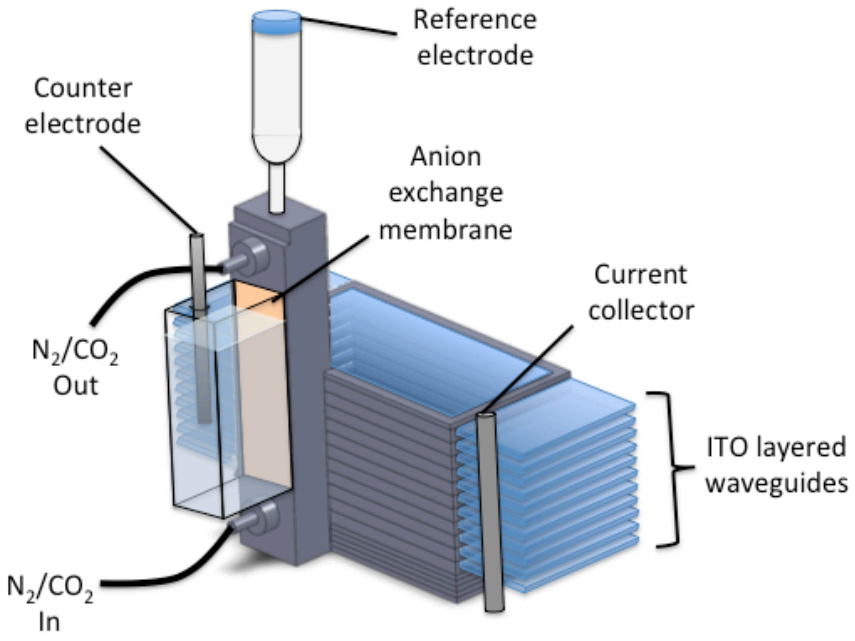

Figure A3.1: Schematic of integrated ITO waveguide photobioreactor for *in-situ* Fe(III) reduction.

8.4 APPENDIX 4

IN-SITU UV DISINFECTION OF A WAVEGUIDE-BASED PHOTOBIOREACTOR

Adapted from: Devin F. R. Doud, Aadhar Jain, Syed S. Ahsan, David Erickson, and Largus T. Angenent. Submitted to *Environmental Science and Technology*, May 2014

8.4.1 Abstract

Compact waveguide-based photobioreactors with high surface area-to-volume ratios and optimum light-management strategies have been developed to achieve high volumetric productivities within algal cultures. The light-managing strategies have focused on optimizing sunlight collection, sunlight filtration, and light delivery throughout the entire bioreactor volume by using light-directing waveguides. In addition to delivering broad-spectrum or monochromatic light for algal growth, these systems present an opportunity for advances in photobioreactor disinfection by using germicidal ultraviolet (UV) light. Here, we investigated the efficacy of *in-situ,* non-chemical UV treatment to disinfect a heterotrophic contaminant in a compact photobioreactor. We maintained a >99% pure culture of *Synechocystis* sp. PCC 6803 for an operating period exceeding three weeks following UV treatment of an intentionally contaminated waveguide photobioreactor. Without UV treatment, the culture became contaminated within only a few days (control). We developed a theoretical model to predict disinfection efficiency based on operational parameters and bioreactor geometry and we verified it with experimental results to predict the disinfection efficiency of a *Bacillus subtilis* spore culture.

8.4.2 Introduction

Ultraviolet (UV) light treatment is an effective non-chemical method for the disinfection of bacterial, eukaryotic, and viral contaminants present in water. Applications include pre-treatment of industrial water (Golimowski and Golimowska 1996), post-treatment of municipal wastewater (Lazarova et al. 1999), disinfection of drinking water (Bukhari et al. 1999), and systems for food safety (Bintsis, Litopoulou-Tzanetaki, and Robinson 2000). Advantages of UV disinfection in these application areas are based on the elimination of chemicals, such as chloramine or hypochlorite, which often remain in the water and exhibit downstream toxicity (Abarnou and Miossec 1992). In addition, UV treatment is fast, minimizes costs and labor, has no hazards associated with chemical handling and disposal, degrades pharmaceuticals (Pereira, Linden, and Weinberg 2007), and does not alter water chemistry.

Ultraviolet C (UVC) (100-280 nm) light has germicidal properties due to its interaction with pyrimidine bases in DNA and RNA at 254 nm. When sufficient UVC is absorbed, the genomic DNA becomes irreversibly cross-linked, restricting replication unless repair mechanisms are activated (Little and Mount 1982). The quantity of UVC light required to achieve a 1-$\log_{10}$ reduction for a particular organism is referred to as the UV dose. This value typically ranges between 1-10 mJ/cm^2 for bacteria, with higher values for viruses, spores, and some eukarya. However, many interferences may be present in waters, such as high suspended solids, low light transmittance, and high iron concentrations, resulting in UV disinfection being more effective for high clarity water treatment than wastewater (Meulemans 1987). One potential application in clear water that has yet to be adopted is UV disinfection within closed photobioreactors.

Closed photobioreactors are designed as highly controlled environments for growing axenic cultures for the production of bio-based chemicals including biofuels and nutraceuticals. However, contamination of these systems periodically occurs, requiring dismantling, disinfection, rinsing, and reculturing. Currently, most contaminated photobioreactors are treated with hypochlorite for disinfection followed by rinsing of the system with water. This labor-intensive process results in chemical consumption, wastewater production, and significant downtime of the system. Harnessing the advantages of *in-situ* UV disinfection for closed photobioreactor systems offers a novel strategy to effectively meet disinfection performance targets with less inconvenience and lower cost.

Photobioreactors that are capable of supporting high-density cultures with internal light-delivery structures, such as slab waveguide bioreactors, have the potential to improve control of optical characteristics and facilitate higher volumetric productivities of microalgal cultures compared to standard photobioreactors (Jung et al. 2012, Gordon 2002, Javanmardian and Palsson 1991). This high volumetric productivity is achieved by reducing the distance light must travel, by installing internal waveguides that are capable of transmitting light (either monochromatic or broad-spectrum). Consequently, internal waveguides allow optimal intensity of light to be delivered throughout the entire working volume of the bioreactor. Although previous projects have designed light collection and distribution systems that intentionally eliminate UV from being transmitted through their light delivery array (An and Kim 2000), we propose that the internal light distribution system could also be a vehicle for UV transmission to disinfect the photobioreactor.

To evaluate whether UVC light could be utilized as a strategy for disinfection of a compact waveguide based photobioreactor, we used *Escherichia coli* K-12 as a model

heterotrophic contaminant in a range of waveguide photobioreactors with different geometries and optical properties. Because the UVC dose required to inactivate a given contaminant is dependent only on the intensity of the UVC irradiance and exposure period, the parameters expected to govern the volumetric disinfection efficiency of the contaminant are: i) UVC light intensity released from the waveguide; ii) absorptivity of the liquid solution; iii) total depth of the bioreactor channel; and iv) exposure period. These parameters were used to construct a predictive model for calculating disinfection efficiency as a function of photobioreactor geometry. To verify the robustness of the model, predictions were made for the treatment of a solution of *Bacillus subtilis* spores, which were subsequently empirically tested.

8.4.3 Materials and methods

8.4.3.1 Bioreactor Construction

Bioreactors were composed of two parts: a single 76 x 25 x 1 mm quartz microscope slide (SPI supplies 01018-AB, Westchester, PA), which functioned as a waveguide capable of delivering UVC light; and a polydimethylsiloxane (PDMS) (Dow Chemicals, Midland, MI) casted chamber attached to the waveguide surface. Three surface conditions of the waveguides - evanescent (i.e., unmodified), chemical etching, and engineered pillars - were tested for enhanced light emission. Chemical etching was accomplished by applying glass-etching cream (Armour Products, Hawthorne, NJ) to the quartz slide for 7 h after which the glass slide was soaked in water and the etching cream was washed away. To fabricate the engineered pillar waveguides, SU-8 was applied using photolithography. The quartz slides were cleaned with soap, and then soaked in Nano-Strip (Cyantek, Fremont, CA) for 10 min. The slides were then heated for 30 min at 200°C on a hot plate. SU-8 2002 (Microchem, Newton, MA) was spun on for 10 s at 500 RPM with 250 r/s acceleration for 2 s, and then 1000 RPM for 30 s with 500 r/s acceleration for 1.5 s to achieve

a 2.8-μm thick layer. Slides were then placed on a hotplate at 95°C for 4 min. The SU-8 was exposed to UV for 7 s using hard contact exposure on a Suss MA6-BA6 Contact Aligner (Suss MicroTech, Sunnyvale, CA). Afterwards, the slides underwent a post-exposure bake at 95°C for 2 min and SU-8 was developed for 1 min (Cornell Nanoscale Science and Technology Facility). Finally, slides were rinsed off with isopropyl alcohol and dried with nitrogen gas. SU-8 was deposited at a gradient from 23% to 50% surface coverage from front to back by patterning an array of 5 μm by 5 μm pillars at varied spacing on the glass.

The bioreactor chambers had a 1 x 4 cm chamber footprint and were cast with different channel depths of 3.2, 1.6, and 0.8 mm. The PDMS chamber molds were fabricated using laser-cut plastic masters (W: 1 cm × L: 4 cm) of different thicknesses. A mixture of 1:100 carbon black to PDMS was poured over the plastic mold and cured at 80°C for 60 min. The PDMS chamber was then plasma-bonded to the waveguide to form the complete bioreactor. All surfaces of the bioreactor, except for the front edge of the waveguide where treatment UVC was coupled, were then coated with carbon black PDMS to block the entry of light. A control bioreactor, which blocked all UVC light, was created by coating all exposed surfaces of the bioreactor with black PDMS.

8.4.3.2 Sterilization Trials

E. coli K-12, which has a 1-$\log_{10}$ UV inactivation dose of ~4 mJ/cm^2 (Sommer et al. 1998), was cultured in Lysogeny broth (LB) at 37°C and grown until mid-exponential phase. Cells were pelleted at 2,000 x g for 10 min at 4°C, washed with sterile 1X phosphate-buffered saline (PBS), and then resuspended in PBS to an OD_{600} of 0.40 (OD_{254} of 1.61) for standard experiments. This bacterial solution was rinsed through all bioreactors prior to inoculation to remove residual liquids and ensure uniformity of the solution between bioreactors. After washing, the entire

bioreactor volume was filled with the solution and needles, which were used during the filling, were removed.

The bioreactors were positioned equidistant at 4 cm below the UV source. UV light was supplied by an Olympus 100 W mercury lamp (Olympus U-LH100HG, Olympus, Center Valley, PA) that was fitted with a narrow bandpass filter for transmission at 254±2.5 nm (50254FNB eSource optics, Whitinsville, MA). A UVC detector (PMA1122 SolarLight, Glenside, PA) was used to quantify the UVC flux at the incident surface of the exposed quartz waveguide edge, which was determined to be 46 $\mu W/cm^2$. Minor increases in local temperature of ~2°C above ambient were measured inside the bioreactor following treatments (1.5 h) in both the exposed and unexposed bioreactors (data not shown).

Following treatments, bioreactor contents were removed and diluted in sterile PBS. 50 µl samples were plated on solid LB media in triplicate using an Autoplate 4000 (Advanced Instruments Inc, Norwood, MA), incubated overnight in the dark at 37°C, and then enumerated from the dilution series with 30-300 colony forming units (CFUs) per plate. Sampling, dilution, and plating were performed rapidly to minimize effects of photoreactivation (Zimmer and Slawson 2002). All disinfection experiments were performed in biological triplicates, each with a technical plating triplicate. For all experiments, log reduction was calculated from the number of surviving organisms (determined by CFU) in the experimental bioreactors compared to the number of surviving organisms in the unexposed control bioreactor.

8.4.4 Axenic growth in a disinfected reactor

Synechocystis sp. PCC 6803 (hereafter *Synechocystis*) was precultured in standard BG-11 media with illumination from a 60-W incandescent lamp. For axenic growth experiments, 2 mL of a 0.05 OD_{600} solution of *Synechocystis* was injected into both a treated (150-min) and untreated 0.8

mm *E. coli* bioreactor (prepared identical to as previously described) and allowed to grow in BG-11 under constant illumination from a 60-W lamp. Purity was determined by daily measurements with both fluorescent and brightfield microscopy (Olympus BX-41 equipped with BF and Cy3 filters). Any organism that appeared in the brightfield image that did not have a corresponding chlorophyll auto-fluorescence signal in the fluorescent image was labeled as a contaminant. Upon high levels of growth, 100 µl was withdrawn from the bioreactor for microscopy and replaced with 100 µl of sterile BG-11 media.

8.4.5 Constructing and validating a predictive model

Predicting the remaining number of cells in a bioreactor following a given treatment can be accomplished using the Chick-Watson model (**Eq. 1**) as a foundation with: N = number of remaining cells; N_O = initial number of cells; k = disinfection rate constant; and t = exposure period.

$$N = N_O \exp(-kt) \quad (1)$$

By substituting our relevant bioreactor and UVC parameters into the disinfection rate constant of the Chick-Watson model, we converted it into a UVC specific form (**Eq. 2**). Relevant terms include: x = channel depth; and K_O = 1/organism UV dose for 1 log reduction

$$\frac{N}{N_O}(x,t) = \exp(-TD(x,t)K_O) \quad (2)$$

$TD_{(x,t)}$, the total dose of UV light delivered as a function of time and depth (**Eq. 3**), I_O = light emitted from waveguide surface, and α = absorption (per meter) of solution at 254 nm (**Eq. 4**)

$$TD_{(x,t)} = I_O t \exp(-\alpha x) \quad (3)$$

$$\alpha = -100 \cdot \ln 10^{-OD_{254}} \quad (4)$$

Because scattering from the surface of the waveguide occurs in all dimensions, the effective channel depth traveled is actually larger than the one dimensional depth corresponding to x. To account for this, we added the depth correction factor f, resulting in the updated total dose formula (**Eq. 5**).

$$\text{Corrected TD} = I_O t \exp(-\alpha f x) \quad (5)$$

To verify the robustness of the model, *B. subtilis* was grown in LB at 30°C for ~six weeks to allow the culture to sporulate. The spores were harvested by centrifugation and washed in sterile PBS. UVC treatment of the *B. subtilis* spore solution was performed identically as described for *E. coli* and was tested at the same OD_{254}.

8.4.6 Results and discussion

8.4.6.1 Waveguide surface activation improves treatment efficacy

Inactivation of bacterial contaminants with UVC proceeds according to the Chick-Watson model with the number of surviving microorganisms computed as a function of the organism lethal dose level, the intensity of UVC light, and the exposure period (**Eq. 2**) (Hassen et al. 2000). Thus, for a bioreactor with a biological contaminant at a specific optical density, the only way to improve disinfection rates is to increase the delivered UVC light intensity. Within a slab waveguide bioreactor, this can be achieved by increasing the level of light that is released from the surface

of the waveguide. Higher light levels from the surface of the waveguide can be accomplished in two ways: 1) increased intensity of the UV light source; and 2) improved efficiency of light emitted from the waveguide *via* modifications to the optical properties of the surface of the waveguide. To assess the potential for improved performance of waveguide-based disinfection by surface modification, three different types of surfaces were tested: 1) evanescent; 2) chemical etch; and 3) engineered pillar.

Unmodified (evanescent) waveguides emit light in the form of evanescent (near-field) waves, which exhibit an exponential decay from the surface of the waveguide without absorption and only travel micrometers (Jung et al. 2012). Chemical etch and engineered pillars, however, alter the refractive index interface at the surface of the waveguide and increase the release of far-field waves, which are capable of further propagating beyond the surface of the waveguide. Chemical etching results in random pitting of the waveguide surface, disrupting the uniformity and allowing emission of internalized light which otherwise would be trapped by total internal reflection. Pillars behave in a similar way, but can be deposited in a controlled manner on the surface of waveguides, allowing rational designs for the emission of light from the waveguide. This technology has recently been demonstrated to allow uniformity of visible light emission across an entire waveguide surface (submitted), but not for UV light. Testing is necessary, because SU-8 is known to absorb UV light (< 350 nm), and therefore we anticipated the possibility that the light releasing advantages conferred by the SU-8 pillar gradient design could be diminished when using UV light instead of visible light. Thus, waveguide-based photobioreactors with these surface modifications were constructed to disinfect a model contaminant solution of *E. coli* for a quantitative evaluation of increased flux of UV emission *via* surface modification (**Fig. A4.1**).

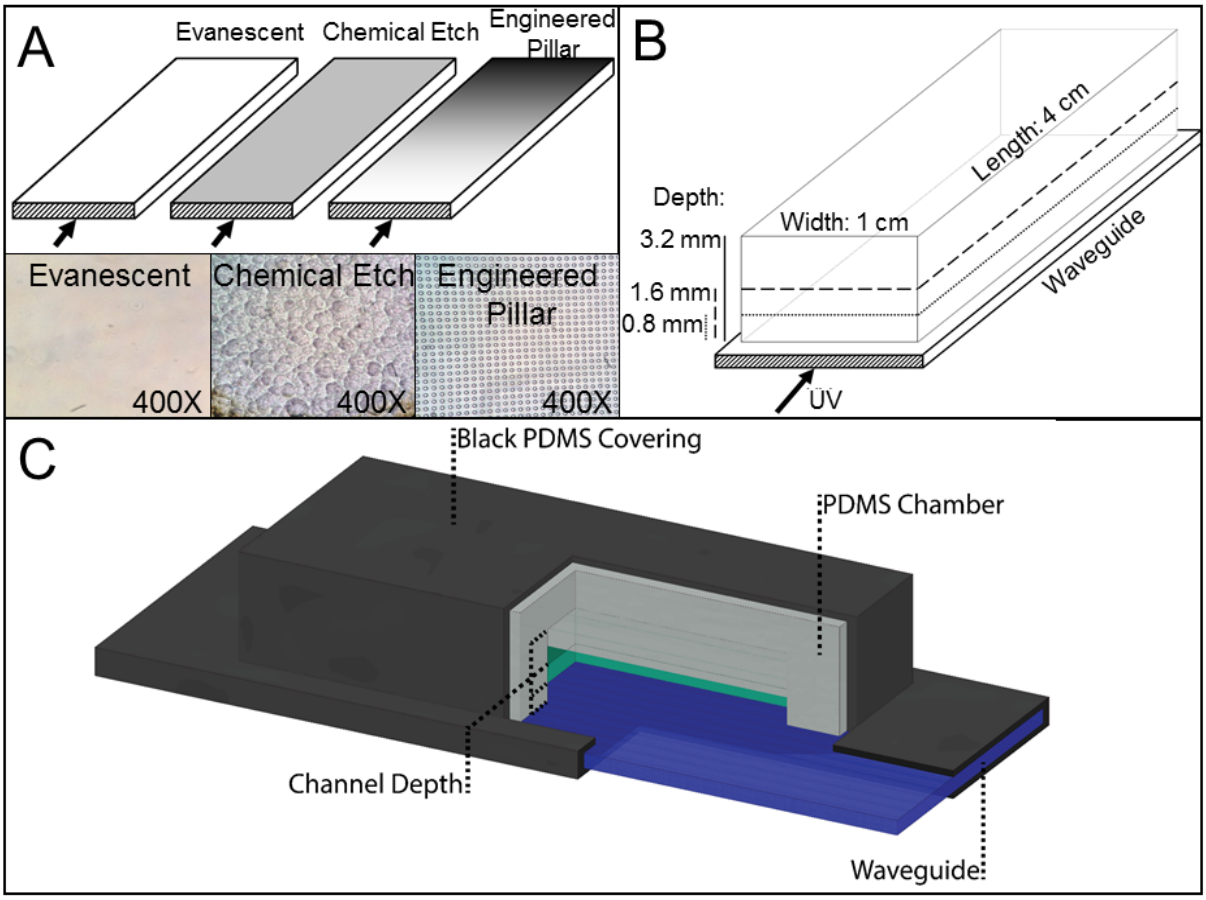

Figure A4.1. Schematic of bioreactors tested. A) Design of surface modifications used for evanescent (unmodified), chemical etch, and engineered pillar waveguides. B) Dimensions of bioreactors constructed for efficacy of disinfection at varying channel depths. C) Representation of assembled bioreactor with all components.

The log reduction of *E. coli* following a 75-min UVC treatment in the 3.2 mm channel depth bioreactors shows the lowest, highest, and middle disinfection efficacy for the evanescent, chemical etch, and engineered pillar waveguides, respectively (**Fig. A4.2 insert**). The efficacy of disinfection was determined as the log reduction in the *E. coli* population in each bioreactor compared to the control bioreactor (no UV). All exposed bioreactors had significantly reduced *E. coli* counts following the 75-min exposure compared to the control as determined by a one-tailed paired t-test ($p<0.01$). In addition, the engineered pillar bioreactor had significantly higher

reduction than the evanescent bioreactor ($p<0.001$), and the chemical etch bioreactor yielded higher reduction than the engineered pillar bioreactor ($p<0.001$). Even though the evanescent waveguide delivered enough UVC to inactivate a significant proportion of the population than the no UV control, the unmodified waveguides with only evanescent waves produced much less disinfection than either of the surface modified waveguides. In addition, although SU-8 surface activation (engineered pillar) has been successfully applied for visible light, one potential reason for its reduced performance compared to the chemical etch surface activation is the absorbance within the UVC spectrum. Therefore, chemical etching as a surface modification was found to be the most effective, and was selected for further investigation.

8.4.6.2 Decreasing channel depth and increasing time improves disinfection

Emitted light attenuates exponentially as it travels through the depth of the bioreactor channel. Because of this, contaminants closer to the surface of the waveguide experience a higher intensity than those farther away, establishing a gradient of cell inactivation through the depth of the bioreactor. As anticipated, when the bioreactor channel depth was decreased, improved disinfection efficiency for the same treatment was obtained (**Fig. A4.2**).

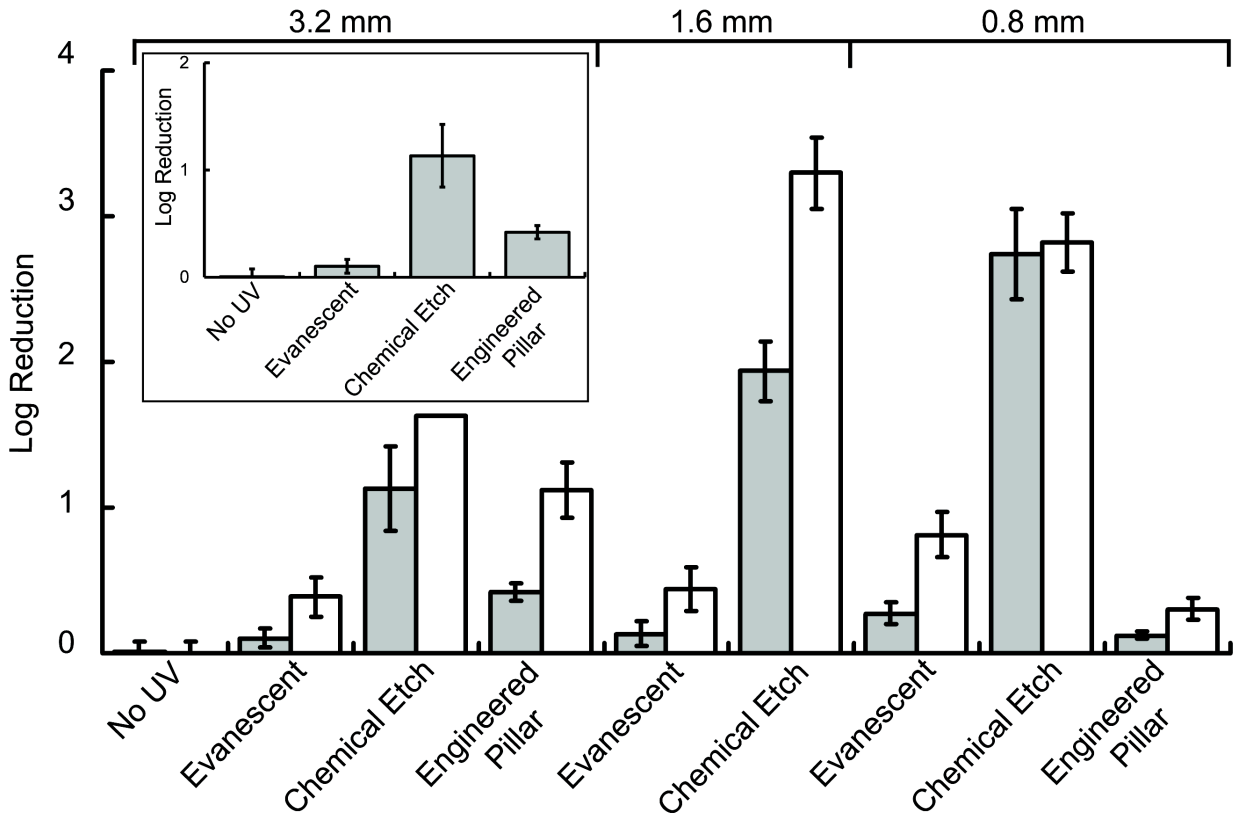

Figure A4.2. Log reduction of *E. coli* for the treatment conditions. Grey bars (75 min) and white bars (150 min) represent different exposure periods. Reduction in *E. coli* from experimental bioreactors was calculated according to the no UV control bioreactor. Insert shows the log reduction of *E. coli* following 75-min UVC treatment in evanescent, chemical etch, and engineered pillar bioreactor types with 3.2 mm channel depth only. Error bars are the standard deviation of triplicates.

With each decrease in bioreactor channel depth, a significant improvement in the disinfection efficiency ($p<0.05$) was attained compared to the previous depth for the 75-min exposure. To further characterize the performance of each bioreactor, an additional experiment with a 150-min exposure period was performed to determine disinfection levels attained after doubling the exposure (**Fig. A4.2**).

The reactor design that demonstrated the least improvement with doubling exposure was the chemical etch. One potential explanation for this non-linear response is an experimental artifact. Due to the superior level of the disinfection levels that the chemical etch bioreactors achieved (99.0-99.9%), any liquid remaining inside the bioreactor that was not exposed to the treatment light, such as very small volumes inside the injection ports, remained untreated and affected the disinfection levels disproportionally. This volume, which was estimated to be 0.1% of the total volume for the 0.8 mm bioreactor, became increasingly influential as the channel volume decreased. Thus, it is likely that disinfection levels attained following the 150-min exposure are underestimated due to contamination from this untreated volume and in reality may be closer to the predicted model value of double the log disinfection from the 75-min exposure.

8.4.6.3 Axenic growth following disinfection of a contaminated bioreactor

Although inactivation of ~99.9% of a bacterial contaminant was demonstrated, the applicability of this technology is dependent upon demonstrating complete inactivation of contaminants in a bioreactor followed by axenic growth of a photosynthetic organism of interest. To investigate if pure culture growth was attainable following disinfection of a contaminated bioreactor, *Synechocystis* was inoculated into an evacuated 0.8 mm chemical etch bioreactor immediately following its 150-min UV disinfection treatment. Purity of the culture was measured *in-situ* with a combination of fluorescence and brightfield microscopy.

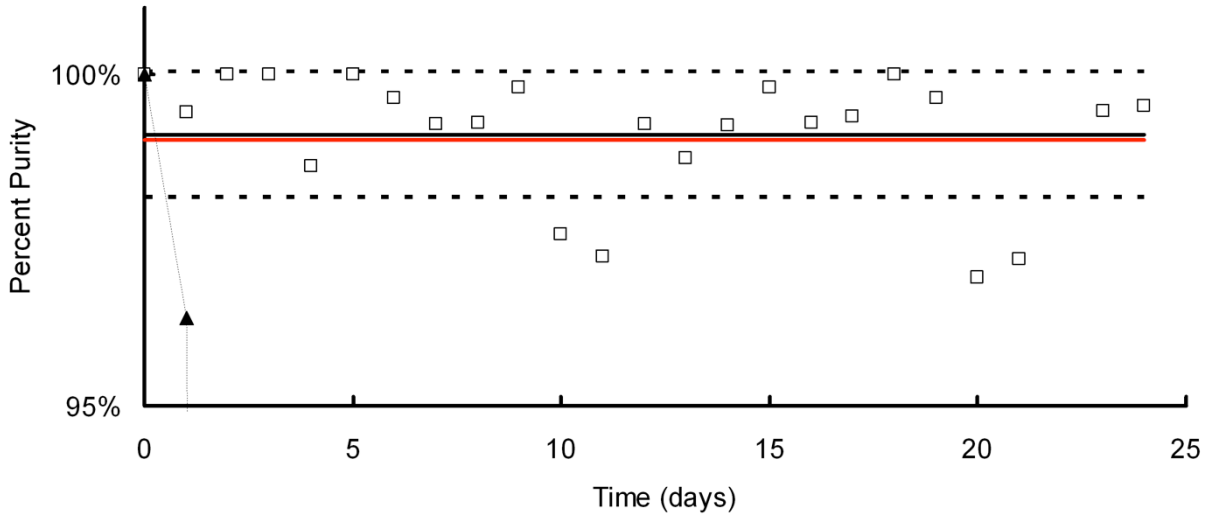

Figure A4.3. Graphical representation of *Synechocystis* purity. Open squares represent daily measurements for the treated bioreactor, closed triangles represent daily measurements for the bioreactor without UVC disinfection. The black horizontal line indicates the average for the measurements from all days, while the red horizontal line indicates the 99% purity threshold. Dotted lines indicate standard deviation of the measured points. Each point was determined by sampling of approximately 500 cells.

An average purity >99% was sustained over a period of 3 weeks in the treated bioreactor (**Fig. A4.3**). The untreated control bioreactor, which was also inoculated with *Synechocystis*, was rapidly contaminated to <10% purity with organisms phenotypically similar to *E. coli*. This result suggests that the treatment inactivated a sufficient proportion of the population of *E. coli* to inhibit recolonization of the bioreactor for at least three weeks. Both control and experimental bioreactors displayed a near 100% purity at Day 0, suggesting that in both cases, a bulk of the heterotroph culture was removed and replaced with the *Synechocystis* culture. However, following only two days of incubation, a steep decrease was observed in the control bioreactor, which did not occur in the treated bioreactor. These findings further attest to the efficacy of UVC disinfection in compact waveguide-based photobioreactors. Beyond achieving a greater than 99.9% reduction as demonstrated with the *E. coli* inactivation experiments, this technology

disabled a contaminant population to the extent that no significant regrowth was observed for more than three weeks, compared to two days when no treatment occurred.

8.4.6.4 Modeling disinfection

Integrating Eq. 5 (materials and methods) over the whole depth of a given bioreactor yields the expression for the proportion of viable cells remaining from an initial culture following a given treatment (**Eq. 6**).

$$\frac{1}{\alpha f d}\left[E_i\left(k \cdot \exp\left(-\alpha f d\right)\right) - E_i\left(k\right)\right] \quad (6)$$

$$k = K_O I_O t \quad (7)$$

This function was then fit to the six data points from the chemical etch bioreactors at different channel depths and exposure treatments to determine the depth correction factor f (**Eq. 5**) and the lumped parameter value k (**Eq. 7**). The k value for the 150-min exposure was held at a factor of 2 larger than the 75-min exposure since doubling the exposure period should result in a doubled k according to Equation 7. The best fit for the empirical *E. coli* data resulted in a k value of 17.5 for the 75-min disinfection series and a k value of 35 for the 150-min exposure (**Fig. A4.4**). This function fit well within the error of measurement for most points. The fitted depth correction factor f was calculated to be 2.6, which also fit well with estimates of three-dimensional scattering of the emitted light (data not shown).

To validate the robustness of the model, we performed a disinfection of *B. subtilis* spores with a 75-min exposure period in the chemical etch bioreactors to investigate whether the experimental results matched the prediction of our model. The organism UVC dose for disinfection of *B. subtilis* spores has previously been determined to be between 20-36 mJ/cm^2

(Sommer et al. 1998, Chang et al. 1985), which is a range approximately 5 to 9 times larger than that of *E. coli*. Washed spores in PBS were inoculated as previously described into the three chemical etch bioreactors to the same OD_{254} as used for *E. coli*. Since all other parameters of the model, other than the organism UV dose, remained the same as in the trials with *E. coli*, it was predicted that the lumped k value (inverse UV inactivation dose, UVC intensity, treatment time) for the 75-min exposure would decrease from 17.5 for *E. coli* to between 3.5 and 1.9 for the spore solution.

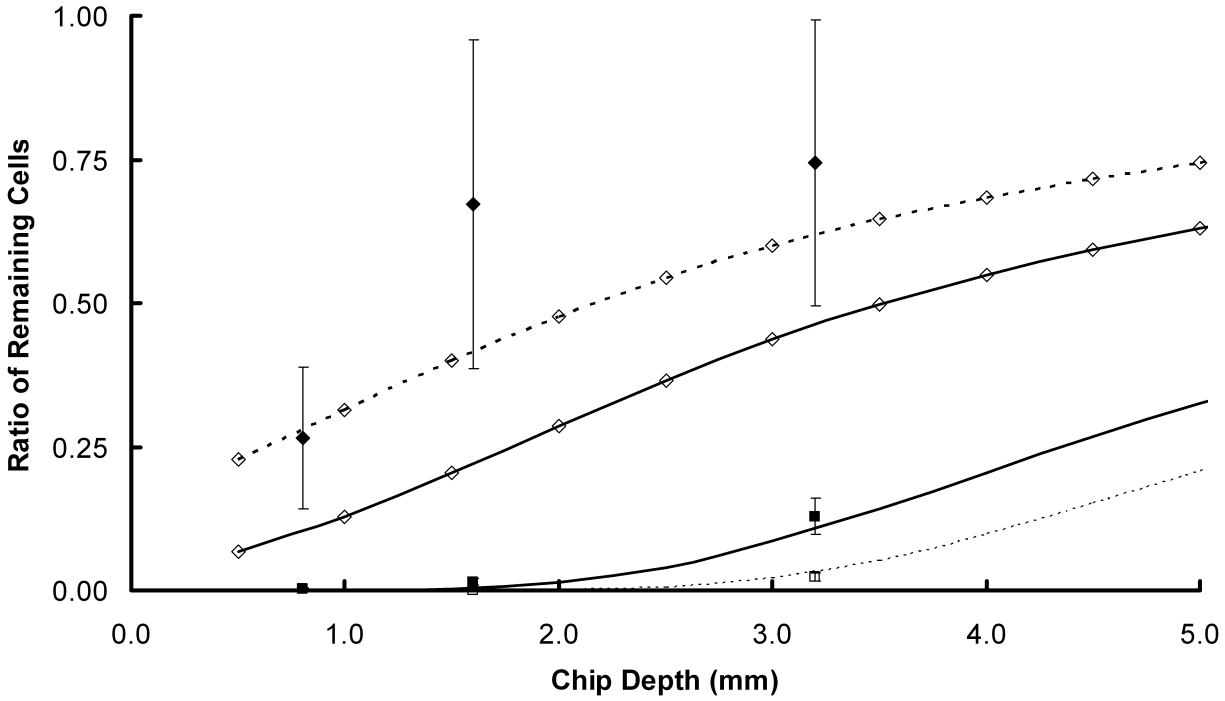

Figure A4.4. Model prediction for *B. subtilis* spore disinfection compared to empirical results. The model was fitted to six *E. coli* data points for chemical etch bioreactors for 75 and 150-min exposures. Solid and open squares indicate 75- and 150-min exposures, respectively, with the standard deviations shown. Solid and dotted lines correspond to predicted disinfection for 75- and 150-min exposures with k values of 17.5 and 35, respectively, with a fitted f value of 2.6. *B. subtilis* spore data is represented by filled diamonds with the standard deviations shown. The function predicted by our model with k value 3.5 is represented by a solid line with open diamonds, while the k value of 1.9 is represented by dotted line with open diamonds.

Both the predicted and experimental disinfection results for the *B. subtilis* spores following a 75-min UV treatment with k values of 3.5 and 1.9 are presented in Fig. 4.4. Within experimental error, the results from the treatment fall into the predicted range expected for *B. subtilis* spore disinfection constants from previous literature. In addition, the correct trend in disinfection as a function of bioreactor channel depth is well maintained with the spore survival. The experimental variation observed for the *B. subtilis* spore solution was much higher than previously attained with *E. coli*. One potential explanation for this is debris remaining in the sporulated culture. Even though the culture was predominantly spores as verified by microscopy, the presence of dead cells, cell debris, or vegetative cells remaining in the washed and resuspended solution following the six-week incubation could have introduced larger variation than the uniform *E. coli* culture. Absorption of UVC by non-viable components of the solution would also account for the slightly higher survival of the spores compared to the predicted results.

UVC light treatment, as demonstrated here, is a potentially advantageous technology for the disinfection of contaminated photobioreactors. By utilizing waveguides capable of internalizing and uniformly delivering UV light, we have shown the potential for this technology. Although we used quartz as the waveguide material, new materials, such as UV-transparent plastics, could minimize the cost associated with engineering UV transmission. We have also utilized optimized bioreactor geometry and modified waveguide surfaces to improve the delivery of UVC light to a defined volume. In addition to high levels of disinfection, this technology was shown to be capable of inactivating a heterotrophic contaminant, allowing sustained axenic growth of a cyanobacterial culture for over three weeks with minimal down time for treatment. In addition, no other forms of disinfection, disassembly, or washing were

required. However, for more UV-resistant contaminants, such as spores, it was demonstrated that this system would require a longer exposure period to reach high inactivation level, extending the downtime of the bioreactor. By fitting the empirical data to a theoretical based model, we were able to predict the required exposure times for inactivation of different biological contaminants with UVC of a known intensity.

8.4.7 Acknowledgements

We would like to thank the Cornell NanoScale Science & Technology Facility. This project was funded by the US DOE Advanced Research Projects Agency – Energy (ARPA-E) Open 2012 program project number DE-AR0000312.

8.4.8 Supplemental information for: In-situ *UV disinfection of a waveguide-based photobioreactor*

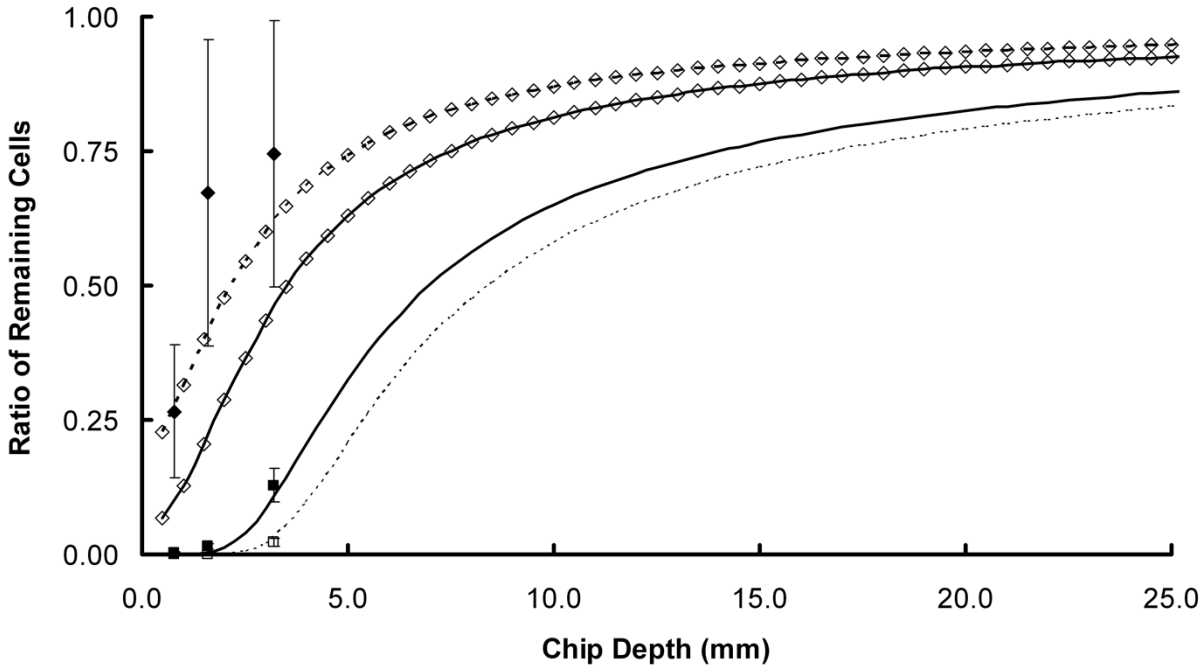

Figure A4.5: Extended model generated from Eq. 5 for deeper bioreactor channel depths.

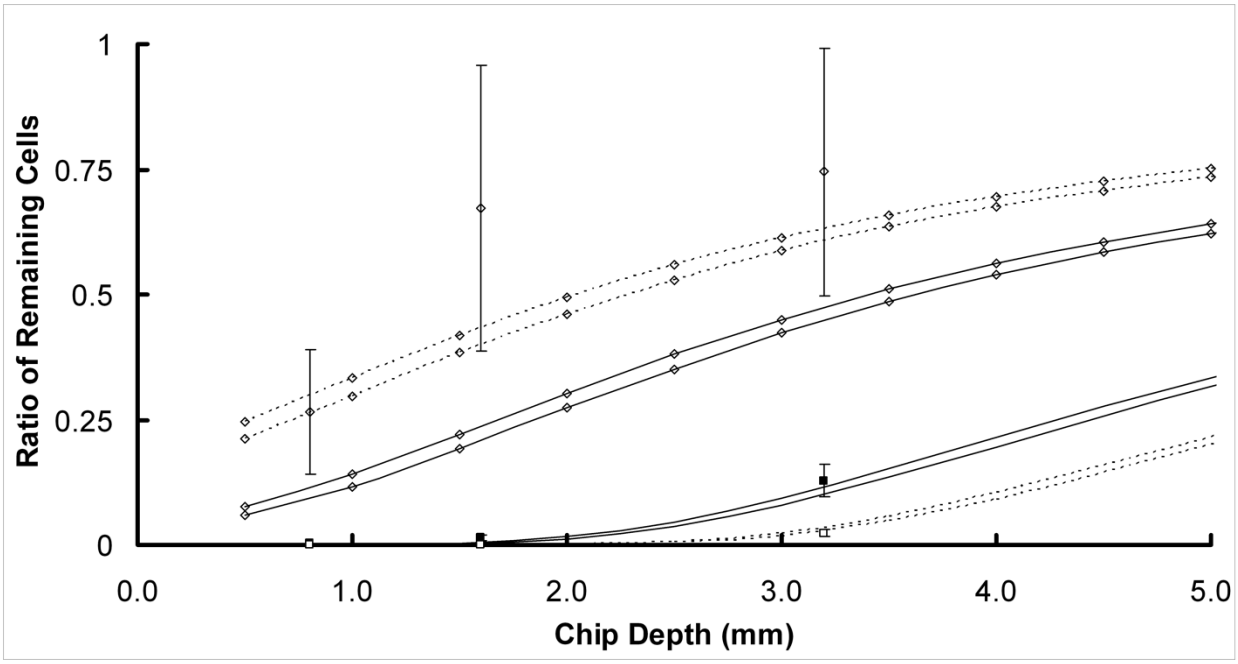

Figure A4.6: 5% sensitivity analysis for k factor. Plain solid line: k=17.5; plain dotted line: k=35; solid line with diamond: k=3.5; dotted line with diamond: k=1.9. Upper and lower boundaries of +/- 5% displayed for each k value. Diamond results represent *B. subtilis* 75-min exposure results, closed squares represent *E. coli* 75-min exposure results, open squares represent *E. coli* 150-min exposure results.

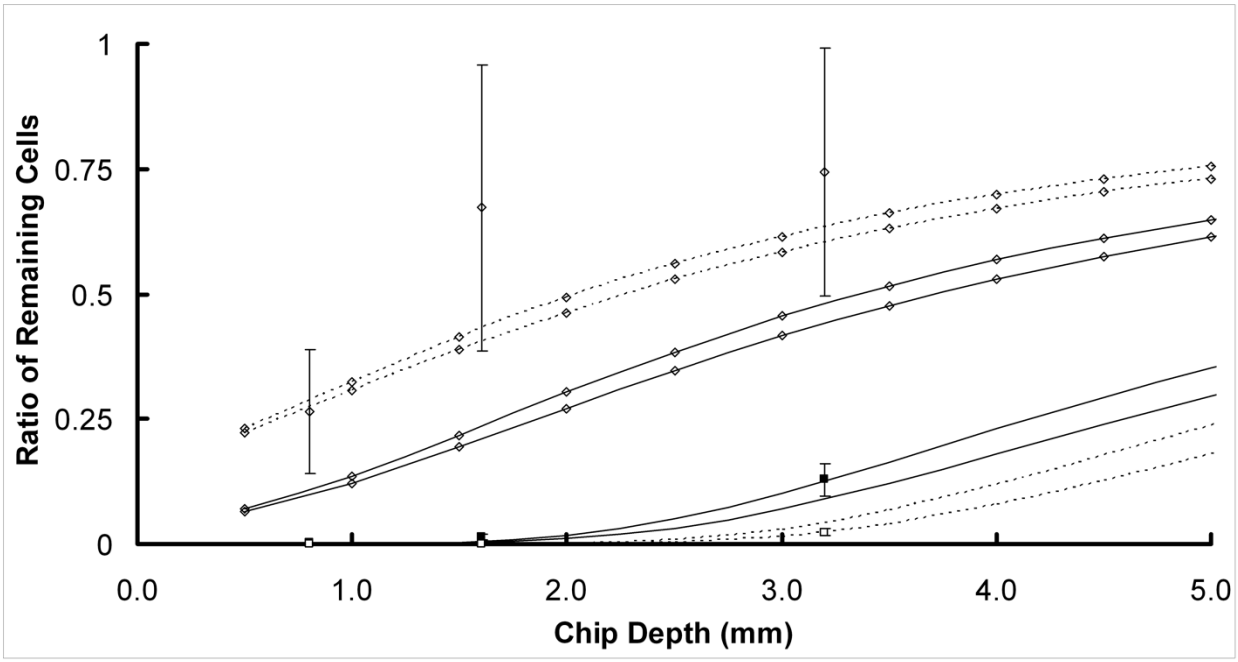

Figure A4.7: 5% sensitivity analysis for f factor. Plain solid line: k=17.5; plain dotted line: k=35; solid line with diamond: k=3.5; dotted line with diamond: k=1.9. Upper and lower boundaries of +/- 5% displayed for the f value of 2.6. Diamond results represent *B. subtilis* 75-min exposure results, closed squares represent *E. coli* 75-min exposure results, open squares represent *E. coli* 150-min exposure results.

8.5 APPENDIX 5

PROTOCOLS

8.5.1 Rhodospirillum Medium

Chemical	Master Stock Weight/100 mL	Volume to Add to Final Media
$KH_2PO_4 + K_2HPO_4$	5.0 g + 5.0 g	10 mL
$MgSO_4\ 7H_2O$	2.0 g	10 mL
NaCl + CaCl $2H_2O$	4.0 g + 0.5 g	10 mL
Fe-Citrate	0.1 g	5 mL
$(NH_4)_2SO_4$	10.0 g	10 mL
SL7 Trace Solution		1 mL
DiH2O		To 0.95 L

Add 2.0 g $NaCH_3CO_2$, adjust pH to 7.0 and autoclave.

After autoclaving and cooling, add 50 mL of sterile 400 mM $NaHCO_3$, and 1 mL of sterile filtered P2 Vitamin Solution

Butyrate +/- HCO_3^-

RM Butyrate media requires the omission of $NaCH_3CO_2$ and addition of sterile of butyrate following autoclaving.

For RM 1 g/L Butyrate + HCO_3^-: To have a pH of 7.0 after the addition of sterile Butyrate, 1.12 mL of 10 M NaOH total should be added prior to autoclaving.

For RM 2 g/L Butyrate + HCO_3^-: To have a pH of 7.0 after the addition of sterile Butyrate, 2.277 mL of 10 M NaOH total should be added prior to autoclaving.

For RM 1 g/L Butyrate No HCO_3^-: To have a pH of 7.0 after the addition of sterile Butyrate, 2.28 mL of 10 M NaOH total should be added prior to autoclaving.

8.5.2 Fresh Water Medium 2 mM p-Coumarate

To 900 ml DI water, add 0.33 g *p*-Coumarate 2.5 g $NaHCO_3$, 0.25 g NH_4Cl, 0.52 g NaH_2PO_4, 0.1 g KCl, 1 mL Trace Metal solution and 10 mL Vitamins, make to 1L with DI water and stir until completely dissolved. Sterilize by filtering media and add directly to reactors or to sterile serum bottles. For serum bottles, sparge solution with sterile N2/CO2 for 20 minutes to make anaerobic

To prepare

Vitamin mix:

- 2 mg biotin,
- 2 mg folic acid,
- 10 mg pyridoxine-HCl,
- 5 mg Thiamine-HCl·$2H_2O$,
- 5 mg Riboflavin,
- 5 mg Nicotinic acid,
- 5 mg D-Ca-pantothenate,
- 0.1 mg vitamin B12,
- 5 mg p-aminobenzoic acid
- 5 mg lipoic acid per liter;

Trace Metal mix:

- 1.5 g nitrilotriacetic acid,
- 3.0 g $MgSO_4 \cdot 7H_2O$,
- 0.5 g $MnSO_4 \cdot H_2O$,
- 1 g NaCl,
- 0.1 g $FeSO_4 \cdot 7H_2O$,
- 0.18 g $CoSO_4 \cdot 7H_2O$,
- 0.1 g $CaCl_2 \cdot 2H_2O$,
- 0.18 g $ZnSO_4 \cdot 7H_2O$,
- 0.01 g $CuSO_4 \cdot 5H_2O$,
- 0.02 g $KAl(SO_4)_2 \cdot 12H_2O$,
- 0.01 g H_3BO_3,
- 0.01 g $Na_2MoO_4 \cdot 2H_2O$,
- 0.025 g $NiCl \cdot 6H_2O$
- 0.3 mg $Na_2SeO_3 \cdot 5H_2O$ per liter.

Note: To make $-HCO_3^-$ media, omit $NaHCO_3$ from the recipe and instead add 1.725 g $NaHPO_4$ and 1.775 g Na_2PO_4. In serum bottles, instead sparge with sterile N_2.

8.5.3 Preparation of 100 mM Fe-NTA

Materials:
DI water
Nitrilotriacetic acid
Iron(III) Chloride Hexahydrate
Sodum Bicarbonate
Sterile Filter and Sterile Bottle
Sterile N_2 for sparging

Procedure:

- Dissolve 1.64 g $NaHCO_3$ in 80 ml water
- Add 2.56 g sodium nitrilotriacetic acid (213.12 g/mol)
  - or 2.30 g Nitrilotriacetic acid (191.14 g/mol) (some base may be necessary to dissolve)
- Then add 2.70 g $FeCl_3$ 6 H_2O (270.3 g/mol)
- Bring solution to 100 ml. Neutralize to just before pH 7 to prevent precipitation.
- Sparge solution with nitrogen and filter sterilize in anaerobic sterile serum bottle. Do not autoclave. Use a final concentration of 5-10 mmol.

8.5.4 Crude Protein Extraction (Whole Cell Extract)

Materials:

Sterile 50 mL Falcon Tube
Sterile 2 mL Microfuge Tube
1X Laemmli Buffer (See References- Cold Spring Harbor Protocols 2006)
Protease inhibitor cocktail (Promega, Fitchburg, WI)
Centrifuge
Sonicator/Cell Disruptor Probe (Branson Sonifier 150, Emerson, Danbury, CT)
Ice
BCA Assay (Pierce BCA protein assay kit, Thermo Scientific, Rockford, IL)

Procedure:

1. Harvest 50 mL of either *E. coli* or *R. palustris* late-exponential cells by centrifugation for 10 min at 12,000 x g and 4°C
2. Pour off supernatant and resuspend the cell pellet in 1 mL 1X Laemmli buffer with a protease inhibitor.
3. Sonicate the suspension on ice using three 30 sec on/1 min off pulses of 20W.
4. After sonication, remove the debris by centrifugation for 10 min at 12,000 x g and 4°C.
5. Transfer the soluble protein to a sterile 2 mL microfuge tube and freeze at -80°C
6. Total soluble protein concentration can be determined by BCA assay using manufacturer suggested protocols.

8.5.5 Preparation of carbon cloth electrodes

Materials:

Graphite Rods (fine, <0.5 cm diameter, >8 cm length)
Carbon Cloth (Panex ® 30- PW06, Zoltek Corp)
Carbon Cement (Leit-C, conductive carbon cement, Electron Microscopy Services)
Zip Ties (6" Black Zip Tie, Home Depot)
Xylenes (ACS reagent, ≥98.5% xylenes + ethylbenzene basis, Sigma-Aldrich)

Procedure:

To prepare carbon cloth electrodes:

1. Clean graphite rod with razor blade and finish with sand paper. Rinse and dry.

IN THE FUME HOOD:

2. Cut carbon cloth into a 9 x 9 cm square.
3. Mix carbon cement with Xylenes solution to a liquid consistency.
4. Dip the tip of the graphite rod in the carbon cement solution and adhere two opposite corners of the carbon cloth square to the tip with a zip tie.
5. Apply another aliquot of carbon cement ~2 cm above the zip tie and adhere the other two corners of the carbon cloth to this location with a zip tie.
6. Allow electrode to dry for 4 hours in the fume hood.
7. Remove excess tail from zip ties.
8. Resistance of the electrode (from carbon rod through carbon cloth) should be less than 1 Ω as measured by a multi-meter.

8.5.6 Preparation of Ag/AgCl sat'd KCl reference electrode

Materials:

Glass reference electrode with magnesia frit (made by Dave Wise, Cornell glassblower)
Silver wire
Rubber stopper to seal reference electrode
DI water
Potassium Chloride
Bacteriological agar
Hotplate + magnetic stirrer
Magnetic stirbar
10 mL syringe with long stainless steel needle
Parafilm

Procedure:

To Oxidize the Silver Wire:

1. Insert a silver wire (~4 cm) through the rubber stopper so that a majority remains inside the body of the electrode and a small tip is available for electrochemical connection
2. Submerge the silver wire intended for the electrode body in a dilute KCl solution in a beaker along with a carbon rod and reference electrode (Ag/AgCl). Connect the end of the silver wire to the working electrode lead of the potentiostat, the carbon rod to the counter electrode lead, and the reference electrode lead to the Ag/AgCl reference electrode.
3. Run the program Prepare_RE with the potentiostat (VSP or SP-200).

To Create the Assembled Reference Electrode:

1. Add 100 mL DI water, 1.5 g bacteriological agar, and a stirbar to a beaker.
2. Heat while stirring until an even boil is achieved and all agar has melted.
3. Add 40.0 g of KCl to the solution and wait until boil returns.
4. Pour the KCl/agar solution into the body of the reference electrode. Remove any air bubbles that occur with the syringe/stainless steel needle. Top off the reference electrode and add the oxidized silver wire/rubber stopper while ensuring there are no air bubbles.
5. Wipe away residual solution ejected from the rubber stopper, and parafilm the seal between the reference electrode and rubber stopper closed.

8.5.7 HPLC Detection of Metabolites (Acetate, Butyrate, Butanol)

Materials:

HPLC Vials (66015-702 Clear Shell Vial with Plugs, VWR)
Waters HPLC System (600 Controller, 717+ Autosampler with 100 sample carousel, 410 Refractive Index Detector)
Aminex Fast-Acid Column (HPX-87H column)
5 mM H2SO4 (HPLC grade) in 18.2 MΩ water

Procedure:

1. Turn on autosampler and detector and wait for initialization to finish.
2. Turn on controller and wait for initialization to finish.
3. Ensure that the 5 mM H_2SO_4 reservoir is full.
4. Set Helium sparging to 100 (mL/min).
5. Set column oven temperature to 60°C.
6. Set autosampler temperature to 4°C.
7. Open the Peak385-32bit program on the detector computer and load the DEFAULT control file.
8. After Helium has sparged the reservoir for 30 minutes, reduce sparging rate to 20.
9. Clear old solution from lines and pump by opening silver valve at face of the pumps and pump at a rate of 1 mL/min for 10 min.
10. Reduce pump rate to 0.05 mL/min and close valve.
11. Slowly ramp pumping rate up to 0.6 mL/min over the course of 30 minutes with 0.05 mL/min intervals. Ensure pressure remains stable at each interval before proceeding to next.
12. Verify settings in program table as: 0.6 mL/min, 100% A eluent
13. Insert samples in desired locations in the carousel and program vial sequence, 30 uL injection volume, and 45 minutes per sample.
14. Ensure in Peak Simple that the Frequency is 2 Hz, and describe the sequence runtime as 44 minutes and designate a save file destination.
15. On the controller, push the operate method button, wait for complete initialization, and then press start run

8.5.8 GC Detection of Metabolites (Butanol, Butyraldehyde)

Materials:

2 mL ROBO Autosampler Vials (46610-722, VWR)
Gas Chromatograph (HP 5890, Hewlett Packard, Palo Alto, CA) with a 7673 autoinjector and flame ionization detector
Custom-made packed bed glass column of 1.8m x 2 mm id (Supelco, Sigma-Aldrich, St. Louis, MO)

Procedure:

1. Start both the GC and communication module.
2. Open all gas tank and needle valves and ensure the GC has proper flow of all gasses (Air, Helium, Hydrogen).
3. Set the inlet and detector temperatures to 220°C and 240°C respectively.
4. Ignite the detector and ensure that the GC has a stable signal readout.
5. Open the Instrument 2 Online icon on the computer.
6. Add samples to the carousel and program the sequences into the computer.
7. Using the SOLVENTS program, run samples.
8. SOLVENTS has been preprogrammed with a temperature profile of 100°C for 2 min, a ramp of 40°C/min to 180°C with a 5 minute hold.

8.5.9 Ion Chromatography Detection of Metabolites (p-Coumarate, 4-Hydroxybenzoate, Benzoate):

Materials:

5 mL Polyvials (P/N 038008, Thermo Scientific)
Ion Chromatograph (Dionex ICS-1100) with a AS-DV autosampler and Variable Wavelength Detector.
1X Dionex AS22 Eluent (063965, Thermo Scientific)

Procedure:

1. Add 1X Dionex AS22 eluent to the reservoir.
2. Open Chromeleon 7.0 IC software.
3. Open the waste valve on the left pump chamber and select "prime" pump. Click OK that the waste valve is open and prime for 5 minutes.
4. Stop flow, close the waste valve, and then click "pump". Pump speed should be operated at 1.2 mL/min.
5. Start Suppressor and UV detector (set to 285 nm).
6. Click "Monitor Baseline" once the UV detector temperature has stabilized.
7. Once a stable signal for UV and conductivity has been attained and pressure in the system is the stable, unclick "monitor baseline".
8. Load samples into the carousel
9. Create a new sample series by clicking create and entering appropriate sample location and names. Select "Devin Method" for the instrument method.
10. Click start to begin analysis

8.5.10 Preparation of E. coli *DH5α electroporation stocks*

Materials

E. coli DH5α
Sterile Lysogeny Broth (LB)
Sterile Glycerol
Sterile DI Water

Procedure:

Day 1:

1. Inoculate a 25 mL overnight culture of in DH5α in LB shaking at 37°C.

Day 2:

2. Inoculate 250 mL of LB with 5 mL culture. Grow at 37 with vigorous shaking til it reaches OD_{600} 0.5- 0.7 (2-3 hrs)
3. Transfer cells to two 250 mL bottles and chill on ice 15+ minutes
4. Harvest cells by centrifucation at 5,000 rpm for 10 minutes at 4°C
5. Pour off supernatant and resuspend each pellet in 40 mL ice cold, sterile ddH2O. Transfer to sterile 50 mL red cap tube. Spin at 2,500 rpm for 15 min at 4°C
6. Pour off (aspirate) all supernatant. Wash cell pellet once again in 50 mL ice cold sterile ddH2O
7. Pour off (aspirate) all supernatant. Resuspend each pellet in 20 mls ice cold sterile 10% glycerol. Pool into one 50 mL tube and spin at 2500 rpm for 15 min at 4°C
8. Resuspend cells with 1 mL ice cold sterile 10% glycerol
9. Aliquot 75 ul cells per 0.5 mL tube and store immediately at -80 C

Note: This protocol can be used for preparing *R. palustris* electrocompetent samples. Preculturing times will be longer for *R. palustris* and can be performed either under aerobic or anaerobic conditions.

8.5.11 Electroporation of E. coli *DH5α*

Materials:

Electrocompetent *E. coli* DH5α
Electroporation cuvette (1 mm)
Super Optimal Broth with Catabolite Repression (SOC)
Lysogeny Broth (LB) and LB 50 μg/mL Kanamycin plates (1.5% agar)
BioRad Electroporator

Procedure:

1. Chill electroporation stock, cuvette, and 1 mL SOC on ice.
2. While keeping all components on ice, add 2 μL of purified DNA to the electrocompetent cells.
3. Transfer the cell/DNA mixture to the chilled electroporation cuvette.
4. Tap down the solution on the benchtop and wipe cuvette with a kim wipe to ensure good connection.
5. Electroporate at 1.8 kV, 200 Ω, 25 μF with an expected time constant of 4 ms.
6. Immediately resuspend the sample with 900 μL of SOC.
7. Incubate at 37°C with no shaking for 1 hr.
8. Pellet the cells at 4,000 g, pour off the supernatant, and resuspend the cells in the small volume that remains.
9. Spread cells on LB 50 μg/mL Kanamycin plates, and incubate upside down overnight at 37°C.

Note: This protocol can be used for transforming *R. palustris* by changing the electroporation resistance to 400 Ω and recovering the cells for 3-4 hours. Following recovery, cells are plated on LB 200 μg/mL Kanamycin plates.